New Aspects of Quantum Interactions:

Acceleration-Induced Transparency, Newton's Cradle Spectra, Superoscillations

by

Barbara Šoda

A thesis
presented to the University of Waterloo
in fulfillment of the
thesis requirement for the degree of
Doctor of Philosophy
in
Physics

Waterloo, Ontario, Canada, 2022

Examining Committee Membership

The following served on the Examining Committee for this thesis. The decision of the Examining Committee is by majority vote.

External Examiner:	Miles Blencowe Professor, Dept. of Physics and Astronomy, Dartmouth College
Supervisors:	Lucien Hardy Professor, Perimeter Institute for Theoretical Physics
	Achim Kempf Professor, Dept. of Applied Mathematics, University of Waterloo
Internal Member:	Niayesh Afshordi Professor, Dept. of Physics, University of Waterloo
Internal-External Member:	Florian Girelli Associate Professor, Dept. of Applied Mathematics, University of Waterloo
Other Member(s):	Robert Myers Professor, Perimeter Institute for Theoretical Physics, Dept. of Physics and Astronomy, University of Waterloo

Author's Declaration

This thesis consists of material all of which I authored or co-authored: see Statement of Contributions included in the thesis. This is a true copy of the thesis, including any required final revisions, as accepted by my examiners. I understand that my thesis may be made electronically available to the public.

Statement of Contributions

This thesis is in part a compilation of articles [85], [156], [108] and [175].

In particular, Chapter 2 and the accompanying Appendix 8 are based on the article [85], which was coauthored with Vivishek Sudhir and Achim Kempf. Exception is the Section 2.8, which is as yet unpublished.

Chapters 4 and 6, and the Appendix 9, are based on articles [175] and [156], both coauthored with Achim Kempf. Exceptions are Section 6.6, based on the [91], Section 6.7 and Section 4.5 which consist of unpublished results of mine. Section 4.6 is partly based on unpublished work with Neeraj Tata.

Finally, Chapter 5 and the Appendix 10 are based on [108], coauthored with Emily Kendall and Achim Kempf.

I am the sole author of all other parts of the thesis, including Chapter 1, Chapter 3 and Chapter 7.

Abstract

We present new results on different aspects of quantum interactions, from new phenomena to new mathematical tools. First, two new phenomena of light-matter interactions are presented: the stimulated Unruh effect and acceleration induced transparency. We show how the two combined lead to improved measurability of the Unruh effect in the laboratory. Building on that, we present a method to modulate the strength of general quantum interactions, which we call the parametrically induced decoupling. Then, as an answer to the mathematical challenges of describing quantum interactions, we present Newton's cradle spectra as a new tool for understanding nonperturbative physics. This is followed by a work describing what influences the rate at which a quantum channel arises at the onset of an interaction between two systems. Finally, we describe a new method to generate superoscillations of arbitrary shape, and the new idea of quantum prison break, whereby a quantum object contained in a finite space may escape it and jump to a predefined region, when triggered by a suitable measurement.

Acknowledgements

First of all, I would like to express sincere gratitude to my supervisors Achim Kempf and Lucien Hardy for giving me the chance to continue my physics path at the Perimeter Institute and University of Waterloo.

I would like to thank Achim Kempf for the encouragement, patience, inspiring discussions with countless tangents, for all the concepts I learned in those discussions, and changing my physics worldview multiple times. In the language of neural networks, your guidance did not just aim to optimize the parameters of my neural network, it helped redesign the architecture, and the set of cost functions, and I am an entirely different physicist as a result, and hopefully a better person. Thank you for everything.

I am grateful for my supervisor Lucien Hardy. Though we did not publish together, I truly enjoyed our meetings and conversations, our idea exchanges. From Lucien I learned physics ideas that I can not imagine I would learn elsewhere, and I am especially grateful for being in the presence of your scientific curiosity and courage. Thank you for your support and kindness.

I would like to thank Jonathan Oppenheim as well, for his support and encouragement.

I have also been lucky to collaborate with Vivishek Sudhir. Not only did I have the good fortune to learn from Vivishek, I was also lucky enough to be on the receiving end of excellent advice and support when I needed them.

I am deeply grateful to Frederic Schuller for his support and guidance at the crucial moments.

I was lucky to be a part of an inspiring research environment: Perimeter Institute and University of Waterloo. I met and befriended more wonderful and interesting people than I would dare to name. I would like to thank everyone at these institutions for making them so wonderful.

To my friends in Waterloo, my friends from good old days in Croatia and all over the world: I am grateful for our times together, you've painted the years with a rainbow of colours, lively and enjoyable, sometimes difficult, all summing up to a deeply meaningful period in my life. Thank you for everything.

Finally, I would like to thank my parents and my brother for their love and unwavering support.

Dedication

To my family: Mladenka, Dane i Lovre.

Table of Contents

List of Figures

Chapter 1

Introduction

The beginning of the 20th century marked the dawn of a new era in physics, one of quantum physics. The mathematical foundations of the theory are well developed by now, and yet, as we shall see, there are still new phenomena hiding in the theoretical framework, left for us to discover. There are mathematical challenges waiting to be resolved, as well.

It is not surprising to discover new phenomena at the intersection of two different fields. When we create a setup where two well-understood physical theories interact with each other, we often find new puzzles, new paradoxes and new physics, perhaps most famously the black hole information paradox [75]. In this thesis though, we will find new aspects of *interactions themselves*, in the context of quantum theory: nonrelativistic quantum physics and quantum field theory.

In the past century, new interaction-related discoveries in quantum physics regularly proved to be fruitful: for example, Rabi oscillations, a simple phenomenon of a qubit interacting with an external field, eventually led to the nuclear magnetic resonance [145], which is now used in medicine, chemistry and has many more applications. Einstein's description of stimulated emission and absorption [54, 55] later led to the discovery of lasers [151], [119], which proved to be useful in many contexts, from precision measurements in industry to medical lasers used in surgery, and others. It is, therefore, compelling to keep exploring and find new such fundamental physical phenomena that might one day contribute in different domains of human endeavours.

We are now faced with new challenges. For example, we are aiming to advance into the era of quantum computing, after a decades-long successful run with silicon-based classical computing. For this, a great challenge seems to be the elimination of noise due to the interaction of a quantum computer with its environment, and due to spurious interactions

between the subsystems of the quantum computer itself. One is faced with the challenge of needing to at the same time maximize the desired interactions between the subsystems of the quantum computer, in order to enhance the spread of entanglement, a valuable resource in quantum computing, while minimizing the spurious interactions contributing to the noise. In order to do that, we need to understand how interactions contribute to the spread of entanglement, and how we may sometimes modulate the strength of some interactions.

Further, we address another challenge in fundamental physics. The weakness of the Unruh effect has led to a decades-long experimental challenge to directly measure it in the laboratory. The effect is small because the interaction terms giving rise to the effect are supressed under the conditions that we can achieve in the laboratory. We will describe this in more details in later chapters. Nevertheles, though the Unruh effect is small, it is important, because it is one of the few acceleration-induced quantum phenomena that we know of. Furthemore, any acceleration-induced effect is necessarily related, via the equivalence principle, to gravitational physics. In this thesis I will present two new acceleration-induced effects: the *stimulated Unruh effect* and the *acceleration-induced transparency*. Interestingly, the two combined will lead to a great improvement in the measurability of the Unruh effect in the laboratory: a modest estimate gives an increase of 16 orders of magnitude over the theoretical predictions for the standard Unruh effect.

The two new phenomena present *an aspect of modulating the strength of interactions*, modelled in the context of light-matter interactions: stimulating the Unruh effect allows us to greatly enhance that part of the interaction between a quantum field and an Unruh-DeWitt detector that is responsible for the Unruh effect. On the other hand, acceleration induced-transparency is a method to suppress the interactions that give rise to the resonant transitions, which may be viewed as the spurious transitions when one is focussed on observing the clean Unruh effect. In summary, these two methods, as we shall see in Chapter 2, allow us to suppress the dominant, resonant interaction terms, and greatly enhance the weak, non-resonant terms, thereby bringing the Unruh effect close to experimental observability.

While gaining control over the strength of an interaction is an important quantitative goal, to complete the understanding, it is also necessary to study its qualitative nature. We aim to understand an interaction's capacity to entangle different subsystems of the total physical system under consideration. This is especially important in quantum computing. After all, in a practical sense, a strong interaction is not considered useful, unless it succeeds in the entangling of some degrees of freedom of interest. For this purpose, in Chapter 5 we study the spread of entanglement at the onset of interactions. More precisely, we investigate how different parameters in the interaction govern the rate at which a quantum

channel arises, at the onset of an interaction between two systems.

A famous mathematical challenge, almost as old as the quantum theory itself, is the problem of understanding how the eigenvalues and eigenvectors of a Hamiltonian change when another Hamiltonian is added to it. It is the problem of understanding how the eigensystem changes when an interaction Hamiltonian is added to the free Hamiltonian. If the matrix elements of the interaction Hamiltonian are small compared to the free Hamiltonian, then we may use perturbation theory. However, when they are comparable in size, and the Hamiltonians do not commute, the problem enters the nonperturbative regime. In this case there only are few mathematical techniques at our disposal, namely the von Neumann-Wigner results on level repulsion, Weyl's inequalities, dualities that relate strong coupling physics to weak coupling physics in some special cases. In Chapter 4 we will add to this repertoir the new mathematical results named 'Newton's Cradle Spectra'. In it, exact expressions are derived for the eigenvalues and the eigenvectors for the case where we add a single rank one projector to a Hamiltonian whose eigenvalues and eigenvectors we know. The expressions are valid irrespective of the size of the coupling, and therefore Newton's cradle spectra presents a new strategy for understanding the nonperturbative regime. We may spectrally decompose any interaction Hamiltonian into a sum of projectors, and so by adding them one by one, we can understand the behaviour of the eigensystem under the addition of Hamiltonians. This will, as I will describe, give us understanding of level repulsion, it will refine Cauchy's interlacing theorem, and find a number of applications to various fields in physics. Since it is a result in linear algebra it may prove to be useful in engineering, as well, and any discipline that applies linear algebra as one of its mathematical tools.

Superoscillations are a phenomenon in Fourier analysis, first discussed in seminal works in the 1980s and 1990s by [30, 6, 7, 9, 21, 22, 144, 94]. They occur when a bandlimited function locally oscillates faster than its largest Fourier component. They are interesting for various applications, perhaps most notably for superresolution (see, e.g., [82, 148]), the ability to image at a better resolution than would be possible with the smallest wavelength of the light available in the spectrum of the light. Though it was plausible that superoscillatory functions exist, at first it was not clear how to efficiently generate them. One of the problems of early methods was numerical instabilities related to the problem of finding inverses of ill-conditioned matrices [102], though that was later resolved by using a multiplicative method [39] instead. The methods to create superoscillatory functions analytically developed over the decades. In Chapter 6 we will describe a new method to analytically construct superoscillatory functions. The advantage of this method over its predecessors is it allows us to freely choose the shape of the superoscillatory part of the function, which might prove useful, e.g., in imaging. The method is numerically stable (un-

like most prior methods), and the error in the analytic construction is under control, which is achieved by rigorously linking it to the convergence properties to Taylor expansions.

Superoscillations can be understood as a phenomenon of quantum physics, arising from weak measurements. Postselected for some outcomes of the measurement of the momentum operator, a special class of quantum states will exhibit superoscillatory behaviour. More generally, for some quantum observable, analogous superphenomena [91] can arise. The common feature of superphenomena is that they allow certain quantum states to locally extract more from a observable than its highest eigenvalue. Analogously, they allow us to locally extract less than the lowest eigenvalue. This is a valuable aspect of quantum interactions, precisely because it allows us to extract more from a quantum state than we would naively expect. Arguably, it has not been extensively explored, and in Chapter 6 we give a new application of the position observable related super-phenomenon: *quantum prison break*. It is an effect due to the superoscillatory nature of the wavefunction in the momentum space, whereby a quantum object initally limited to a finite support in position, can escape to a predetermined position, conditioned on the postselection of the momentum measurement.

This thesis will present all the above mentioned aspects of quantum interactions in the following order: first, in Chapter 2 we describe the stimulation of the Unruh effect and the acceleration-induced transparency, as new effects in light-matter interactions. They are followed by Chapter 3 where we describe the generalization of acceleration-induced transparency, applicable to any interacting quantum systems, named *parametrically induced decoupling*. This method allows us to modulate the strength of some (or all) transitions induced by the interaction Hamiltonian, by varying the coupling strength or the interaction Hamiltonian in time. We then describe Newton's cradle spectra in Chapter 4, a new mathematical tool for understanding non-perturbative physics. In Chapter 5 we discuss the spread of entanglement between subsystems at the onset of interactions. Finally, in Chapter 6 we describe a new, efficient method to generate superoscillatory functions of a desired shape, the generalizations of superoscillations to super-phenomena, and the new idea, *quantum prison break*.

Chapter 2

Acceleration-Induced Effects in Stimulated Light-Matter Interactions

This chapter will first introduce a simplified model of light-matter interactions, the model of an Unruh-DeWitt detector interacting with a scalar quantum field. This is followed by a review of the conventional, or spontaneous Unruh effect. The two new phenomena follow, stimulated Unruh effect and acceleration-induced transparency, which combined lead to a new way to measure the Unruh effect in the laboratory. Finally, we summarize the work described in the chapter and discuss its outlook.

2.1 Introduction

Gravity and acceleration are locally equivalent, so says the equivalence principle. This means that acceleration-induced quantum effects are closely related to gravity-induced quantum effects. For example, the well-known acceleration-induced Unruh effect [164, 166, 43] is closely related to the Hawking effect [76, 27, 162].

In this work, we demonstrate that there are two new basic quantum effects that are caused by acceleration. These effects bridge the conceptual gap between phenomena well-known in atomic physics — such as a stimulated emission and absorption — and the Unruh effect, while simultaneously generalizing all of them. Schematically, the interaction between two levels of an atom and a quantized field is described by an interaction Hamiltonian of the form $\hat{H}_{\text{int}} \propto (\hat{\sigma}_- + \hat{\sigma}_+)(\hat{a} + \hat{a}^\dagger)$ where $\hat{\sigma}_+ = |e\rangle\langle g|$ raises and $\hat{\sigma}_- = \hat{\sigma}_+^\dagger$ lowers the atomic level, while $\hat{a}^\dagger$ and $\hat{a}$ create and annihilate field quanta respectively. When the atom moves

inertially in free space, and its coupling with the field is weak, energy conservation leads to the condition that the energy of an absorbed or emitted photon matches the atomic energy gap. As a consequence, in the interaction Hamiltonian the so-called counter rotating terms $\hat{\sigma}_-\hat{a} + \hat{\sigma}_+\hat{a}^\dagger$ can be neglected, resulting in the so-called Jaynes-Cummings model [87] of the form, $\hat{H}_{\rm JC} \propto \hat{\sigma}_-\hat{a}^\dagger + \hat{\sigma}_+\hat{a}$, which is paradigmatic in atomic physics and quantum optics [12, 41]. If the atom is accelerated by an external agent (which of course has to invest energy), counter-rotating terms of the form $\hat{\sigma}_+\hat{a}^\dagger$ can contribute and can lead to the excitation of the accelerated atom while emitting a photon. This is the crux of the Unruh effect.

Here, we show, first, that acceleration not only activates the counter-rotating terms (the conventional Unruh effect) but that acceleration can impact the physics of the rotating-wave terms as well. We show that this effect can be made so strong that it leads to the new phenomenon of acceleration-induced transparency. Second, we consider stimulated emission and absorption. Here, we show the new phenomenon that, in the presence of acceleration, it is possible to stimulate not only the rotating wave terms (conventional stimulation [52]) but also the counter-rotating terms. This leads to a new phenomenon that we dub the stimulated Unruh effect. Through the stimulated Unruh effect, the probability for acceleration-induced counter rotating transitions can be vastly enhanced. This is remarkable because, in the absence of acceleration, effects of counter-rotating wave terms are conventionally essentially only accessible in the ultrastrong coupling regime [65].

2.2 Simplified model of the light-matter interaction

The basic mathematical principles underlying the two new phenomena arise as part of all quantum field theories and can be demonstrated already in the simplified model of the light matter interaction outlined above: a two-level atom with states $\{|g\rangle, |e\rangle\}$ separated in the atom's rest frame by an energy gap Ω (in units of $\hbar = 1$) interacts with a massless scalar quantum field $\hat{\varphi}(\mathbf{x}, t)$. The free Hamiltonian reads:

$$\hat{H}_0 = \Omega\hat{\sigma}_z + \tfrac{1}{2} : (\partial_\mu\hat{\varphi})^2 := \Omega\hat{\sigma}_z + \int (dk)\, \omega_{\mathbf{k}}\, \hat{a}^\dagger_{\mathbf{k}}\hat{a}_{\mathbf{k}}$$

Here, $\hat{\sigma}_z = \frac{1}{2}(|e\rangle\langle e| - |g\rangle\langle g|)$, $\omega_{\mathbf{k}} = ck$ is the frequency of the field mode whose annihilation/creation operators are $\hat{a}_{\mathbf{k}}, \hat{a}^\dagger_{\mathbf{k}}$, $(dk) = \mathrm{d}^3k/[(2\pi)^{3/2}\omega_{\mathbf{k}}^{1/2}]$ is the Lorentz invariant integration measure and $: \cdots :$ represents normal order. Note that this simplified model captures the electromagnetic interaction between an atom and a single polarization of the electromagnetic field when the radiation of interest is of a wavelength long compared to the

size of the atom [69, 41, 141, 118]. (Qualitative aspects of the electromagnetic interaction arising from polarization are neglected in this model.)

The interaction between the two systems, modelled after the minimal coupling between a charge distribution and the electromagnetic field, is taken to be [166],

$$\hat{H}_{\rm int} = G\,\hat{\mu}\,\hat{\varphi}\left(\mathbf{x}(\tau), t(\tau)\right), \tag{2.1}$$

where G is the coupling strength, $\hat{\mu} = |e\rangle\langle g| + |g\rangle\langle e|$, and $\hat{\varphi}[\mathbf{x}(\tau), t(\tau)]$ is the field along the detector's trajectory $(t(\tau), \mathbf{x}(\tau))$ in terms of its proper time τ. (The form of the interaction we consider here matches the dipole approximated form of the electromagnetic interaction which is valid as long as the wavelength of all radiation involved is longer than the typical size of the atom [118] — this is true in all that follows.)

We are, in general, interested in the probability that an initial state $|\psi_{\rm i}\rangle$ produces a state $|\psi_{\rm f}\rangle$ via the interaction. Moving to the interaction picture, the interaction Hamiltonian becomes time-dependent, $\hat{H}_{\rm int}(\tau) = G\,\hat{\mu}(\tau)\hat{\varphi}(\mathbf{x}(\tau), t(\tau))$, where,

$$\begin{aligned}\mu(\tau) &= e^{i\Omega\tau}\hat{\sigma}_+ + h.c.\\ \hat{\varphi}(\mathbf{x}, t) &= \int (dk)\,\left(e^{-i\omega_{\mathbf{k}}t + i\mathbf{k}\cdot\mathbf{x}}\hat{a}_{\mathbf{k}} + h.c.\right).\end{aligned}$$

Restricting attention to the weak-coupling regime, the transition amplitude for the process $|\psi_{\rm i}\rangle \to |\psi_{\rm f}\rangle$ is (up to a phase),

$$\mathcal{A}_{\rm i\to f} = \int \langle\psi_{\rm f}|\hat{H}_{\rm int}(\tau)|\psi_{\rm i}\rangle\, d\tau = \int (dk)\,\mathcal{A}_{\rm i\to f}(\mathbf{k}),$$

where,

$$\begin{aligned}\mathcal{A}_{\rm i\to f}(\mathbf{k}) = G\int d\tau\,\langle\psi_{\rm f}|\left(e^{i\Omega\tau}\hat{\sigma}_+ + h.c.\right)\\ \times\left(e^{-i\omega_{\mathbf{k}}t + i\mathbf{k}\cdot\mathbf{x}}\hat{a}_{\mathbf{k}} + h.c.\right)|\psi_{\rm i}\rangle\,,\end{aligned} \tag{2.2}$$

is the amplitude for the transition $|\psi_i\rangle \to |\psi_{\rm f}\rangle$ mediated by a field quantum of momentum $\mathbf{k}$ in proper time τ. Defining the integrals,

$$I_\pm(\Omega, \mathbf{k}) = \int d\tau\, e^{i\Omega\tau \pm ik^\mu x_\mu(\tau)}, \tag{2.3}$$

the transition amplitude can be expressed as:

$$\mathcal{A}_{\rm i\to f}(\mathbf{k}) = G\Big[I_-(\Omega, \mathbf{k})\,\langle\psi_{\rm f}|\,\hat{\sigma}_+\hat{a}_{\mathbf{k}}\,|\psi_{\rm i}\rangle + h.c.\Big]$$

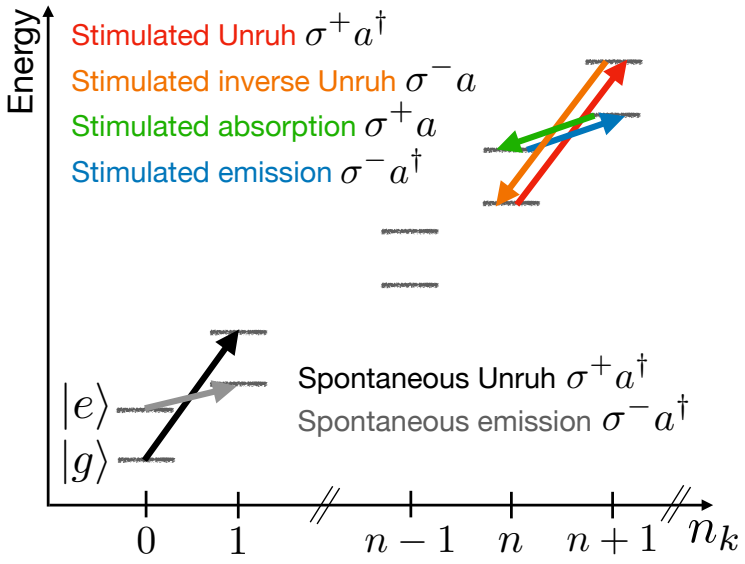

Figure 2.1: Comparison between conventional first order processes in light-matter interaction that happens in inertial motion (gray, green, blue), and those that happen only in the presence of non-inertial motion (black, orange, red). Shown here are the pairs of states $\{|g\rangle \otimes |n_k\rangle\,, |e\rangle \otimes |n_k\rangle\}$ as the field photon number n_k increases, and the transitions between them due to the various processes together with the terms that describe the processes.

$$+ G\left[I_+(\Omega, \mathbf{k}) \langle \psi_{\rm f}| \hat{\sigma}_+ \hat{a}^\dagger_{\mathbf{k}} |\psi_{\rm i}\rangle + h.c.\right].$$

We note that in general both the rotating-wave terms (first line) and counter-rotating-wave terms (second line) contribute, weighted by I_- and I_+ respectively.

2.3 Conventional inertial absorption and emission

Oft-studied phenomena [52] such as spontaneous emission (i.e., $|e, 0\rangle \to |g, 1_{\mathbf{k}}\rangle$), stimulated emission (i.e., $|e, n_{\mathbf{k}}\rangle \to |g, (n+1)_{\mathbf{k}}\rangle$), and absorption (i.e., $|g, (n+1)_{\mathbf{k}}\rangle \to |e, n_{\mathbf{k}}\rangle$) all arise from the rotating-wave terms when the atom is in inertial motion (see Fig. 2.1). (Here, $|n_{\mathbf{k}}\rangle = (n!)^{-1/2} \hat{a}^\dagger_{\mathbf{k}} |0\rangle$ is the Fock state of the field.) Indeed in inertial motion — given by the trajectory $x^\mu(\tau) = (\gamma\tau, \gamma\mathbf{v}\tau)$ where $\gamma = (1 - |\mathbf{v}|^2)^{-1/2}$ —the emission and absorption amplitudes,

$$\begin{aligned} \mathcal{A}_{|e,n\rangle \to |g,n+1\rangle}(\mathbf{k}) &= G\sqrt{n+1} \cdot \delta[\Omega - \gamma(\omega_{\mathbf{k}} - \mathbf{k}\cdot\mathbf{v})] \\ \mathcal{A}_{|g,n+1\rangle \to |e,n\rangle}(\mathbf{k}) &= G\sqrt{n} \cdot \delta[\Omega - \gamma(\omega_{\mathbf{k}} - \mathbf{k}\cdot\mathbf{v})] \end{aligned} \tag{2.4}$$

are non-zero only on resonance, i.e., when the excitation energy of the atom matches the (relativistically Doppler-shifted) energy of the photon. This implies that in inertial motion, emission and absorption processes are strictly due to the rotating-wave terms in the interaction. Here, the δ distribution arises from the integral I_-, which quantifies the contribution of the rotating-wave terms.

For later reference we note that the probabilities for these processes satisfy the Einstein relations,

$$\begin{aligned} \left|\mathcal{A}_{|e,n\rangle\to|g,n+1\rangle}\right|^2 &= (n+1)\times\left|\mathcal{A}_{|e,0\rangle\to|g,1\rangle}\right|^2 \\ \left|\mathcal{A}_{|g,n+1\rangle\to|e,n\rangle}\right|^2 &= n\times\left|\mathcal{A}_{|e,0\rangle\to|g,1\rangle}\right|^2 \end{aligned} \tag{2.5}$$

i.e., stimulated emission and absorption are respectively $(n+1)$ and n times more probable than spontaneous emission.

2.4 The conventional (i.e. spontaneous) Unruh effect

The conventional Unruh effect [164, 162] is the possibility that an atom in its ground state which is accelerating through the field vacuum transitions to an excited state while emitting a photon. Let us denote the atom's trajectory by $x^\mu(\tau)$. The amplitude for the conventional (i.e. spontaneous) Unruh process then reads:

$$\mathcal{A}_{|g,0\rangle\to|e,1\rangle}(\mathbf{k}) = G\int d\tau\, e^{i\Omega\tau+ik^\mu x_\mu(\tau)} = G\, I_+(\Omega,\mathbf{k}). \tag{2.6}$$

For inertial motion, we have that, $I_+ = \delta[\Omega + ck - \mathbf{k}\cdot\mathbf{v}]$, which does not contribute since $c > |\mathbf{v}|$ always; so in inertial motion, the above amplitude is identically zero. For non-inertial trajectories, for example, for uniform acceleration of magnitude a, e.g., $x^\mu(\tau) = (\sinh(a\tau)/a, \cosh(a\tau)/a, 0, 0)$, we have that [166, 162, 19],

$$\left|\mathcal{A}_{|g,0\rangle\to|e,1\rangle}\right|^2 = G^2\frac{2\pi/(\Omega a)}{e^{\Omega/(k_B T_{\rm U})}-1};\quad T_{\rm U} = \frac{a}{2\pi k_B}, \tag{2.7}$$

which is a Bose-Einstein distribution at temperature $T_{\rm U}$. An atom uniformly accelerated through the vacuum perceives an apparently thermal field.

We note a few key aspects. First, I_+ and therefore the probability of the spontaneous Unruh process can be non-zero because acceleration leads to a time-dependent and therefore chirped Doppler shift between the atom and the field modes. Mathematically, this

phenomenon traces to the peculiar Fourier phenomenon of 'concomitant' frequencies [10]: the Fourier transform of chirped positive frequencies necessarily also contains negative frequencies. Here, I_+, see Eq. (2.3), represents negative concomitant frequencies arising in the Fourier transform of the trajectory-dependent function $e^{ik^\mu x_\mu(\tau)}$ which represents a chirp of positive frequencies. As a consequence, even for realistically accelerated trajectories that do not involve eternal uniform acceleration, the Unruh process has a non-zero probability.

Second, the energy required to simultaneously excite the atom and create a photon comes from the accelerating agent; indeed in a more complete treatment, the excitation of the detector is accompanied by a recoil of the atom's center-of-mass degree of freedom [135, 136, 161]. Third, despite it being a robust quantum feature of accelerated bodies [153], the Unruh temperature (restoring constants), $T_U = \hbar a/(2\pi k_B c) \approx 10\,\mathrm{mK}\left(\frac{a}{10^{18}\,\mathrm{m/s^2}}\right)$ is, so far, too small to make its experimental study feasible. (It is worth noting that the term 'Unruh effect' is sometimes reserved for the class of trajectories which possess horizons or for which the accelerated system is driven to a thermal or near-thermal state. We will consider general trajectories and will call any excitation of quantum systems due to non-inertial motion an Unruh effect.)

2.5 Stimulated Unruh effect

Given the central importance of the conventional Unruh process, we now examine whether acceleration induces further phenomena in the light matter interaction and to what extent those may be amenable to experimental observation. Deriving inspiration from the stimulated processes that happen in inertial motion [Eq. (2.4)], we now consider the possibility of stimulating an Unruh-like process. That is, instead of the initial state $|g,0\rangle$, we consider the state $|g,n_{\mathbf{k}}\rangle$. The interaction leads to the transformation:

$$\begin{aligned}|g,n_{\mathbf{k}}\rangle \to G\Big[&I_+\sqrt{n+1}\,|e,(n+1)_{\mathbf{k}}\rangle \\ &+ I_-\sqrt{n}\,|e,(n-1)_{\mathbf{k}}\rangle\Big];\end{aligned} \tag{2.8}$$

Here, the transformed state is unnormalized for brevity. The first term ($\propto I_+$) corresponds to a stimulated Unruh process, which arises from counter-rotating terms in the interaction, is absent in inertial motion, and does not depend on the stimulating photon being resonant with the atom. The second term ($\propto I_-$) corresponds to conventional (resonant) absorption, which is due to rotating wave terms in the interaction, and therefore relies on atom-photon resonance. The stimulated Unruh process stands in the same relation to the conventional

(spontaneous) Unruh process in an accelerating frame, as conventional stimulated emission is to spontaneous emission in an inertial frame. Importantly, the probability of the stimulated Unruh processes is enhanced by a factor of $n+1$ compared to the spontaneous version,

$$\left|\mathcal{A}_{|g,n\rangle\to|e,n+1\rangle}\right|^2 = (n+1)\times\left|\mathcal{A}_{|g,0\rangle\to|e,1\rangle}\right|^2, \tag{2.9}$$

where $\left|\mathcal{A}_{|g,0\rangle\to|e,1\rangle}\right|^2$ is the probability for the spontaneous Unruh process (which is, e.g., for the special case of uniform acceleration, given in Eq. (2.7)). This equation elicits the well known Einstein relation [Eq. (2.5)] for inertial stimulated emission.

The scaling with photon number immediately suggests that the experimental obstruction to observing the spontaneous Unruh effect can be alleviated by stimulation. However two aspects need to be addressed. First, in order to take advantage of the $n-$scaling, realistic experiments would need to use a large mean photon number, whereas large-n Fock states are challenging to prepare. Second, the state transformation in Eq. (2.8) produces an undesirable resonant absorption component in addition to the stimulated Unruh process. (Processes higher order in the interaction Hamiltonian are suppressed, since they roughly scale as some power of the first order process, which, even with stimulation, has a less-than-unity probability in the weak-coupling regime.) In the following we show that both issues can be solved.

First we show that stimulation with the desired scaling can also be achieved with readily available states rather than with Fock states. To see this, we represent general field states in terms of the (over-)complete coherent state basis [160, 68]. The transition amplitude for the stimulated Unruh process where the field is in these basis states is (up to a phase factor),

$$\mathcal{A}_{|g,\alpha\rangle\to|e,\beta\rangle}(\mathbf{k}) = \frac{Ge^{-|\alpha-\beta|^2/2}}{(2\pi)^{3/2}\sqrt{\omega_{\mathbf{k}}}}(\alpha I_- + \beta^* I_+). \tag{2.10}$$

Here $|\alpha\rangle, |\beta\rangle$ are non-orthogonal field coherent states: $|\langle\alpha|\,\beta|^2 = e^{-|\alpha-\beta|^2}$). The probability that the atom gets excited, irrespective of the final field state in mode $\mathbf{k}$, is,

$$\begin{aligned}\mathcal{P}_\alpha(\mathbf{k}) &= \int\frac{d^2\beta}{\pi}\left|\mathcal{A}_{|g,\alpha\rangle\to|g,\beta\rangle}(\mathbf{k})\right|^2 \\ &= \frac{G^2}{(2\pi)^2\omega_{\mathbf{k}}}\left(|\alpha|^2|I_+ + I_-|^2 + |I_+|^2\right).\end{aligned} \tag{2.11}$$

In the special case $\alpha = 0$, i.e., if the initial field state is the vacuum, this expression reduces to $\mathcal{P}_0(\mathbf{k}) \propto |G\,I_+|^2$, i.e., we recover the conventional, i.e., spontaneous Unruh effect for a general trajectory.

For an arbitrary initial field state, $\hat{\rho}_{\rm i} = \int P(\alpha) {\rm d}^2\alpha/\pi$, where $P(\alpha)$ is a generalized probability distribution in the coherent state basis [160, 68], the probability that the atom is excited on an arbitrary trajectory can be shown to be, $\mathcal{P}(\mathbf{k}) = \int P(\alpha)\mathcal{P}_\alpha(\mathbf{k}){\rm d}^2\alpha/\pi$, or explicitly,

$$\mathcal{P}(\mathbf{k}) = \frac{G^2}{(2\pi)^3\omega_{\mathbf{k}}}\left(\langle \hat{a}^\dagger_{\mathbf{k}}\hat{a}_{\mathbf{k}}\rangle |I_+ + I_-|^2 + |I_+|^2\right). \tag{2.12}$$

Here we have used the relation between integrals of P and expectations of normal-ordered operators [68]. The implication is that in general — irrespective of the input field state — the probability of the stimulated Unruh process grows with the average photon number.

We note that the atom can get excited through three different processes [see Eq. (2.12)]: (1) The spontaneous Unruh effect (last term $\propto |I_+|^2$) — which is challenging to observe. (2) The new phenomenon of the stimulated Unruh effect ($\propto \langle \hat{a}^\dagger\hat{a}\rangle |I_+|^2$) — whose probability can be dramatically larger. (3) Conventional (resonant) absorption ($\propto \langle \hat{a}^\dagger\hat{a}\rangle |I_-|^2$). In fact, as Eq. (2.12) shows, stimulation amplifies resonant and non-resonant terms equally: the actual probability is $\propto \langle \hat{a}^\dagger\hat{a}\rangle |I_+ + I_-|^2$. Excitation due to the new stimulated Unruh effect appears, therefore, to be 'contaminated' by conventional resonant absorption.

We will now continue our search for new acceleration induced effects in the light matter interaction. We will thereby find a new effect that happens to provide means to suppress I_- relative to I_+, i.e., that will allow one to remove the contamination of the stimulated Unruh effect by conventional absorption.

Indeed, on one hand, it is clear that it is possible to make I_- smaller than I_+ simply by choosing the stimulating field mode to be far detuned from the atomic resonance. This is because absorption is a resonant process whereas the Unruh process is non-resonant. In this case, assuming a finite linewidth γ for the resonant transition, and a detuning Δ from resonance, the probability of exciting the resonance decreases as [41], $(1 + (\Delta/\gamma)^2)^{-1} \approx (\gamma/\Delta)^{-2}$. On the other hand, we can now demonstrate a new effect that allows not only for an attenuation of conventional absorption but, in principle, for its complete suppression, $I_- = 0$.

2.6 Acceleration-induced transparency

As we now show, acceleration impacts not only the counter rotating but also the rotating wave terms: in fact, by choosing suitably accelerated trajectories, one can, in principle, completely suppress resonant absorption, $I_- = 0$, while also keeping $I_+ \neq 0$. This phenomenon may be called "acceleration-induced transparency". (Acceleration-induced

transparency is unrelated to the so-called electromagnetically-induced transparency [64] which is caused by destructive interference of excitation amplitudes in a three-level atom induced by resonant excitation with coherent field states).

To demonstrate acceleration-induced transparency, let us assume that an atomic gap, Ω, and the stimulating mode's wave vector, $\mathbf{k}$, are chosen. Our task is to show that there are trajectories for which $I_- = 0$ and $I_+ \neq 0$. To this end, we consider for any trajectory $x_\mu(\tau)$ its 'phase function' $\alpha(\tau) = k^\mu x_\mu(\tau)$, so that $I_\pm(\Omega, \mathbf{k}) = \int \mathrm{d}\tau\, e^{i\Omega\tau \pm i\alpha(\tau)}$. The phase functions of physical trajectories obey: $\dot{\alpha}(\tau) > 0 \ \forall\tau$. This is because $\dot{\alpha}(\tau)$ is scalar and, in an instantaneous rest frame, it reads $\dot{\alpha}(\tau) = k^\mu \dot{x}_\mu(\tau) = k^0 \dot{x}_0(\tau) > 0$ since $k_0, \dot{x}_0 > 0$. Conversely, and more importantly, to any phase function $\alpha(\tau)$ obeying $\dot{\alpha}(\tau) > 0 \ \forall\tau$, there exists a corresponding physical trajectory. We prove this by construction: choose a coordinate system such that $k = (k_0, 0, 0, k_0)$; then the trajectory,

$$\dot{x}_\mu(\tau) = \left(\frac{1}{2}\left(\frac{k_0}{\dot{\alpha}(\tau)} + \frac{\dot{\alpha}(\tau)}{k_0}\right), 0, 0, \frac{1}{2}\left(\frac{k_0}{\dot{\alpha}(\tau)} - \frac{\dot{\alpha}(\tau)}{k_0}\right)\right) \tag{2.13}$$

is timelike with τ its proper time (i.e., $\dot{x}^\mu \dot{x}_\mu = 1$). It is straightforward to verify that this trajectory obeys $k^\mu \dot{x}_\mu(\tau) = \dot{\alpha}(\tau)$, i.e., that it produces the desired phase function $\alpha(\tau)$ up to an irrelevant integration constant that translates the trajectory. Notice that the trajectory is inertial if $\dot{\alpha}$ is constant, and accelerating otherwise.

Our remaining task is to find examples of phase functions $\alpha(\tau)$ obeying $\dot{\alpha}(\tau) > 0 \ \forall\tau$ for which $I_- = 0$ and $I_+ \neq 0$. Through Eq. (2.13) we then obtain corresponding trajectories for which the Unruh effect can be arbitrarily strongly stimulated while conventional absorption vanishes. To this end, consider a phase function satisfying,

$$\dot{\alpha}(\tau) := k^0 \begin{cases} s_0 & \tau < 0 \\ s_0 + \frac{s_1 - s_0}{T_1}\tau & \tau \in [0, T_1) \\ s_1 + \frac{s_2 - s_1}{T_2 - T_1}(\tau - T_1) & \tau \in [T_1, T_2) \\ s_2 & \tau \geq T_2, \end{cases} \tag{2.14}$$

where the constants $\{s_i, T_i\}$ can be chosen arbitrarily except that we require $\dot{\alpha} > 0$ and $0 < T_1 < T_2$.

The corresponding trajectories are relatively simple. They are initially inertial, then possess two phases of acceleration, followed by inertial motion. In the non-relativistic regime, the trajectories further simplify, since then the accelerations are uniform.

The question is whether among these trajectories there are ones which exhibit acceleration-induced transparency for some arbitrarily fixed gap Ω. To produce explicit examples, we

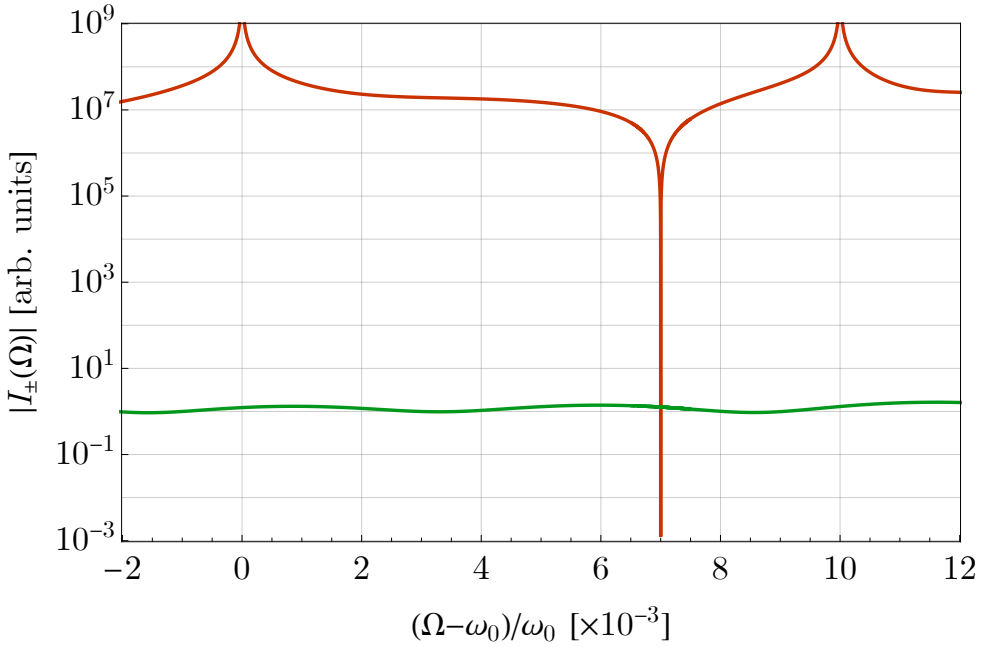

Figure 2.2: The two curves display $|I_\pm(\Omega)|$ for an example of a trajectory of the form given in Eq. (2.14). The red curve is the resonant contribution $|I_-|$ which shows the strength of conventional absorption while the green curve is the non-resonant contribution $|I_+|$ which shows the strength of Unruh-type counter-rotating effects. Importantly, we see that the resonant contribution dips below that of the latter (here $|I_-/I_+| \approx 10^{-3}$), so that at that frequency, the probability of resonant absorption is $\sim 10^{-6}$ of the stimulated Unruh process. The frequency at which the resonant contribution dips is designed to be the detector gap frequency. The two peaks in I_- correspond to absorption at the Doppler shifted frequencies $\omega_0 = k^0 s_0$, $\omega_2 = k^0 s_2$ that are due to the initial and final inertial velocities of the trajectory.

held the parameters s_0, s_2 and T_1 fixed and varied the parameters s_1 and T_2. In the (s_1, T_2)-plane, we plotted the curves for which $\mathrm{Re}\,[I_-] = 0$ or $\mathrm{Im}\,[I_-] = 0$. These curves intersect (see Appendix 8), which shows that there are parameter values for which the corresponding trajectory possesses acceleration-induced transparency at the chosen gap Ω. This means that it is possible, in principle, to make the stimulated Unruh process dominate arbitrarily strongly over all conventional, i.e., resonant processes, at this order in perturbation theory and for a given gap Ω.

In Fig. 2.2, we plot $|I_\pm(\Omega)|$ for such a trajectory. The plot shows that the resonant effects described by I_- tend to dominate over the non-resonant effects described by I_+, except

for the arbitrarily strong acceleration-induced suppression of I_- at the chosen value of Ω. Notice that this plot in effect also shows the k_0 dependence. Mathematically, we have here shown a phenomenon of Fourier theory (related to that of concomitant frequencies, [10]): by suitably chirping positive frequencies, a single positive frequency can always be suppressed in the overall Fourier spectrum. Physically, this means that the amplitude for resonant absorption, being a coherent superposition of contributions from all parts of the trajectory, can be made to vanish for suitable trajectories. The corresponding trajectories can be experimentally realized, for example, by accelerating a charged UDW detector using external electromagnetic fields (see also the Appendix 8).

In addition to the effects considered above where the accelerating atom starts in the ground state, it is possible to consider the case where the atom starts in the excited state. Variants of the stimulated Unruh effect can then be considered with this initial condition for the atom's internal state. Such processes are time-reversed versions of the ones already studied above. The amplitudes for such processes are obtained by replacing $I_\pm \to I_\mp^*$ in the equations above.

2.7 Summary

We have shown that, beyond the Unruh effect and the dynamical Casimir effect, there are two new phenomena by which acceleration impacts the light matter interaction: On one hand, we showed that acceleration not only activates the counter rotating terms (the Unruh effect) but that it also impacts the rotating wave terms, leading to the new phenomenon of acceleration-induced transparency. On the other hand, we also showed that, in the presence of acceleration, stimulation can be used not only on the rotating wave terms (conventional stimulation) but also on the counter-rotating terms, leading to the new phenomenon of a stimulated Unruh-like effect.

Further, we showed that by using suitably designed trajectories and by simultaneously stimulating, these two new phenomena can be combined to highly enhance acceleration-induced counter rotating transitions while simultaneously arbitrarily strongly suppressing the conventional rotating wave effects. While the Unruh effect is as yet unobservable, the new findings could bring acceleration-induced activations of the counter-rotating terms into the range of observability, even in the weak-coupling regime.

For example, the stimulated Unruh effect can be detected via the recoil of the emitted/absorbed photon on an accelerated low-mass two-level system [161]. A single electron, whose spin state degeneracy is lifted by a magnetic field, and whose motion can be

continuously monitored is such a transducer. Although accelerations of $\sim 10^{20}\,\mathrm{m/s^2}$ are possible for a trapped electron, corresponding to an Unruh temperature $T_{\mathrm{U}} \sim 1\,\mathrm{K}$, the challenge so far has been the exceedingly small rate of the spontaneous Unruh process [18] $\Gamma_0 \approx 10^{-18}/\mathrm{s}$. We have shown that, in a scalar model of the electromagnetic interaction, the rate scales to [Eq. (2.9)] $\Gamma_n = (n+1)\Gamma_0$ when stimulated with n photons on average. Thus, the accelerated motion of a single electron trapped in a Penning trap (a combination of a static axial magnetic field and a quadrupolar electric field) [120], which is co-located inside a microwave cavity loaded with photons can serve as a potential experimental platform for detecting the stimulated Unruh effect. Indeed, state-of-the-art microwave cavities resonating at $\omega \sim 2\pi \times 1\,\mathrm{GHz}$ with modest quality factors [134, 146] of $Q \sim 10^5$ can store on average $n = (4Q/\omega)(P/\hbar\omega) \approx 10^{15}(P/1\,\mathrm{mW})$ photons. That is, the stimulated counter-rotating processes that we have described here can be made 15 orders of magnitude more likely than the spontaneous Unruh process, and therefore resolvable in a few hours of observation.

2.8 Outlook

We can explore extending these results to more general contexts. In Chapter 8 we have given details on how to prove the existence of a trajectory giving rise to acceleration induced transparency. In the Fig. 8.1 one can see the parameter space of trajectories we searched for, where the crossings of blue and red lines give instances of desired parameters. In this figure, one can see that there is more than one crossing, though we later used only one in our numerical optimizations. For convenience, we limited the parameter space to only two parameters, and found indications of existence of multiple solutions in finite intervals. We may then ask what would happen if we increased the parameter space to a higher-dimensional one. We conjecture that we would find the real and imaginary zero point surfaces crossing, not only in points, but generically, also in higher dimensional codimension-2 surfaces, in analogy to our example where points were codimension-2 'surfaces' of solutions in 2 dimensions. In other words, we conjecture that the trajectories giving rise to acceleration-induced transparency are not rare.

This conjecture is relevant for two reasons. One is that we may want to have acceleration-induced transparency for more than one wavenumber (wavevector) of light. In the example where we've proven its existence, we fixed a value k for the mode of the quantum field. We might be interested in suppressing other transitions as well, for example, when the Unruh-DeWitt detector is an N-dimensional quantum system, as opposed to the simplest 2-dimensional, as we used in the work above. In that case, there would be transitions

between any two energy levels of the detector, every transition generically having a different energy split. If we want to suppress more than one of those transitions, we would need to produce trajectories giving rise to acceleration-induced transparency for each of those transitions.

The second reason the conjecture on ubiquity of acceleration-induced transparency could prove important is extending the applicability of this phenomenon beyond weak coupling. We've assumed, all throughout this chapter, that the coupling constant G is small, therefore we worked in first order perturbation theory. We may use the Unruh-DeWitt model of quantum system coupled to a quantum field in a different context where the model is still useful, however the coupling G is no longer small. If we still want to suppress the resonant transitions, while keeping the non-resonant, we have to find trajectories preserving acceleration-induced transparency beyond the first order of perturbation. We conjecture that this is also possible.

If this conjecture is proven to be right, we would find a new way to control the interactions of N-dimensional quantum systems interacting with a quantum field. On one hand, the resonant transitions would be suppressed, meaning we would have control over the spurious decoherence arising from the presence of field excitations. At the same time, the non-resonant transitions would still be present, though small. Using their stimulation (stimulation of the Unruh effect interaction terms), we may turn them on at will.

Gravity and acceleration are related via the equivalence principle. The two new phenomena, stimulated Unruh effect and acceleration-induced transparency, suggest the existence of their gravity-induced analogs. Work in this direction is in progress, on the phenomena of gravity-induced translucency or transparency and the stimulation of Hawking radiation.

Finally, in the next chapter we will see that the new phenomenon of acceleration-induced transparency can be generalized to arbitrary quantum systems.

Chapter 3

Parametrically Induced Decoupling

3.1 Introduction

In this chapter, I will introduce[1] a generalization of the phenomenon of acceleration-induced transparency, described in Chapter 2. Acceleration-induced transparency can then be understood as a special case of a more general phenomenon, which will be called *parametrically induced decoupling*. We will show how, analogously to acceleration-induced transparency, we can modulate the strengths of transitions arising from the interaction Hamiltonian. The strength modulations, and even decoupling, arise due to a suitable choice of time variation of a parameter in the interaction Hamiltonian.

Let us consider the typical situation of two interacting quantum systems, named A and B. The total free Hamiltonian H_0 acts on the tensor product of their respective Hilbert spaces, $H_0 : \mathcal{H}_A \otimes \mathcal{H}_B \to \mathcal{H}_A \otimes \mathcal{H}_B$. We can in general write the free Hamiltonian as follows:

$$H_0 = H_A \otimes \mathbb{1} + \mathbb{1} \otimes H_B, \tag{3.1}$$

where the Hamiltonians $H_A : \mathcal{H}_A \to \mathcal{H}_A$ and $H_B : \mathcal{H}_B \to \mathcal{H}_B$ act on the respective Hilbert spaces of A and B.

We will add an interaction Hamiltonian H_{int}, which is a rank-one projector onto a vector $|v(t)\rangle \in \mathcal{H}_A \otimes \mathcal{H}_B$, with a coupling constant $\mu(t) \in \mathbb{R}$:

$$H_{\text{int}} = \mu(t) |v(t)\rangle \langle v(t)| . \tag{3.2}$$

[1] This work has not yet been published.

The reason the interaction Hamiltonian which is a rank-one projector is the effect we will later described is visible already with this simple choice. To easily draw the parallel to acceleration-induced transparency, we will do the computations in the interaction picture of quantum mechanics. Therefore, we will have to evolve the interaction Hamiltonian in time, using the free Hamiltonian Hamiltonian, while the states evolve according to the interaction Hamiltonian.

According to the interaction picture, the time evolution of H_{int} is the following:

$$H_{\text{int}}(t) = e^{iH_0 t} H_{\text{int}} e^{-iH_0 t}. \tag{3.3}$$

We find that, due to the interaction Hamiltonian being a rank-one projector, the expressions simplify. In particular, we can make use of the assumption that the eigenvalues and the eigenvectors of the free Hamiltonian are known, as is typically the case:

$$H_0 = \sum_{j=1}^{N_A N_B} s_j \left|s_j\right\rangle \left\langle s_j\right|. \tag{3.4}$$

Therefore, we have:

$$H_{\text{int}}(t) = e^{iH_0 t} \mu(t) \left|v(t)\right\rangle \left\langle v(t)\right| e^{-iH_0 t}, \tag{3.5}$$

$$H_{\text{int}}(t) = \mu(t) \left[\sum_j e^{is_j t} \langle s_j | v(t)\rangle \left|s_j\right\rangle\right] . \left[\sum_k e^{-is_k t} \langle v(t) | s_k\rangle \left\langle s_k\right|\right], \tag{3.6}$$

$$H_{\text{int}}(t) = \mu(t) \sum_{j,k} e^{i(s_j - s_k)t} \langle s_j | v(t)\rangle \langle v(t) | s_k\rangle \left|s_j\right\rangle \left\langle s_k\right|. \tag{3.7}$$

Finally, the expression we will use is the following:

$$H_{\text{int}}(t) = \mu(t) \sum_{j,k} e^{i(s_j - s_k)t} v_j(t) v_k^*(t) \left|s_j\right\rangle \left\langle s_k\right|, \tag{3.8}$$

where $v_n(t)$ are the components of $\left|v(t)\right\rangle$, as $v_n(t) = \langle s_n | v(t)\rangle$, $n \in \{1, ..., N_A N_B\}$.

Assuming that the coupling constant μ is small, we can expand the time evolution unitary operator into a Taylor series and keep only the linear approximation in μ:

$$U_I(t) = e^{i\int_{t_0}^{t} d\tau H_{\text{int}}(\tau)} \approx \mathbb{1} + i\int_{t_0}^{t} d\tau H_{\text{int}}(\tau) + ..., \tag{3.9}$$

$$U_I(t) \approx \mathbb{1} + i\int_{t_0}^{t} d\tau \mu(\tau) \sum_{j,k} e^{i(s_j - s_k)\tau} v_j(\tau) v_k^*(\tau) |s_j\rangle \langle s_k| . \tag{3.10}$$

Let us take as the initial state the ground state of the free Hamiltonian H_0:

$$|\Psi_0\rangle = |s_0\rangle . \tag{3.11}$$

Then, we evolve it with the first order approximation to the time evolution operator $U_I(t)$, and find the probability $p_{\text{exc.}}$ of the excitation to the first excited state $|s_1\rangle$:

$$p_{\text{exc.}} = |\langle s_1|U_I(t)|s_0\rangle|^2, \tag{3.12}$$

$$p_{\text{exc.}} = \left|\int_{t_0}^{t} d\tau \mu(\tau) e^{i(s_1 - s_0)\tau} v_1(\tau) v_0^*(\tau)\right|^2 . \tag{3.13}$$

In the case where the interacton Hamiltonian is not simply a rank-one projector, but a sum of rank-one projectors $H_{\text{int}} = \sum_i \mu_i(t) |v_i(t)\rangle \langle v_i(t)|$, the expression for $p_{\text{exc.}}$ is straightforwardly modifed, due to the calculation being done in first order perturbation theory in μ_i's:

$$p_{\text{exc.}} = \left|\int_{t_0}^{t} d\tau e^{i(s_1 - s_0)\tau} \sum_i \mu_i(\tau) v_{i,1}(\tau) v_{i,0}^*(\tau)\right|^2 . \tag{3.14}$$

Here, $v_{i,j}(t)$ for $j \in \{0, 1\}$, are the components of $|v_i(t)\rangle$, e.g., $v_{i,0}(t) = \langle s_0|v_i(t)\rangle$.

We may now compare the expression in Eq. (3.14) to the total excitation probability of an Unruh-DeWitt detector, for a fixed wavevector $\vec{k}$ of a field excitation. As introduced in Chapter 2:

$$p_{\text{exc.}}(k) = G^2 \left| \int d\tau\, e^{i\Omega\tau + ik^\mu x_\mu(\tau)} + \int d\tau\, e^{i\Omega\tau - ik^\mu x_\mu(\tau)} \right|^2 \tag{3.15}$$

Recall that G is the coupling constant, Ω the energy of the excited state, and x_μ the trajectory of the detector. In this expression, $e^{i\Omega\tau}$ part of the integrand is analogous to $e^{i(s_1-s_0)\tau}$ in Eq. (3.14). Both are phases arising from the energy split between the ground and the excited state. Furthermore, both expressions feature additional time dependence inside the time integrals. In the light-matter interactions, it is the phase function $e^{\pm ik^\mu x_\mu(\tau)}$ induced by the detector's trajectory, while for the general description in Eq. (3.14), $\mu_i(t)$, $v_{i,1}(t)$, $v_{i,0}(t)$ all may be time dependent functions.

In the discussion on acceleration-induced transparency, in Section 2.6, we showed that we may turn off resonant transitions in the UDW model of light-matter interactions, by choosing a suitable trajectory. Mathematically, this translates to the vanishing time integral:

$$\mathcal{I}_- = \int d\tau e^{i\Omega\tau - ik^\mu x_\mu(\tau)} = 0, \tag{3.16}$$

for the suitable choice of trajectory $x_\mu(\tau)$.

In the following sections, we will demonstrate that this is a more general interaction phenomenon, which can occur when the interaction Hamiltonian has some parametric time dependence. Since the analogue of the acceleration (trajectory)-induced time dependence in $e^{\pm ik^\mu x_\mu(\tau)}$ is the parametric time dependence of the coupling constants' $\mu_i(t)$ and the vectors' $|v_i(t)\rangle$, we will call the phenomenon *parametrically-induced decoupling*. Mathematically, it arises from one or more of the time integrals in Eq. (3.14) vanishing:

$$\mathcal{I}_a = \int_{t_0}^{t} d\tau e^{i(s_1-s_0)\tau} \mu_a(\tau) v_{a,1}(\tau) v^*_{a,0}(\tau) = 0, \tag{3.17}$$

for some $a \in \{1, 2, ..., N_A N_B\}$.

Note that the problem of suppressing the probability $p_{\text{exc.}}$ is ultimately about the vanishing of an integral over the product of functions (see Eq. (3.14)). It may be seen as an orthogonality condition in the Hilbert space of functions. In the case of acceleration-induced transparency, finding the orthogonal function was nontrivial, due to the constraint that the trajectory-dependent function $e^{ik^\mu x_\mu(\tau)}$ is always of modulus one. The function space spanned by such transparency-inducing functions has not been widely explored, only its existence was proved. In this chapter, we used the solution whose existence was proved. It would be interesting to find solutions which go beyond the modulus one constraint, and to explore and understand the space of solutions more deeply.

3.2 Time-varying coupling constant

We will first focus on the simple case of rank-one projector as the interaction Hamiltonian. Then, the excitation probability from the ground to the excited state is:

$$p_{\text{exc.}} = \left| \int_{t_0}^{t} d\tau \mu(\tau) e^{i(s_1 - s_0)\tau} v_1(\tau) v_0^*(\tau) \right|^2. \tag{3.18}$$

In this section, we will fix the projector $|v\rangle\langle v|$. Therefore, it will not depend on time, $v_i(t) = v_i = \text{const.}$, for $i = 0, 1$, while the coupling constant will, $\mu = \mu(t)$.

Say that the experiment runs for a long time, where we may set the boundaries of the time integral to be $t_0 = -\infty$, $t = +\infty$. Then, only a specific sinusoidal dependence on time, with $\omega = s_1 - s_0$, will yield a non-zero excitation probability:

$$\mu(t) = \mu_0 \cos(\omega t + \varphi), \tag{3.19}$$

where $\mu_0 \in \mathbb{R}$ is a constant. This is reminiscent of the resonance phenomenon in light-matter interactions. For frequencies $\omega \neq s_1 - s_0$, the probability $p_{\text{exc.}}$ integrates to zero.

Generically, for $\mu(t)$ some function of time $\mu(t) = f(t)$, the probability is non-zero. However, in chapter Chapter 2 we proved that there are some functions $f(t) \in \mathbb{C}$ for which $p_{\text{exc.}} = 0$. This is because we can choose it to be the function:

$$f(t) = e^{ik^\mu x_\mu(t)}, \tag{3.20}$$

where $x_\mu(t)$ is a trajectory that gives rise to acceleration-induced transparency. In the case where we have only one projector as the interaction Hamiltonian, we can not use the time-varying coupling constant $\mu(t) \in \mathbb{R}$ to induce decoupling. This is due to, as we learned from Chapter 2, $f(t)$ crucially having both real and imaginary parts, in order to cancel the absolute value of the time integral and induce the transparency:

$$p_{\text{exc.}} = \left| \int_{t_0}^{t} d\tau e^{ik^\mu x_\mu(t)} e^{i(s_1 - s_0)\tau} \right|^2 = 0. \tag{3.21}$$

Instead, we will add one more projector to obtain the sum of $|v^{(1)}\rangle\langle v^{(1)}|$ and $|v^{(2)}\rangle\langle v^{(2)}|$ as the interaction Hamiltonian, each with its coupling constant, $\mu_1(t)$ and $\mu_2(t)$. Then the excitation probability changes to (see Eq. (3.14)):

$$p_{\text{exc.}} = \left| \int_{t_0}^{t} d\tau \mu_1(\tau)\, e^{i(s_1-s_0)\tau} v_1^{(1)} v_0^{(1)*} + e^{i(s_1-s_0)\tau} \mu_2(\tau)\, v_1^{(2)} v_0^{(2)*} \right|^2 . \tag{3.22}$$

If we choose $\mu_1(t)$ and $\mu_2(t)$, and the vectors $|v^{(1)}\rangle$ and $|v^{(2)}\rangle$, in the following way:

$$\mu_1(t) = \frac{\text{Re}\left[e^{ik^\mu x_\mu(t)}\right]}{\left| v_1^{(1)} v_0^{(1)*} \right|}, \tag{3.23}$$

$$\mu_2(t) = \frac{\text{Im}\left[e^{ik^\mu x_\mu(t)}\right]}{\left| v_1^{(2)} v_0^{(2)*} \right|}, \tag{3.24}$$

with

$$\frac{v_1^{(2)} v_0^{(2)*}}{\left| v_1^{(2)} v_0^{(2)*} \right|} = i\, \frac{v_1^{(1)} v_0^{(1)*}}{\left| v_1^{(1)} v_0^{(1)*} \right|}, \tag{3.25}$$

in the expression for $p_{\text{exc.}}$ we get precisely the accleration-induced transparency integral in Eq. (3.21), assuming the integral limit $t = +\infty$, $t_0 = -\infty$. Therefore, with these choice for the time dependences of $\mu_1(t)$ and $\mu_2(t)$, and the constant phase ratio of the projector components in Eq. (3.25), we get that the transition probability is equal to zero:

$$p_{\text{exc.}} = \left| \int_{-\infty}^{+\infty} d\tau \mu_1(\tau)\, e^{i(s_1-s_0)\tau} v_1^{(1)} \left(v_0^{(1)}\right)^* + e^{i(s_1-s_0)\tau} \mu_2(\tau)\, v_1^{(2)} \left(v_0^{(2)}\right)^* \right|^2 = 0. \tag{3.26}$$

We showed the example of adding a pair of rank-one projectors, with carefully chosen time dependences. Generically, if we had a sum of m such pairs of projectors, in total $2m$ projectors, with analogously chosen parameters to Eq. (3.23) and Eq. (3.25):

$$H_{\text{int}} = \sum_{i=1}^{m} \mu_{1,i}(t) \left|v_{1,i}\right\rangle \left\langle v_{1,i}\right| + \mu_{2,i}(t) \left|v_{2,i}\right\rangle \left\langle v_{2,i}\right|, \tag{3.27}$$

all of the transitions would be suppressed as well. This is because for each pair of projectors individually, the respective time integral exactly equal to zero, so all of them sum up to zero in the expression for total probability $p_{\text{exc.}}$ (see Eq. (3.14)).

We call this parametrically-induced decoupling, since choosing the suitable time dependences of the coupling constants leads to the suppression of transitions induced by the interaction Hamiltonian.

3.3 Time-varying projector

In this section, we will describe parametrically induced decoupling using a time-varying rank-one projector. We assume that the coupling constant is true to its name, $\mu(t) = \mu =$ const., while the projector varies:

$$H_{\text{int}} = \mu \left|v\left(t\right)\right\rangle \left\langle v\left(t\right)\right| . \tag{3.28}$$

Let us assume that the time-dependence of a component $v_i\left(t\right)$ of $\left|v\left(t\right)\right\rangle$ is as follows:

$$v_i\left(t\right) = \sum_k \langle s_i|h_k\rangle\langle h_k|v\left(t_0\right)\rangle e^{ih_k(t-t_0)}. \tag{3.29}$$

Here, note that the only time dependence is in the phase function $e^{ih_k(t-t_0)}$, while $\langle s_i|h_k\rangle$, $\langle h_k|v\left(t_0\right)\rangle$ are fixed complex numbers.

Now, we take Eq. (3.29) and insert it into the expression in Eq. (3.18) for excitation probability for the system to go from the ground to the excited state:

$$p_{\text{exc.}} = \left| \int_{t_0}^{t} d\tau\mu \; e^{i(s_1-s_0)\tau} \sum_{j,k} e^{i(h_j-h_k)\tau} \langle s_1|h_j\rangle\langle h_j|v\left(t_0\right)\rangle\langle s_0|h_k\rangle\langle h_k|v\left(t_0\right)\rangle^* \right|^2 . \tag{3.30}$$

Here, the time dependence is found only sum over phase functions $e^{i(s_1-s_0)\tau}e^{i(h_j-h_k)\tau}$. If we take, as before the limits of the integral to be $t_0 = -\infty$, $t = +\infty$, generically these time integrals will be equal to zero, unless for some indices j, k, $h_j - h_k = s_1 - s_0$. If such a condition is satisfied, it is once again reminiscent of the resonance phenomenon.

However, a more interesting case is when the time dependence of interaction Hamiltonian's components $v_i\left(t\right)$ is not the simple one in Eq. (3.29). Assume this time that the time dependence of a more general form:

$$v_i\left(t\right) = e^{if_i(t)}v_i^{(0)}, \tag{3.31}$$

where $f_i(t) \in \mathbb{R}$ are some functions of time. Now, the norm of $|v(t)\rangle$ is still 1, if we assume that $\sum_i \left|v_i^{(0)}\right|^2 = 1$, since $\left|e^{if_i(t)}\right|^2 = 1$, for real functions $f_i(t)$.

Again, we can argue that there will be a transition which is suppressed:

$$p_{\text{exc.}} = \left| \int_{t_0}^{t} d\tau\mu \; e^{i(s_1-s_0)\tau} v_1 v_0^* \right|^2 \tag{3.32}$$

$$= \left| \int_{t_0}^{t} d\tau\mu \; e^{i(s_1-s_0)\tau} e^{if_1(t)-if_0(t)} v_1^{(0)} \left(v_0^{(0)}\right)^* \right|^2, \tag{3.33}$$

if we can produce $f_1(t)$ and $f_0(t)$ such that:

$$e^{if_1(t)-if_0(t)} = e^{ik^\mu x_\mu(t)}, \tag{3.34}$$

for $k^\mu x_\mu$ that result in acceleration-induced transparency, for an energy gap $\Omega = s_1 - s_0$.

The question of how to create the time dependences of the interaction Hamiltonian that give rise to the desired functions $f_1(t)$ and $f_0(t)$, or the one in Eq. (3.29) in the laboratory is of interest for applications. Note that throughout this chapter, we simply assumed that we can prescribe the time dependence of the interaction Hamiltonian, and showed that the ones which give rise to parametrically induced coupling exist. We leave the study of how to create the desired time dependence for specific applications to future work.

3.4 Summary and Outlook

In this chapter we described the generalization of the idea of acceleration-induced transparency. The parametrically-induced decoupling was described as a phenomenon arising from carefully chosen time dependence of either the coupling constants of the interaction Hamiltonian, or the time dependence of the interaction Hamiltonian itself. It was shown that some choices of time dependences lead to suppression of transitions which would otherwise be present, if the coupling constants and the interaction Hamiltonian were constant in time. Though this work is preliminary, it shows a path towards new ways of controlling transitions between different states of a quantum system, and may be interesting in various applications, such as in quantum control, or in quantum computing, where it could prove useful as a tool to suppress decoherence. Especially, since it is a tool to prevent transitions,

it may prove to be useful in adiabatic quantum computing as a method for preventing the system from jumping to an excited state. Usually this is achieved by slowing down the computation in order to remain in the adiabatic regime. We may be able to speed up adiabatic quantum computation simply by choosing the suitable time dependence of some parameters, and it should also be interesting to its applicability in Quantum Approximate Optimization Algorithms [57, 174].

Chapter 4

Newton's Cradle Spectra

4.1 Introduction

The behavior of eigenvalues and eigenvectors plays important roles throughout science and engineering [159, 47, 133]. Of particular interest is, for example, their behavior under the addition of Hermitian operators, such as Hamiltonians, and under the multiplication of unitaries, such as time evolution operators. In the literature, this problem is often investigated perturbatively. Nonperturbative results, such as level repulsion [130, 81, 40] and Cauchy interlacing [35, 48], are particularly valuable but few in number [51]. Here, we present new broadly applicable nonperturbative results on the behavior of the spectra and eigenvectors of Hermitian and unitary operators in finite dimensions.

4.2 The Behaviour of the Eigensystem Under Addition of a Rank One Projector

4.2.1 Addition of Hermitian operators

Let us consider an arbitrary Hermitian operator S with nondegenerate spectrum, acting on an N-dimensional Hilbert space $\mathcal{H}$. We ask how the eigenvalues change when adding to S an arbitrary Hermitian operator R. To this end, by the spectral theorem, we write R as a weighted sum of rank 1 projectors: $R = \sum_{j=1}^{N} \mu^{(j)} |v^{(j)}\rangle\langle v^{(j)}|$. Since the sum $S + R$ can

be obtained by successively adding these weighted projectors to S, we can focus on how the spectrum of S changes under the addition of a single weighted projector:

$$S(\mu) := S + \mu|v\rangle\langle v| \tag{4.1}$$

Here, $|v\rangle$ is an arbitrary fixed normalized vector and we let the weight μ range from $-\infty$ to $+\infty$. We denote the eigenvalues and eigenvectors of S by $\{s_n\}, \{|s_n\rangle\}$ with the ordering $s_1 < s_2 < \ldots < s_N$. We denote the eigenvalues and eigenvectors of $S(\mu)$ by $\{s_n(\mu)\}, \{|s_n(\mu)\rangle\}$ and we have $s_n(0) = s_n, |s_n(0)\rangle = |s_n\rangle$. The ordering of the $s_n(\mu)$ is inherited from the ordering of the s_n, taking into account possible level crossings. The phases of the $|s_n(\mu)\rangle$ are left arbitrary for now.

First, the trivial special cases. If $|v\rangle$ is chosen so that $\langle s_m|v\rangle = 0$ for some m, then the eigenspaces of S spanned by the $|s_m\rangle$ remain unaffected, i.e., their eigenvalues and eigenvectors do not change with μ: $s_m(\mu) = s_m, |s_m(\mu)\rangle = |s_m\rangle \ \forall \mu \in \mathbb{R}$. If we choose $|v\rangle$ to be an eigenvector, $|v\rangle := |s_r\rangle$, then $\langle s_m|v\rangle = 0 \ \ \forall m \neq r$ and all eigenvectors and eigenvalues are frozen except that $s_r(\mu) = s_r + \mu, |s_r(\mu)\rangle = |s_r\rangle \ \forall \mu \in \mathbb{R}$.

4.2.2 Newton's cradle for Hermitian operators

We now consider the generic case in which $|v\rangle$ is not orthogonal to any eigenvectors of S. For this case, we can show that, as μ runs from $-\infty$ to $+\infty$, all $s_n(\mu)$ strictly monotonously move to the right, akin to Newton's cradle: s_1 arrives from $-\infty$, the eigenvalues s_2 to s_{N-1} each move a small distance to the right to take the next eigenvalue's place and finally s_N escapes to $+\infty$. As illustrated in Fig. 2.1, interlaced between the eigenvalues s_n, there exist numbers s_n^* obeying $s_n < s_n^* < s_{n+1}$ for $n = 1, \ldots, (N-1)$ so that, as we let μ run from $-\infty$ to $+\infty$, each eigenvalue $s_n(\mu)$ runs from s_{n-1}^* to s_n^*, passing through s_n when $\mu = 0$. Here, $s_0^* := -\infty$ and $s_N^* := +\infty$.

4.2.3 Exact evolution of Hermitian Newton's cradles

Due to the Newton cradle behavior of the eigenvalues, the full set of eigenvalues $\{s_n(\mu)\}$ for all $n = 1 \ldots N$ and all $\mu \in \mathbb{R} \cup \{+\infty\}$ cover the real line exactly once. For any $s \in \mathbb{R}$, there therefore exists a unique pair (n, μ) such that $|s\rangle := |s_n(\mu)\rangle$ obeys $S(\mu)|s\rangle = s|s\rangle$. Defining $v_n := \langle s_n|v\rangle$, we can show that for any $s \in \mathbb{R}$, the corresponding μ reads:

$$\mu(s) = \left(\sum_{n=1}^{N} \frac{|v_n|^2}{s - s_n} \right)^{-1} \tag{4.2}$$

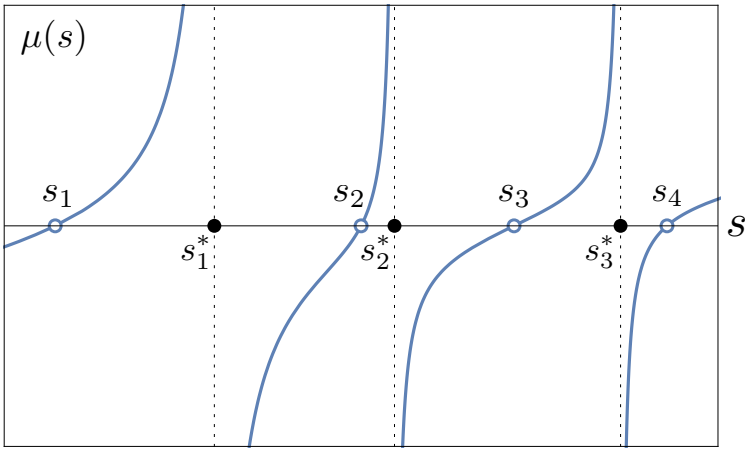

Figure 4.1: Plot of $\mu(s)$ using Eq. (4.2) for a random choice of Newton cradle of four eigenvalues. From bottom to top, the four curves show the evolution of the four eigenvalues $\{s_n(\mu)\}_{n=1}^4$ with increasing μ. For $\mu = 0$, the eigenvalues are s_1, s_2, s_3, s_4. As $\mu \to +\infty$, the eigenvalues tend to s_1^*, s_2^*, s_3^* and $s_4^* = +\infty$ respectively.

Eq. (4.2) can also be viewed as reexpressing the characteristic equation for $S(\mu)$. Eq. (4.2) implies that the values s_n^* for $n = 1 \dots (N-1)$ are the solutions to:

$$\sum_{m=1}^{N} \frac{|v_m|^2}{s_n^* - s_m} = 0 \tag{4.3}$$

Differentiating Eq. (4.2) yields:

$$\frac{d\mu(s)}{ds} = \left(\sum_{m=1}^{N} \frac{|v_m|^2}{s - s_m} \right)^{-2} \sum_{r=1}^{N} \frac{|v_r|^2}{(s - s_r)^2} \tag{4.4}$$

The inverse, $ds/d\mu$, is the velocity of the eigenvalues, s, with respect to μ. The special case of the velocity $ds_n(\mu)/d\mu$ of an eigenvalue $s_n(\mu)$ at $\mu = 0$ reads:

$$\left. \frac{\mathrm{d}s_n(\mu)}{\mathrm{d}\mu} \right|_{\mu=0} = |v_n|^2 \tag{4.5}$$

These velocities are positive and stay positive for all finite μ. This is because if a velocity $ds_n/d\mu$ vanished for a finite μ, we would have $\langle s_n(\mu)|v\rangle = 0$, hence this eigenvalue would be frozen for all μ, in contradiction to the assumption that $\langle s_n|v\rangle \neq 0$. Further, since

$\sum_{m=1}^{N} |v_m|^2 = 1$, the velocities sum to one. Since $d\,\mathrm{Tr}(S(\mu))/d\mu = \mathrm{Tr}(|v\rangle\langle v|) = 1$ for all μ, each Newton cradle conserves its total momentum in the sense that for all $\mu \in \mathbb{R}:\quad \sum_{n=1}^{N} \frac{\mathrm{d}s_n(\mu)}{\mathrm{d}\mu} = 1$.

4.2.4 Newton's cradles for unitaries

An analogous result holds for unitaries. Let us consider an arbitrary fixed unitary U acting on $\mathcal{H}$. Instead of adding a 1-parameter family of projectors as we did above, we now multiplicatively act on U from the left with a $U(1)$ group. The elements of this $U(1)$ act nontrivially on the dimension spanned by an arbitrary fixed vector, $|w\rangle$, and act as the identity on all other dimensions, i.e., we multiply U from the left with the $U(1)$-family of unitaries $(\mathbb{1} + (e^{i\alpha} - 1)\,|w\rangle\,\langle w|)$ for $\alpha \in [0, 2\pi)$ to obtain a family of unitaries $U(\alpha)$:

$$U(\alpha) := (\mathbb{1} + \left(e^{i\alpha} - 1\right)|w\rangle\,\langle w|)\,U \tag{4.6}$$

Let us denote the eigenvalues of U by $\{u_n\}$, ordered counterclockwise on the complex unit circle, starting from 1. We denote the eigenvalues of $U(\alpha)$ by $u_n(\alpha)$, i.e., we have $u_n(0) = u_n$. We define $w_n := \langle u_n|w\rangle$. Clearly, if $|w\rangle$ is chosen to obey $\langle u_m|w\rangle = 0$ for some m then the corresponding eigenvalues and eigenvectors are frozen, $u_m(\alpha) = u_m,\ |u_m(\alpha)\rangle = |u_m\rangle\ \forall\alpha$. Excluding these trivial cases, we can show again a Newton cradle behavior: as α runs from 0 to 2π, each eigenvalue $u_n(\alpha)$ runs counterclockwise on the complex unit circle, reaching u_{n+1} as $\alpha \to 2\pi$. Except, $u_N(\alpha)$ runs towards $u_1(\alpha)$.

4.2.5 Equivalence of unitary and Hermitian Newton's cradles

We can show that the left multiplication of a unitary operator by a representation of the group $U(1)$ is equivalent to the addition of a weighted rank 1 projector to a Hermitian operator. The equivalence is established by this Cayley transform:

$$U(\alpha) = (S(\mu) - i\mathbb{1})(S(\mu) + i\mathbb{1})^{-1} \tag{4.7}$$

$$S(\mu) = -i(U(\alpha) + \mathbb{1})(U(\alpha) - \mathbb{1})^{-1} \tag{4.8}$$

Therefore, $U(\alpha)$ and $S(\mu)$ possess the same eigenspaces and their eigenvalues are related by a Möbius transform: $u_n(\alpha) = (s_n(\mu) - i)/(s_n(\mu) + i)$. We can show that

$$|v\rangle = \frac{2}{\sqrt{\sum_{m=1}^{N} |w_m|^2 \left(s_m^2 + 1\right)}} \left(\mathbb{1} - U\right)^{-1} |w\rangle \tag{4.9}$$

and in coefficients:

$$v_n = \frac{1}{\sqrt{\sum_{m=1}^{N} |w_m|^2 (s_m^2+1)}} \frac{s_n+i}{i} w_n \tag{4.10}$$

$$w_m = \frac{1}{\sqrt{\sum_k \frac{|v_k|^2}{s_k^2+1}}} \frac{i}{s_m+i} v_m \tag{4.11}$$

Further, μ and α are related by:

$$\alpha(\mu) = 2\,\mathrm{arccot}\left[\frac{\sum_m |w_m|^2 (s_m^2+1)}{\mu} + \sum_k |w_k|^2 s_k\right] \tag{4.12}$$

$$= 2\,\mathrm{arccot}\left[\left(\sum_k \frac{|v_k|^2}{s_k^2+1}\right)^{-1} \left(\frac{1}{\mu} + \sum_m \frac{|v_m|^2 s_m}{s_m^2+1}\right)\right]$$

$$\mu(\alpha) = \frac{\sum_{m=1}^{N} |w_m|^2 (s_m^2+1)}{\cot\left(\frac{\alpha}{2}\right) - \sum_{k=1}^{N} |w_k|^2 s_k} \tag{4.13}$$

$$= \left(\sum_{m=1}^{N} \frac{|v_m|^2}{s_m^2+1} \cot\left(\frac{\alpha}{2}\right) - \sum_{k=1}^{N} \frac{|v_k|^2 s_k}{s_k^2+1}\right)^{-1} \tag{4.14}$$

We read off that $\mu(\alpha) = 0$ for $\alpha = 0$ and that as α increases from 0 to the finite value $\alpha^* := 2\,\mathrm{arccot}(\sum_k |w_k|^2 s_k)$ we have that $\mu(\alpha)$ runs to $+\infty$. As α further increases, $\mu(\alpha)$ comes back up from $-\infty$ and finally $\mu(\alpha) \to 0$ as $\alpha \to 2\pi$.

In this context, let us recall that the addition of Hermitians does not turn into the multiplication of unitaries under exponentiation, and that one obtains instead the Baker Campbell Hausdorff formula [29]. In contrast, we here see that the Cayley transform turns addition into multiplication in the sense that adding a multiple of a rank-1 projector to a Hermitian operator does map into left multiplying a unitary by a $U(1)$ unitary, a process that can also be iterated with successive projectors. Correspondingly, we obtain for any element of $U(N)$ a decomposition into a product of $U(1)$ elements.

4.2.6 Newton's cradle eigenvectors

Recall from above that in a Newton cradle every real number occurs exactly once as an eigenvalue, i.e., we have that for any $s \in \mathbb{R}$, there exists a pair (n, μ) so that $|s\rangle := |s_n(\mu)\rangle$

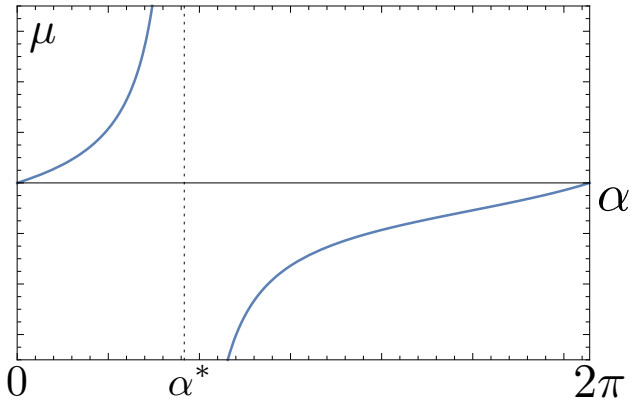

Figure 4.2: Plot of $\mu(\alpha)$ for the example used in Fig.1.

obeys $S(\mu)|s\rangle = s|s\rangle$. The normalized eigenvectors $|s\rangle$ are defined only up to phases and so is their inner product. But the magnitude of their overlap is unique and we can prove that for all $s \in \mathbb{R}$:

$$|\langle s|s_n\rangle| = \frac{|v_n|}{|s - s_n|} \left(\sum_{m=1}^{N} \frac{|v_m|^2}{(s - s_m)^2} \right)^{-1/2} \tag{4.15}$$

It is possible to choose the phases of the eigenvectors such that the overlap function $\langle s|s_n\rangle$ is real and continuous:

$$\langle s|s_n\rangle = \frac{(-1)^n |v_n|}{s - s_n} \left(\sum_{m=1}^{N} \frac{|v_m|^2}{(s - s_m)^2} \right)^{-1/2} \prod_{r=1}^{N} (-1)^{\theta(s - s_r)} \tag{4.16}$$

Here, the singularity at $s = s_n$ is trivially removable and θ is the Heaviside function with $\theta(0) := 0$. Using Eq. (4.16), the eigenvectors $|s_n(\mu)\rangle$ of the operators $S(\mu) = S + \mu|v\rangle\langle v|$ can be expressed explicitly in terms of the eigenvectors $|s_k\rangle$ of the operator S.

4.2.7 Iteration of Newton's cradles to obtain S + R

The Newton cradle for $|v\rangle := |v^{(1)}\rangle$ and $\mu := \mu^{(1)}$ yields the first step in the evolution of S to $S + R$. For the second step, we need the coefficients $v_n^{(2)}$ of $|v^{(2)}\rangle$ in the eigenbasis $\{|s_r^{(1)}(\mu^{(1)})\rangle\}_{n=1}^{N}$ of the operator $S + \mu^{(1)}|v^{(1)}\rangle\langle v^{(1)}|$. Using Eq. (4.16), we obtain them exactly:

$$v_n^{(2)} = \langle s_n(\mu^{(1)})|v^{(2)}\rangle = \sum_{r=1}^{N} \langle s_n(\mu^{(1)})|s_r\rangle\langle s_r|v^{(2)}\rangle \tag{4.17}$$

Successively turning on all of the projectors that comprise R yields $S + R$ as the result of N Newton cradles.

4.2.8 Proofs

The key elements of the proofs are described in the Appendices Chapter 9. They are inspired by [95, 96, 105, 97, 74] and by von Neumann's theory of the self-adjoint extensions of simple symmetric operators [129, 11], in particular for the case of deficiency indices $(1, 1)$. Von Neumann's theory itself does not apply in finite dimensions since in finite dimensions there are no symmetric non-self-adjoint operators. However, unitary extensions of isometries do exist in finite dimensions and, as we prove in the Appendix 9, they map, via the Cayley transform, into the addition of weighted projectors, rather than into the so-called abstract boundary conditions of von Neumann's method.

4.3 Applications

4.3.1 Level repulsion

The important phenomenon of level repulsion, see, e.g., [139, 13], arises as a special case: Let us consider a $|v\rangle$ which obeys $v_m = \langle s_m|v\rangle = 0$ for one m. Then the corresponding eigenvalue is frozen, $s_m(\mu) = s_m \ \forall \mu$. The remaining eigenvalues $s_n(\mu)$ for $n \neq m$ form a Newton cradle and $s_{m-1}(\mu)$ will cross s_m as μ runs from 0 to ∞. In general, however, $|v_m| \neq 0$. In this case, no matter how small $|v_m|$ is, the eigenvalue $s_m(\mu)$ does participate in Newton's cradle and is, therefore, not being crossed as μ runs. For very small $|v_m|$, the eigenvalue $s_{m-1}(\mu)$ can at most closely approach $s_m(\mu)$ while $s_m(\mu)$ barely moves until eventually $s_{m-1}(\mu)$ must repel $s_m(\mu)$ to send it on its way to s_m^* as $\mu \to \infty$. Let us now consider the generating of the sum of two Hermitian operators, $S + R$, by successively continuously turning on one after the other of the weighted projectors that comprise R. Since each turning on of a weighted projector is a Newton cradle process, we conclude that the eigenvalues cannot cross during that process, i.e., we must have level repulsion, except when and only when the projector $|v^{(i)}\rangle\langle v^{(i)}|$ that is being added is orthogonal to an eigenvector of the operator that it is being added to.

4.3.2 Cauchy interlacing

The Cauchy interlacing theorem also arises as a special case. The theorem states that the $N-1$ eigenvalues $a_1 < a_2 < \ldots < a_{N-1}$ of any Hermitian $(N-1)\times(N-1)$ matrix A obtained by deleting the r-th row (r is arbitrary) and r-th column of a Hermitian $N \times N$ matrix S with nondegenerate spectrum are interlaced in the N eigenvalues of S, i.e.,: $s_n < a_n < s_{n+1}\ \forall n = 1 \ldots (N-1)$. We can show that one obtains this result as the special case of the Newton cradle of S in which $|v\rangle$ is chosen to be the vector with the components $\delta_{r,i}$ in the basis in which the matrix S is given, and letting $\mu \to \infty$. Using Eq. (4.2) for $\mu \to \infty$, we can conclude more, namely that each of the interlaced eigenvalues a_n is a solution of Eq. (4.3), which means that we can identify the interlaced eigenvalues as $a_n = s_n^*$ for $n = 1, \ldots, N-1$.

4.3.3 Generalization of Shannon sampling

Shannon sampling theory is central in information theory, where it establishes the equivalence of continuous and discrete representations of information [154, 88, 123, 172, 20]. Applied to physical fields, spacetime could be described as simultaneously discrete and continuous in the same way that information can, [96, 98, 36]. Shannon sampling also possesses a close relationship to generalized uncertainty principles [93, 95]. The basic Shannon sampling theorem [154] concerns Ω-bandlimited functions, i.e., functions f for which there exists an $\tilde{f}$ so that $f(s) = \int_{-\Omega}^{\Omega} e^{i\omega s}\tilde{f}(\omega)d\omega$. The theorem states that if the amplitudes $\{f(s_n)\}_{n=-\infty}^{\infty}$ of an Ω-bandlimited function f on the real line are sampled at the so-called Nyquist spacing π/Ω, e.g., $s_n := n\pi/\Omega\ \ \forall n \in \mathbb{Z}$, then f can be exactly reconstructed from these samples for all $s \in \mathbb{R}$:

$$f(s) = \sum_{n=-\infty}^{\infty} f(s_n)\,\frac{\sin(s\Omega - n\pi)}{s\Omega - n\pi} \tag{4.18}$$

While abundantly useful, this theorem has the drawbacks of assuming a constant bandwidth and a correspondingly constant Nyquist rate as well as requiring an infinite number of samples. In practice, these drawbacks can lead to inefficiencies and truncation errors respectively. In the literature, Shannon sampling has been generalized to varying Nyquist sampling rates, corresponding to varying bandwidths, see, e.g., [95, 74, 124]. These results still required taking infinitely many samples, the obstacle being the use of von Neumann's method of self-adjoint extensions which does not apply in finite dimensions.

The present Newton cradle results are derived in finite dimensions and we now show that they can be applied to generalize Shannon sampling theory to enable both variable Nyquist

rates and finite numbers of samples. To this end, let us assume given a Newton cradle, i.e., a family of Hermitian operators $S(\mu) = S + \mu|v\rangle\langle v|$ for fixed S, fixed $|v\rangle$ and for μ running through $\mathbb{R}$. We can then uniquely associate to every vector $|f\rangle$ in the Hilbert space the function $f(s) := \langle s|f\rangle$. These functions obey

$$f(s) = \langle s|f\rangle = \sum_{n=1}^{N} \langle s|s_n\rangle\langle s_n|f\rangle = \sum_{n=1}^{N} \langle s|s_n\rangle \; f(s_n), \tag{4.19}$$

and more generally, for any μ:

$$f(s) = \sum_{n=1}^{N} \langle s|s_n(\mu)\rangle \; f(s_n(\mu)) \tag{4.20}$$

Here, $\langle s|s_n(\mu)\rangle$ can be assumed real and continuous as given in Eq. (4.16). On one hand, Eqs. (4.19) and (4.20) reduce sampling theory to the fact that knowing the coefficients of a vector, $|f\rangle$, in the eigenbasis of one $S(\mu)$ implies knowing its coefficients in all bases, including the eigenbases of all other $S(\mu')$. On the other hand, Eq. (4.20) shows that knowledge of the discrete set of amplitude samples $\{f(s_n(\mu))\}_{n=1}^{N}$ for a fixed μ suffices to reconstruct $f(s)$ for all $s \in \mathbb{R}$, establishing the equivalence of discrete and continuous representations of the information contained in $|f\rangle$. We can show that this result generalizes the sampling theory of [95, 74, 124] by allowing not only variable Nyquist rates but also finitely many samples without incurring truncation errors, while recovering the sampling results of [95, 74, 124] in the limit $N \to \infty$. In turn, [95, 74, 124] yield the Shannon sampling theorem [154] as the special case of an eternally constant Nyquist rate.

It will be interesting to explore applications of the new sampling result given in Eq. (4.16) and Eq. (4.19) in circumstances with known varying Nyquist rate, such as in synthetic aperture experiments. For example, in the planned SKA experiment [167], the effective bandwidth between a pair of antennas depends on their apparent distance as seen by the observed object and therefore varies predictably with the earth's rotation. Since large communication costs demand maximally efficient data taking, the generalized Shannon sampling method could be useful by enabling sampling and reconstruction at continuously-adjusted Nyquist rates, without incurring truncation errors at the beginning and end of sample taking.

4.3.4 Algorithmic complexity in adiabatic quantum computing

Adiabatic quantum computing [59, 67] is polynomially equivalent [2] to algorithmic quantum computing [132] and is therefore in that sense as powerful. An adiabatic quantum

computation starts at a time $t = 0$ by preparing a system with a simple Hamiltonian, H_S, in its ground state. The Hamiltonian is then gradually changed from H_S at $t = 0$ to a different Hamiltonian H_C at a time $t = T$ through $H(t) := (1 - \frac{t}{T})H_S + \frac{t}{T}H_C$. Here, H_C is a cost function Hamiltonian designed to implement the calculation by energetically penalizing errors. The ground state of H_C represents the solution. For example, to implement a combinatorial satisfiability problem, e.g., from the NP-complete set of 3-SAT problems, [58], H_C would be a sum of positive operators, $H_C = \sum_i H_{C,i}$, each of which implements a logical clause: a state $|\psi\rangle$ fulfils a clause $H_{C,i}$ iff it obeys $H_{C,i}|\psi\rangle = 0$.

For an adiabatic quantum computation to succeed, the ground state $|E_1(t = 0)\rangle$ of H_S has to evolve between $t = 0$ and $t = T$ into a state that matches the desired ground state $|E_1(t = T)\rangle$ of H_C with high fidelity. By the adiabatic theorem, see, e.g., [59], this is achieved if the process of switching over from H_S to H_C is slow enough: $T \gg \frac{a}{g_{min}^2}$. Here, a is the transition matrix element $a := \max_{0\leq t\leq T} |\langle E_2(t)|H_C - H_S|E_1(t)\rangle|$ and g_{min} is the minimum of the spectral gap $E_2(t) - E_1(t)$ of $H(t)$ over the ground state as t runs from $t = 0$ to $t = T$. The dominant behavior is that the smaller the spectral gap, the more time, T, is needed for the computation.

The question arises as to what it is that makes an adiabatic quantum computation problem computationally complex, in the sense that only a slow evolution will let the ground state of the simpler system H_S adiabatically evolve into the desired ground state of H_C. In particular, what properties of the cost function Hamiltonian H_C and the low lying states of the Hamiltonian H_S cause the gap to narrow during the computation?

For a preliminary application of the Newton cradle results, we write $H(t) = S + \frac{t}{T}R$ where $S := H_S$ and $R := H_C - H_S$. Without incurring significant overhead, we can turn on R by changing only one at a time of the prefactors $\mu^{(n)}$ of the projectors $|v^{(n)}\rangle\langle v^{(n)}|$ that comprise R. Let us now focus on one of these intermediate steps in the adiabatic quantum computation, say a step in which the prefactor $\mu^{(n)}$ of the projector $|v^{(n)}\rangle\langle v^{(n)}|$ is being increased. (In the example of satisfiability problems, we may intuitively think of this as adding a new clause.) The ground and first excited states at the beginning of this step shall be called $|g\rangle$ and $|e\rangle$.

The question now is what property of $|g\rangle$, $|e\rangle$ and the projector $|v^{(n)}\rangle\langle v^{(n)}|$ determines whether the gap narrows during the computation, i.e., whether the addition of $\mu^{(n)}|v^{(n)}\rangle\langle v^{(n)}|$ increases the computational complexity in the sense that it slows down the computation.

From the behavior of Newton cradles, we know that as a prefactor $\mu^{(n)}$ is being increased, all eigenvalues increase. Therefore, the gap over the ground state narrows iff the ground state eigenvalue increases faster than the first exited state's eigenvalue. From Eq. (4.5), we know that $ds_1/d\mu^{(n)} = |v_1^{(n)}|^2 = |\langle g|v^{(n)}\rangle|^2$ and $ds_2/d\mu^{(n)} = |v_2^{(n)}| = |\langle e|v^{(n)}\rangle|^2$. Therefore,

the gap narrows iff:

$$|\langle g|v^{(n)}\rangle|^2 > |\langle e|v^{(n)}\rangle|^2 \tag{4.21}$$

Defining $H^{(n)} := \mu^{(n)}|v^{(n)}\rangle\langle v^{(n)}|$, Eq. (4.21) becomes:

$$\langle g|H^{(n)}|g\rangle > \langle e|H^{(n)}|e\rangle \tag{4.22}$$

Therefore, at any point within an adiabatic quantum computation, the addition of a new contribution $H^{(n)} := \mu^{(n)}|v^{(n)}\rangle\langle v^{(n)}|$ to the Hamiltonian is algorithmically complex in the sense that a slight increase in $\mu^{(n)}$ narrows the gap and therefore forces a slowdown of the computation if and only if $H^{(n)}$ energetically penalizes the current ground state $|g\rangle$ more than the current first excited state, $|e\rangle$, i.e., iff the current ground state fulfills the condition posed by $H^{(n)}$ less than the current first excited state does. This indicates that it is desirable, for example, to choose an H_S whose ground state is a better approximation to the solution than its low lying states.

While Eq. (4.22) could be obtained from first order perturbation, the nonperturbative Newton cradle results may also enable a nonperturbative analysis for the full time evolution. First, Eq. (4.4) yields the eigenvalue velocities and accelerations for all s. An analysis that takes into account the Newton cradles of all projectors comprising R, could, therefore, yield nonperturbative insights into when, where and why the eigenvalue traffic on the s-axis decelerates and, therefore, leads to the narrowing of gaps between eigenvalues. Second, given knowledge of the evolving eigenvalues, Eq. (4.16) yields nonperturbative information on the evolution of the eigenvectors, including the ground state. In this context, it should also be very interesting to explore the role of the Newton cradle mechanism in Quantum Approximate Optimization Algorithms (QAOA), [57, 174].

For completeness, we add that the turning on of the projectors comprising R can generate not only right-moving but also left-moving Newton cradles. This is because even with H_S and H_C positive, $R = H_C - H_S$ may not be positive and can possess positive as well as negative eigenvalues $\mu^{(n)}$. For negative $\mu^{(n)}$, the gap narrows if the leftward speed of the ground state is smaller than that of the first excited state, i.e., if $|\langle g|v\rangle|^2 < |\langle e|v\rangle|^2$. Since $\mu^{(n)} < 0$, this yields again Eq. (4.22).

4.4 Outlook

Dynamics of quantum channels. Quantum channels are established through physical interactions and the question arises as to how the quantum channel capacity, i.e., the channel's ability to transmit entanglement or coherent information, depends on the dynamics of

the interactions involved. The dynamics of the negativities and coherent information are functions of the dynamics of the spectra of density operators and their partial transpose. Building on [108], decomposing the dynamics of interactions into Newton cradles may, therefore, yield new insight into the establishing of quantum channel capacities in interactions.

Casimir-like forces. Newton cradle decompositions should also be interesting to apply to the analysis of the dynamics of the spectra, and therefore the ground state energies, of quantum field mode decompositions under the variation of classical parameters, [66, 28], leading to effective forces. An example is the Casimir force that arises when the parameters describe the distances and shapes of conductors, such as parallel conducting plates [34, 126]. Another example is the inducing of gravitational forces in Sakharov's approach [149].

Generalization to infinite-dimensional Hilbert spaces. The present results apply in finite-dimensional Hilbert spaces and, for this case, it should be very interesting to apply them also, for example, to random matrix theory [70] where they could help shed light on the dynamics of the BBT transition [16, 138] in quantum chaotic systems. In infinite-dimensional Hilbert spaces, the Cayley transform of the unitaries $U(\alpha)$ can yield bounded or unbounded self-adjoint operators. In the unbounded case, von Neumann's theory of self adjoint extensions can be applied and it shows that the operators $S(\mu)$ differ not by a multiple of a projector but a domain extension, such as boundary conditions in the case of differential operators [11], though interestingly they can differ by a self-adjoint operator by using an auxiliary Hilbert space [140]. For the resulting generalization of Shannon sampling see, e.g., [95, 74, 93, 124]. It will be interesting to explore the generalization of the present results in the limit $N \to \infty$ and to families of bounded operators, $S(\mu)$, in infinite-dimensions, i.e., for finite-size Newton cradles with infinitely many eigenvalues.

Spectral geometry. Spectral geometry asks to what extent the spectra of Hermitian Laplacian and Dirac operators on Riemannian manifolds determine the metric of the manifold, see, e.g., [46]. Spectral geometric methods have also been applied to bridge between the differential geometric language of general relativity and the functional analytic language of quantum theory [105, 1, 100]. In this context, a Newton cradle analysis could yield new insights into the dynamics of the spectra of wave operators as a function of parametrized changes to the metric.

4.5 An Application of Newton's Cradle Spectra: Dressed Vacuum in Light-Matter Interactions

In an earlier chapter, the Unruh-DeWitt model of light-matter interactions was introduced. In this model a two-level quantum system, called the Unruh-DeWitt detector, interacts with a scalar quantum field.

In the usual derivation of the Unruh effect, it is assumed that the detector is initially in its ground state, while the field is also in its lowest energy state, in the vacuum state of its free Hamiltonian. Though the tensor product of the detector's ground state and the field's vacuum is the lowest energy state of the total free Hamiltonian, it is not the ground state of the total Hamiltonian including the interactions.

We will use the expressions derived in this chapter to find the dressed vacuum, i.e. the vacuum of the total Hamiltonian.

As a reminder, let us write down the total free Hamiltonian:

$$H_0 = \frac{\Omega}{2}\left(|e\rangle\langle e| - |g\rangle\langle g|\right) + \int (dk)\ \omega_{\mathbf{k}} a^\dagger_{\mathbf{k}} a_{\mathbf{k}}. \tag{4.23}$$

We see that the energy gap Ω separates the ground state $|g\rangle$ from the excited state $|e\rangle$ of the detector, while the vacuum state of the field, which we will denote $|0\rangle$ is its lowest energy state, and it contains no excitations, $a_{\mathbf{k}}|0\rangle = 0$.

The interaction Hamiltonian, as a reminder, is the following:

$$H_{\text{int}} = G\left(|e\rangle\langle g| + |g\rangle\langle e|\right) \otimes \varphi(x), \tag{4.24}$$

where G is the coupling strength and $\varphi(x)$ is the field along the detector's trajectory $x = (t(\tau), \mathbf{x}(\tau))$ in terms of its proper time τ.

In order to use the Newton's cradle spectra technique, we need to express the interaction Hamiltonian as a sum of projectors. We first find that the field $\varphi(x)$ can be expressed in terms of Fock states:

$$H_{int} = G(|v_D\rangle\langle v_D| - |e\rangle\langle e| - |g\rangle\langle g|) \otimes (|v_F\rangle\langle v_F| - |0\rangle\langle 0| - \int (dk_1)(dk_2) e^{i(\vec{k_1}-\vec{k_2})\cdot\vec{x}} |\mathbf{k}_1\rangle\langle \mathbf{k_2}| \ldots), \tag{4.25}$$

where the states $|v_D\rangle$ and $|v_F\rangle$ are defined as:

$$|v_D\rangle = \frac{1}{\sqrt{2}}(|g\rangle + |e\rangle),\ |v_F\rangle = |0\rangle + \int (dk) e^{-i\vec{k}\vec{x}} |k\rangle + ... \tag{4.26}$$

Our aim is to find the dressed vacuum, i.e. the new lowest energy state after adding the interaction Hamiltonian. The free vacuum state was the state $|\Psi_0\rangle = |g\rangle \otimes |0\rangle$. Let us identify how different projectors in the interaction Hamiltonian may affect the ground state. For this, we may use what we learned from Newton's cradle spectra.

First of all, if the expected value of a projector Π in the initial ground state $|\Psi_0\rangle$ is zero, then the ground state will be unaffected. For example, if we take the projector $\Pi = |e\rangle\langle e| \otimes |v_F\rangle\langle v_F|$, its expected value $\langle\Psi_0|\Pi|\Psi_0\rangle = 0$, since $\langle e|g\rangle = 0$, and this projector will affect other states, but not the ground state. This means we can freely drop a vast number of terms from the interaction Hamiltonian, for the purposes of calculating the dressed vacuum. Let us write only the leftover terms, and name the resulting operator the 'relevant' interaction Hamiltonian:

$$H_{int}^{(rel.)} = G(|v_D\rangle\langle v_D| - |g\rangle\langle g|) \otimes (|v_F\rangle\langle v_F| - |0\rangle\langle 0|). \tag{4.27}$$

Of these terms, $G|g\rangle\langle g|) \otimes |0\rangle\langle 0|$ affects the ground state trivially, since it is just the projector on the free ground state $|\Psi_0\rangle$, and it only elevates its energy by the coupling constant G.

The projector $G|g\rangle\langle g| \otimes |v_F\rangle\langle v_F|$ affects each of the subsystems separately, i.e. it changes the vacuum state of the detector trivially by just shifting its energy, as mentioned above, while it nontrivially affects the vacuum of the field, and all its excited states, due to $|v_F\rangle$ being a superposition over all Fock states. Analogous is true for the projector $G|v_D\rangle\langle v_D| \otimes |0\rangle\langle 0|$.

Therefore, we will focus our attention to the only projector that affects both subsystems nontrivially, the projector $G|v_D\rangle\langle v_D| \otimes |v_F\rangle\langle v_F|$. Then the full Hamiltonian can be written as the sum of the free Hamiltonian and a projector:

$$H = H_0 + G|v_D\rangle\langle v_D| \otimes |v_F\rangle\langle v_F|. \tag{4.28}$$

This allows us to directly apply the expressions derived in the chapter on Newton's cradle spectra. First of all, let us identify the ground state energy λ_0 of the free Hamiltonian:

$$H_0 \left|\Psi_0\right\rangle = \lambda_0 \left|\Psi_0\right\rangle, \tag{4.29}$$

$$\left[\frac{\Omega}{2}\left(\left|e\right\rangle\left\langle e\right| - \left|g\right\rangle\left\langle g\right|\right) + \int (dk)\ \omega_{\mathbf{k}} a^\dagger_{\mathbf{k}} a_{\mathbf{k}}\right] \left|g\right\rangle\left|0\right\rangle = -\frac{\Omega}{2}\left|g\right\rangle\left|0\right\rangle. \tag{4.30}$$

Therefore we find that $\lambda_0 = -\frac{\Omega}{2}$. After the addition of the interaction Hamiltonian, that we have simplified to a projector, this energy will change to a new value, namely the energy of the dressed vacuum λ_0':

$$\lambda_0 = -\frac{\Omega}{2} \rightarrow \lambda_0' = -\Omega + \Delta E \tag{4.31}$$

We may find λ_0' by directly using one of the Newton's cradle expressions. The following expression relates the coupling constant G to the new eigenvalue λ_0':

$$G(\lambda_0') = \left(\sum_{n=1}^{N} \frac{\left|v_n\right|^2}{\lambda_0' - \lambda_n}\right)^{-1}. \tag{4.32}$$

Here, $\left|v_n\right|^2 = \left|\langle\Psi_0|v_n\rangle\right|^2$, where $\left|v_n\right\rangle$ is one of the states in the superposition $\left|v_D\right\rangle \otimes \left|v_F\right\rangle = \frac{1}{\sqrt{2}\sqrt{\mathcal{N}}}\left(\left|g\right\rangle \otimes \left|0\right\rangle + \left|e\right\rangle \otimes \left|0\right\rangle + ...\right)$. Note that, when the field and detector are in free space, the sum over n should be replaced by an integral, corresponding to the real-number valued spectrum $\mathbf{k}$ of the momentum operator. In order to use Newton's cradle expressions straightforwardly, we put the detector and the field in a box, and set a finite cutoff. This will ensure that the sum over n is a finite sum.

Instead of finding the root of Eq. (4.32) to find λ_0' for a fixed coupling G, the numerically easier strategy is to guess a solution for λ_0', and find what is the corresponding coupling G, using the same Eq. (4.32). If the resulting coupling is higher than the real G, we know that we need to guess a smaller λ_0'. This is due to the monotonicity property of Newton's cradle spectra, proved in the Eq. (4.4), and visually clear from Fig. 4.1. Iteratively, one settles on an approximation of λ_0', to a desired accuracy.

Perhaps even more interestingly, we can also find the overlap between the dressed vacuum $\left|0_D\right\rangle$ and the free states λ_n of the detector and the field:

$$\left|\langle 0_D|\lambda_n\rangle\right| = \frac{\left|v_n\right|}{\left|\lambda_0' - \lambda_n\right|}\left(\sum_{m=1}^{N} \frac{\left|v_m\right|^2}{(\lambda_0' - \lambda_m)^2}\right)^{-1/2} \tag{4.33}$$

From this equation, we learn that the dressed vacuum is a weighted superposition over all free states $|\lambda_n\rangle$. This is due to the fact that $|v_D\rangle$ is a superposition over detector's free states $|g\rangle$ and $|e\rangle$, and similarly $|v_F\rangle$ over the Fock states of the field.

4.6 Spectral Dynamics Beyond Newton's Cradle

Newton's cradle spectra provided insights into the nonperturbative dynamics of the spectra and the eigenvectors of a Hamiltonian when a projector is added to it. The expressions we derived allow us to trace the trajectories of the eigenvalues as we change the coupling constant μ. Interestingly, they seem to behave as though they were point-like Newtonian particles, interacting with one another via some potential $V(s_1, s_2, ..., s_N)$ that depends on the "positions" of each of the eigenvalues.

In order to make these statements more precise, we start by demonstrating conservation of momentum. We first identify the set of eigenvalues $s_i(\mu)$, depending on the coupling constant μ, with a set of classical particles, whose trajectories are time-dependent $x_i(t)$. The identification is as follows:

$$s_i(\mu) \leftrightarrow x_i(t),$$
$$\mu \leftrightarrow t.$$

We will take the mass of the Newtonian particles $x_i(t)$ to be $m = 1$. Momentum conservation can then be stated as the sum of velocities being a constant function of time:

$$\sum_i p_i = \sum_i \frac{dx_i(t)}{dt} = const. \tag{4.34}$$

The analogue of the conservation of momentum in the dynamics of the eigenvalues is the constant total "trace velocity":

$$\sum_i \frac{ds_i}{d\mu} = \frac{d}{d\mu}\mathrm{Tr}\left[S(\mu)\right] = 1. \tag{4.35}$$

In addition, we can identify the force of interaction between the 'particles', i.e. the eigenvalues in the spectra. First, we write the "eigenvalue velocity", $\frac{ds(\mu)}{d\mu}$, derived from Newton's cradle spectra expressions:

$$\frac{ds(\mu)}{d\mu} = \frac{\sum_n \frac{|v_n|^2}{s-s_n}}{\sum_m \frac{|v_m|^2}{(s-s_m)^2}}. \tag{4.36}$$

We can then in principle also calculate the "acceleration", $\frac{d^2s(\mu)}{d\mu^2}$, though the expressions quickly become laborious and long:

$$\frac{d^2s(\mu)}{d\mu^2} = \frac{d}{d\mu}\frac{(\sum_n \frac{|v_n|^2}{s-s_n})^2}{\sum_m \frac{|v_m|^2}{(s-s_m)^2}}. \tag{4.37}$$

Since all the masses are equal to 1, this is the expression for the force. Interestingly, the force seems to generically always be the result of N-point interactions.

In future work, it will be interesting to study what we may learn about the behaviour of eigenvalues, given that we know that they can be described with Newtonian mechanics in the case of adding one rank-one projector.

Interestingly, let us assume we could derive an expression for the addition of multiple projectors, analogously to the one in Section 4.6. This would imply that we could simulate the behaviour of eigenvalues of a Hamiltonian using a classical system. If the Hamiltonian is an N by N matrix, we could simulate the changes of its eigenvalues using N classical objects, if we are clever enough to engineer the forces as in Section 4.6. Presumably, such N-point interaction forces would be hard to generate, but possible in principle. It would be interesting to study if this would imply something of interest for the study of advantages of quantum over classical computing, since it would be an example of a classical simulation of something seemingly inherently quantum, the evolution of eigenvalues as the coupling constants in a Hamiltonian vary.

Chapter 5

Transmission of Coherent Information at the Onset of Interactions

5.1 Introduction

Over the past decade, progress in the field of quantum information has seen rapid acceleration, with the physical realisation of a large number of quantum technologies in disciplines such as communication, computing, machine learning, and cryptography. Recently, for example, successful quantum key distribution over distances of thousands of kilometers has been achieved using a ground-to-satellite quantum communication network [38]. Other recent advances include the development of programmable, scalable photonic quantum chips [14], and the demonstration of computational performance advantages over classical methods, see, e.g., [109].

A key challenge in the general field of quantum technologies is to control coherence and entanglement during quantum processes. Depending on the application, different behaviours are desired. Often, it is necessary that entanglement be transferred efficiently from one system to another, such as in quantum communication within or in between quantum processors. Conversely, in other applications it can be important to retain pre-existing entanglement for as long as possible, in particular, to minimize its transfer to the environment [155, 128].

It is therefore important to explore the factors that determine the efficiency with which quantum information is transmitted between two systems as they start interacting. A

key tool with which to investigate this is the coherent information [152]. The coherent information serves as an indicator of the degree of preservation of initial entanglement as a quantum system undergoes a quantum channel.

Moreover, the coherent information is of particular importance in the determination of the capacity of a quantum channel. Specifically, the quantum channel capacity is determined via maximising the coherent information over input states and many parallel uses of the channel [117, 71, 110, 44]. Via other optimizations, the coherent information also yields the one-way and two-way distillable entanglements.

In the present work, we analyze the factors that determine the rate at which pre-existing coherent information is transferred at the onset of an interaction. We adopt a perturbative framework, in which we Taylor expand the evolution of the coherent information at early times. Because the coherent information is defined as a difference between von Neumann entropies, we calculate the changes in these entropies perturbatively to yield the overall change in coherent information.

We find that, while the von Neumann entropies themselves are well-defined for any given channel configuration, the leading order expansion coefficient in their time evolution may diverge, thereby yielding a divergent leading order change in the coherent information. To overcome this problem, we extend our analysis by considering a generalisation to a class we refer to as the $n-$coherent information. Whereas the traditional coherent information is defined as a difference of von Neumann entropies, the $n-$coherent information is analogously defined as a difference between the n^{th} Rényi entropies. From this perspective, the traditional coherent information may be referred to as the '1-coherent information', since the von Neumann entropy is the limit of the n^{th} Rényi entropy as $n \to 1$.

There are a number of benefits to considering the full family of $n-$Rényi entropies rather than only the von Neumann entropy. First, we find that for all integers $n > 1$, there are no divergences in the leading order expansion coefficient, and we are therefore able to obtain finite values for the early time behaviour of the corresponding $n-$coherent information. Furthermore, by determining the behavior of the entire family of $n-$Rényi entropies we capture a more comprehensive picture of the dynamics. For example, the von Neumann entropy of a density matrix yields little specific information about that density matrix. By contrast, knowledge of the full family of integer Rényi entropies for $n > 1$ of a density matrix allows one to reconstruct the entire spectrum of the density matrix [116, 63, 32, 169]. Recall also that the family of Rényi entropies with $n > 1$ satisfy the additivity and majorisation criteria of suitable information measures [147].

Using the perturbative method, we find that the leading contribution to the time evolution of the n-coherent information occurs at second order for all n. Moreover, we show that

to second order, the evolution of the $n-$coherent information is independent of the free Hamiltonians of either subsystem. This markedly simplifies the computations, and implies that complicated resonance phenomena do not affect the leading order behaviour of the coherent information, since such phenomena necessarily involve the free Hamiltonians in their mathematical descriptions [80, 170].

Interestingly, we show that the second order change in the n-coherent information is not a simple function of the degree of pre-existing entanglement. Instead, it depends upon the extent to which the initial entanglement in the $A\tilde{A}$ system is accessible to the interaction Hamiltonian H_{int} of A with B. Specifically, we identify a new quantity, which we term the $n-$exposure, to which the leading order change in the $n-$coherent information is proportional. This is an important point, as it implies that initial preparations of the $\tilde{A}A$ system which possess the same level of entanglement may nevertheless exhibit vastly different behaviours at the onset of interaction with system B. Therefore, the notion of n-exposure could help, for example, to identify regions in a system's space of states (such as regions in the Bloch sphere in the simple case of a qubit), that are desirable because they have little $n-$exposure and are therefore relatively resistant to transmission of quantum information to the environment.

To illustrate the utility of the $n-$coherent information and $n-$exposure, we apply our results to simple physical scenarios. We first apply our approach to the Unruh-DeWitt model (UDW) [125] model of the light-matter interaction. In this simple model, we can solve for the time evolution of the qubit exactly. This allows us to verify our perturbative results non-perturbatively. We can then also use the $n-$exposure to identify which regions in the state space have greater propensity to transmit pre-existing entanglement at the onset of interactions. We also apply our results to a simple scenario involving a qutrit as the input to a quantum channel in order to explore the utility of the $n-$exposure in larger systems. We explicitly demonstrate regions of state space which are prone to either retaining or transmitting pre-existing entanglement at the onset of the the interaction.

The structure of this paper is as follows. In Section 5.2, we prove that free Hamiltonians do not contribute to second order in our calculations and may therefore be neglected in the following sections without loss of generality. We then discuss the notion of coherent information in Section 5.3 and describe the quantum channel setup which we will work with throughout the remainder of the paper. In Section 5.4, we consider the early time evolution of the traditional coherent information, and demonstrate the divergences which can arise in derivatives of the von Neumann entropy. In Section 5.5 we introduce the generalised n-coherent information, and demonstrate that, unlike the traditional coherent information, the leading order behaviour is well-defined and finite across state space for $n > 1$. In Section 5.6 and Section 5.7 we apply our results to the light-matter interaction

and to a qutrit scenario. In Section 5.8 we discuss the potential significance of our results in the context of quantum communication and computing technologies and address the scope for future work.

5.2 Preliminaries: Free Hamiltonians Do Not Contribute up to Second Order

In this work, we calculate the transfer of coherent information perturbatively in time, i.e., for the onset of the interaction between two systems. We begin by showing that the transfer of coherent information sets in at second order and that the presence of the free Hamiltonians of the two interacting systems does not contribute to the evolution of the quantities of interest until third order. This means that, in the remainder of this paper, we will be able to work to leading (i.e., second) order while neglecting the free Hamiltonians.

To see this, let us start by considering a system AB composed of two subsystems A and B, described by density matrix $\rho(t)$, which is separable at $t = 0$ such that: $\rho_0 = \rho_A \otimes \rho_B$. We allow the total Hamiltonian $\hat{H}$ for the time evolution of the combined system AB to be fully general, i.e., of the form:

$$\hat{H} := \sum_j \hat{A}_j \otimes \hat{B}_j, \tag{5.1}$$

where the operators $\{\hat{A}_j\}$ act only on subsystem A, and the operators $\{\hat{B}_j\}$ act only on subsystem B. Note that this general expression for $\hat{H}$ encompasses both interaction terms (with non-trivial action on both subsystems), as well as the free evolution of each subsystem through terms of the form $\hat{A}_j \otimes \mathbb{I}$ (for subsystem A) and $\mathbb{I} \otimes \hat{B}_j$ (for subsystem B). We now expand the time-evolved state of the total system in the Schrödinger picture as:

$$\rho(t) = e^{it\hat{H}} \rho_o e^{-it\hat{H}} = \rho_0 + it\big[\hat{H}, \rho_0\big] + \frac{(it)^2}{2!}\Big[\hat{H}, \big[\hat{H}, \rho_0\big]\Big] + ... \tag{5.2}$$

A key quantity for which we wish to prove that its time evolution is independent of the free Hamiltonians to second perturbative order is the n-purity, γ_n. The n-purity of subsystem B is defined as

$$\gamma_{n,B}(t) := \mathrm{Tr}_B\left[\rho_B(t)^n\right] = \mathrm{Tr}_B\left[\,\mathrm{Tr}_A[\rho(t)]^n\right], \tag{5.3}$$

and likewise for subsystem A. The first and second time derivatives of the n-purity of B are as follows:

$$\dot{\gamma}_{n,B}(t) = n\,\mathrm{Tr}_B\Big[\,\mathrm{Tr}_A[\rho(t)]^{n-1}\,\mathrm{Tr}_A[\dot{\rho}(t)]\Big], \tag{5.4}$$

$$\ddot{\gamma}_{n,B}(t) = n \operatorname{Tr}_B \Bigg[\operatorname{Tr}_A[\dot{\rho}(t)] \sum_{j=0}^{n-2} \operatorname{Tr}_A[\rho(t)]^j \operatorname{Tr}_A[\dot{\rho}(t)] \operatorname{Tr}_A[\rho(t)]^{n-2-j} + \operatorname{Tr}_A[\rho(t)]^{n-1} \operatorname{Tr}_A[\ddot{\rho}(t)] \Bigg]. \tag{5.5}$$

We will first show that, irrespective of the precise form of $\hat{H}$, $\dot{\gamma}_{n,B}(t)$ and $\dot{\gamma}_{n,B}(t)$ vanish at $t = 0$. To do this, we use that $\operatorname{Tr}_A[\rho(0)] = \rho_B$, and Eq. (5.2) to find that $\dot{\rho}(0) = i[\hat{H}, \rho_0]$. Now, substituting the full expression for $\hat{H}$ we have:

$$\begin{aligned} \dot{\gamma}_{n,B}(0) &= in \operatorname{Tr}_B \left[\rho_B^{n-1} \operatorname{Tr}_A \left[\sum_j \hat{A}_j \otimes \hat{B}_j, \rho_A \otimes \rho_B \right] \right] \\ &= in \sum_j \operatorname{Tr}_A[\hat{A}_j \rho_A] \operatorname{Tr}_B \left[\rho_B^{n-1} [\hat{B}_j, \rho_B] \right] = 0 \end{aligned} \tag{5.6}$$

The expression vanishes because the trace over system B vanishes for every j due to the cyclicity of the trace.

We now consider Eq. (5.5) at $t = 0$. Again we note that $\operatorname{Tr}_A[\rho(0)] = \rho_B$ and from Eq. (5.2) we have $\ddot{\rho}(0) = -\big[\hat{H}, [\hat{H}, \rho_0]\big]$. Hence,

$$\ddot{\gamma}_{n,B}(0) = -n \operatorname{Tr}_B \left[\operatorname{Tr}_A \left[[\hat{H}, \rho_0] \right] \sum_{j=0}^{n-2} \rho_B^j \operatorname{Tr}_A \left[[\hat{H}, \rho_0] \right] \rho_B^{n-2-j} + \rho_B^{n-1} \operatorname{Tr}_A \left[\hat{H}, [\hat{H}, \rho_0] \right] \right]. \tag{5.7}$$

Substituting in the general expression for $\hat{H}$ and simplifying we find:

$$\ddot{\gamma}_{n,B}(0) = -2n \sum_{jk} \Bigg(\operatorname{Tr}_A \left[\hat{A}_j \rho_A \right] \operatorname{Tr}_A \left[\hat{A}_k \rho_A \right] \operatorname{Tr}_B \left[\rho_B^{n-1} [\hat{B}_j, \rho_B] \hat{B}_k \right] + \operatorname{Tr}_A \left[\hat{A}_j \hat{A}_k \rho_A \right] \operatorname{Tr}_B \left[\rho_B^{n-1} [\rho_B \hat{B}_j, \hat{B}_k] \right] \Bigg). \tag{5.8}$$

To prove that the free Hamiltonians do not contribute here, we must show that any terms of the form $\hat{A} \otimes \mathbb{I}$ or $\mathbb{I} \otimes \hat{B}$ do not contribute to the sum. To this end, let us consider the Hamiltonian $\hat{H} = \sum_j \hat{A}_j \otimes \hat{B}_j$ where the term with index $j = m$ is of the form $\hat{H}_A \otimes \mathbb{I}_B$. We can now divide the sum over j, k in Eq. (5.8) as follows:

$$\sum_{jk} = \sum_{j,k \neq m} + \sum_{j,(k=m)} + \sum_{k,(j=m)} . \tag{5.9}$$

There is no contribution from $\hat{H}_A \otimes \mathbb{I}_B$ in the first term on the right of the above equation. Hence, we need only consider the two final terms. We have:

$$\begin{aligned}
-2n \sum_{j,(k=m)} \Big(& \mathrm{Tr}_A \left[\hat{A}_j \rho_A\right] \mathrm{Tr}_A \left[\hat{H}_A \rho_A\right] \mathrm{Tr}_B \left[\rho_B^{n-1} [\hat{B}_j, \rho_B] \mathbb{I}_B\right] \\
& + \mathrm{Tr}_A \left[\hat{A}_j \hat{H}_A \rho_A\right] \mathrm{Tr}_B \left[\rho_B^{n-1} [\rho_B \hat{B}_j, \mathbb{I}_B]\right] \Big) \\
-2n \sum_{k,(j=m)} \Big(& \mathrm{Tr}_A \left[\hat{H}_A \rho_A\right] \mathrm{Tr}_A \left[\hat{A}_k \rho_A\right] \mathrm{Tr}_B \left[\rho_B^{n-1} [\mathbb{I}_B, \rho_B] \hat{B}_k\right] \\
& + \mathrm{Tr}_A \left[\hat{H}_A \hat{A}_k \rho_A\right] \mathrm{Tr}_B \left[\rho_B^{n-1} [\rho_B \mathbb{I}_B, \hat{B}_k]\right] \Big).
\end{aligned} \tag{5.10}$$

We see immediately that there is no contribution from these partial sums because each trace over B either includes a commutator with the identity, or is of the form $\mathrm{Tr}_B \left[\rho_B^{n-1} \hat{B}_j \rho_B - \rho_B^n \hat{B}_j\right]$, which is zero by the cyclicity of the trace. Hence, we see that terms of the form $\hat{H}_A \otimes \mathbb{I}_B$ do not contribute to Eq. (5.8). Let us now consider terms of the form $\mathbb{I}_A \otimes \hat{H}_B$. Again, we will assume that the term of this form is indexed by m, and split the double sum over i, j as shown in Eq. (5.9). Again, the first partial sum, which does not include $j = m$ or $k = m$ does not contain any instances of the $\mathbb{I}_A \otimes \hat{H}_B$ term. Looking at the final two partial sums, we have:

$$\begin{aligned}
-2n \sum_{j,(k=m)} \Big(& \mathrm{Tr}_A \left[\hat{A}_j \rho_A\right] \mathrm{Tr}_A \left[\mathbb{I}_A \rho_A\right] \mathrm{Tr}_B \left[\rho_B^{n-1} [\hat{B}_j, \rho_B] \hat{H}_B\right] \\
& + \mathrm{Tr}_A \left[\hat{A}_j \mathbb{I}_A \rho_A\right] \mathrm{Tr}_B \left[\rho_B^{n-1} [\rho_B \hat{B}_j, \hat{H}_B]\right] \Big) \\
-2n \sum_{k,(j=m)} \Big(& \mathrm{Tr}_A \left[\mathbb{I}_A \rho_A\right] \mathrm{Tr}_A \left[\hat{A}_k \rho_A\right] \mathrm{Tr}_B \left[\rho_B^{n-1} [\hat{H}_B, \rho_B] \hat{B}_k\right] \\
& + \mathrm{Tr}_A \left[\mathbb{I}_A \hat{A}_k \rho_A\right] \mathrm{Tr}_B \left[\rho_B^{n-1} [\rho_B \hat{H}_B, \hat{B}_k]\right] \Big).
\end{aligned} \tag{5.11}$$

We now use the fact that $\mathrm{Tr}_A[\mathbb{I}_A \rho_A] = \mathrm{Tr}_A[\rho_A] = 1$, and rename the index $k \to j$ in the second sum to write

$$\begin{aligned}
-2n \sum_j \mathrm{Tr}_A[\hat{A}_j \rho_A] \, \mathrm{Tr}_B \Big[\rho_B^{n-1} \Big(& [\hat{B}_j, \rho_B] \hat{H}_B + [\rho_B \hat{B}_j, \hat{H}_B] \\
& + [\hat{H}_B, \rho_B] \hat{B}_j + [\rho_B \hat{H}_B, \hat{B}_j] \Big) \Big] = 0,
\end{aligned} \tag{5.12}$$

where again we have made use of the cyclicity of the trace.

Hence, we have shown that terms of the form $\hat{A} \otimes \mathbb{I}$ and $\mathbb{I} \otimes \hat{B}$ (i.e., free Hamiltonians) do not contribute to either the first or second time derivatives of the n-purity, and therefore we can neglect free evolution when working to second perturbative order in the following sections without loss of generality.

5.3 Quantum Channels and Coherent Information

The controlled isolation or transfer of quantum information among quantum systems is of great importance in quantum technologies [112, 15]. Of particular interest is the degree to which pre-existing quantum correlations with an ancilla system as measured, e.g., by coherent information (or also, e.g., by negativity) are preserved or transmitted under the action of a quantum channel.

Let us now consider the direct channel described in the introduction, i.e., the channel from the density matrix of system A at the initial time to the density matrix of system A at a later time, namely after A interacted with a system B. In this interaction, A may transmit some of its pre-existing quantum correlations with an ancilla, $\tilde{A}$, to system B. Therefore, we also consider the complementary channel from the density matrix of system A at the initial time to the density matrix of system B after the onset of the interaction.

We assume that among the three systems, A, $\tilde{A}$ and B, systems A and $\tilde{A}$ are initially entangled, such that $\tilde{A}$ purifies A. B is assumed initially unentangled with both A and $\tilde{A}$, and for now we will assume that system B is initially pure. Therefore, the total tripartite system $A\tilde{A}B$ is also pure. We then consider an interaction which takes place between systems A and B only. This arrangement is illustrated in Fig. 5.1.

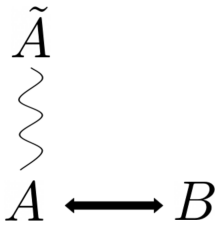

Figure 5.1: A tripartite system in which, initialy, A is purified by $\tilde{A}$, and B is initially pure. An interaction then proceeds between Systems A and B only.

We consider the direct quantum channel $A \to A'$ and the complementary channel $A \to B'$. Here, primes represent the time evolved systems. We will study the coherent information of these channels since they are the building blocks for the channel capacity. Moreover, as

mentioned before, maximising over all possible input states and parallel executions of the channel gives rise to the overall quantum channel capacity [117, 113, 114]. The coherent information for our two channels is defined as

$$I^d = S(A') - S((A\tilde{A})'), \tag{5.13}$$

$$I^c = S(B') - S((B\tilde{A})'), \tag{5.14}$$

where the superscripts d and c stand for 'direct' and 'complementary', respectively, and S represents the von Neumann entropy.

Though the coherent information is not an entanglement monotone, by definition, the coherent information quantifies the degree to which the entropy of a subsystem exceeds that of its supersystem. Since, classically, this quantity can never be positive, a positive coherent information indicates the presence of quantum correlations between the subsystems [171].

Since system B starts out pure and system $B\tilde{A}$ starts out mixed, the coherent information, I^c, of the complementary channel starts out negative and therefore requires at least a finite amount of time to turn positive. Since $I^c = -I^d$, this means that I_d, which starts out positive, needs to decrease. Our aim here is to find out what determines the speed with which the two channel's coherent informations change at the onset of interactions.

5.4 Perturbative Expansion of the Coherent Information

We now study the evolution of the coherent information perturbatively, calculating the leading order derivatives of the von Neumann entropies in Eq. (5.13). We will find that there can be divergences in the leading derivatives, which will motivate the introduction of a generalisation of the coherent information in Section 5.5.

Let us begin by revisiting the definition of the coherent information, Eq. (5.13), which can be re-expressed as follows:

$$I^d = S(A') - S(B'), \tag{5.15}$$

$$I^c = S(B') - S(A'). \tag{5.16}$$

Here we have made use of the fact that the entire tripartite system $A\tilde{A}B$ is pure, and therefore any bipartition of the whole must result in a symmetric configuration of entropies. Since the coherent information of the complementary channel is the negative of that of the direct channel, it is sufficient to study the latter.

To compute the leading order change in I^d at the onset of the quantum channel, we note that the von Neumann entropies in Eq. (5.15) can be expressed as the limit of the n-Rényi entropy, H_n, as $n \to 1$. That is

$$S(A) = \lim_{n\to 1} H_n(A) = \lim_{n\to 1} \frac{1}{1-n} \log\left(\gamma_{n,A}\right), \tag{5.17}$$

where $\gamma_{n,A} = \mathrm{Tr}_A[\rho_A^n]$. To obtain the time evolution of the von Neumann entropy, we can therefore compute the evolution of H_n in the limit $n \to 1$. Thereby we will find that it is not possible to obtain an analytic expression for the leading time derivative of the von Neumann entropy which is valid across the entire state space.

To see this, let us now consider the case where the interaction Hamiltonian between systems A and B is of the form $H_{int} = \hat{A} \otimes \hat{B}$, generating the unitary time evolution operator $U = \exp\left(it\hat{A} \otimes \hat{B}\right)$. As illustrated in Fig. 5.1, systems A and B are assumed initially unentangled with a combined density matrix of the form $\rho_A \otimes \rho_B$. In previous work, see ([107]), we already showed that for this situation, the first derivative of the n-Rényi entropy vanishes for either subsystem, and that the leading (second) order is given by

$$\ddot{H}_n(A)|_{t=0} = \frac{\ddot{\gamma}_{n,A}}{(1-n)\gamma_{n,A}}\bigg|_{t=0} = \frac{-2n(\Delta B)^2\,\mathrm{Tr}_A\left[\rho_A^{n-1}\left[\hat{A},\rho_A\right]\hat{A}\right]}{(n-1)\,\mathrm{Tr}_A\left[\rho_A^n\right]}, \tag{5.18}$$

and likewise for system B.[1] In ([107]) we assumed the absence of free Hamiltonians of either subsystem. In fact, as we now showed in Section 5.2, these results hold even with free Hamiltonians as they do not contribute to second order in the evolution of γ.

In order to obtain the leading derivative of the von Neumann entropy, we must now evaluate Eq. (5.18) in the limit $n \to 1$. We will first attempt to find an analytic expression for the second time derivative as $n \to 1$. This limit exists, except for states possessing one or more vanishing eigenvalues. To see this, let us first set $n = 1+\varepsilon$, and re-express Eq. (5.18) accordingly. We have

$$\ddot{H}_{1+\varepsilon}(A)|_{t=0} = \frac{-2(1+\varepsilon)(\Delta B)^2\,\mathrm{Tr}_A\left[\rho_A^{\varepsilon}\left[\hat{A},\rho_A\right]\hat{A}\right]}{\varepsilon\,\mathrm{Tr}_A\left[\rho_A^{1+\varepsilon}\right]}, \tag{5.19}$$

which we may re-express as:

$$\ddot{H}_{1+\varepsilon}(A)|_{t=0} = \frac{-2(1+\varepsilon)(\Delta B)^2\,\mathrm{Tr}_A\left[\exp\left(\varepsilon\log\rho_A\right)\left[\hat{A},\rho_A\right]\hat{A}\right]}{\varepsilon\,\mathrm{Tr}_A\left[\rho_A^{1+\varepsilon}\right]}. \tag{5.20}$$

[1] The simplicity of Eq. (5.18) highlights the advantage of this perturbative approach. By contrast, in Appendix 10.1 we demonstrate the complexity arising in an exact calculation, from which expressions of this kind cannot be straight-forwardly derived.

Let us now consider the trace term in the numerator. It can be expanded as a power series in ε:

$$\mathrm{Tr}_A\left[\exp\left(\varepsilon\log\rho_A\right)\left[\hat{A},\rho_A\right]\hat{A}\right] = \mathrm{Tr}_A\left[(1+\varepsilon\log\rho_A+...)\left[\hat{A},\rho_A\right]\hat{A}\right]. \tag{5.21}$$

Note that, due to the cyclicity of the trace, the first term in this expansion vanishes since

$$\mathrm{Tr}_A\left[\left[\hat{A},\rho_A\right]\hat{A}\right] = \mathrm{Tr}_A\left[\hat{A}\rho_A\hat{A}\right] - \mathrm{Tr}_A\left[\rho_A\hat{A}\hat{A}\right] = 0. \tag{5.22}$$

Hence, prior to taking any limits, Eq. (5.19) can be written as:

$$\begin{aligned}\ddot{H}_{1+\varepsilon}(A)|_{t=0} &= \frac{-2(1+\varepsilon)(\Delta B)^2\,\mathrm{Tr}_A\left[\left(\varepsilon\log\rho_A+\mathcal{O}(\varepsilon^2)\right)\left[\hat{A},\rho_A\right]\hat{A}\right]}{\varepsilon\,\mathrm{Tr}_A\left[\rho_A^{1+\varepsilon}\right]},\\ &= \frac{-2(1+\varepsilon)(\Delta B)^2\,\mathrm{Tr}_A\left[\left(\log\rho_A+\mathcal{O}(\varepsilon)\right)\left[\hat{A},\rho_A\right]\hat{A}\right]}{\mathrm{Tr}_A\left[\rho_A^{1+\varepsilon}\right]}.\end{aligned} \tag{5.23}$$

For density matrices ρ_A whose eigenvalues are all nonzero, we obtain an analytic expression for the limit $\varepsilon \to 0$:

$$\ddot{H}_1(A)|_{t=0} = -2(\Delta B)^2\,\mathrm{Tr}_A\left[\log\rho_A\left[\hat{A},\rho_A\right]\hat{A}\right], \tag{5.24}$$

It can be re-expressed in terms of the eigenvalues (λ_i) of ρ_A:

$$\ddot{H}_1(A)|_{t=0} = -2(\Delta B)^2\sum_{i,j}\log(\lambda_j)(\lambda_i-\lambda_j)|a_{ij}|^2. \tag{5.25}$$

Taking the limit $n \to 1$ (or equivalently $\varepsilon \to 0$) is non-trivial for states ρ_A possessing a vanishing eigenvalue. In fact, if ρ_A possesses a vanishing eigenvalue then we cannot neglect higher order terms in the above expansion, as this would require that the matrix elements of $\varepsilon\log(\rho_A)$ are $<< 1$. The problem for states with a vanishing eigenvalue, say λ, arises from the noncommutativity of the two limits $\varepsilon \to 0$ and $\lambda \to 0$. To see this, let us consider the trace term in the numerator of Eq. (5.19), expressed in the eigenbasis of ρ_A:

$$\mathrm{Tr}_A\left[\rho_A^{\varepsilon}\left[\hat{A},\rho_A\right]\hat{A}\right] = \sum_{i,j}\lambda_j^{\varepsilon}(\lambda_i-\lambda_j)|a_{ij}|^2 = \sum_{i,j}(\lambda_j^{\varepsilon}\lambda_i-\lambda_j^{1+\varepsilon})|a_{ij}|^2. \tag{5.26}$$

The right hand side of the above equation illustrates the issue at hand. Namely, we must consider the term λ^{ε}, as both quantities tend to zero. However,

$$\lambda^{\varepsilon} = \begin{cases}0, & \text{for } \lambda = 0, \varepsilon > 0\\ 1, & \text{for } \lambda > 0, \varepsilon = 0\end{cases} \tag{5.27}$$

In Appendix 10.3, we numerically illustrate the small ε and λ behavior of the trace term. The noncommutativity of the two limits $\varepsilon \to 0$ and $\lambda \to 0$ is a kind of instability in the sense that dimensions in the Hilbert space which initially have zero probability tend to immediately become populated. An initial divergence does not imply that their corresponding probability increases to a large value, but merely that the rise possesses a large acceleration initially. We discuss this further in Appendix 10.5.

To summarize our findings so far: when System A (of Fig. 5.1) possesses only finite eigenvalues $\{\lambda_i\}$, we obtain a well defined limit of $\ddot{H}_{1+\varepsilon}(A)|_{\underset{t=0}{\cdot}}$ as $\varepsilon \to 0$, i.e., for the von Neumann entropy. Conversely, as one or more $\lambda_i \to 0$, $\ddot{H}_{1+\varepsilon}(A)$ diverges. This includes the case where all eigenvalues but one approach zero, i.e., a pure state. Hence, while the von Neumann entropy itself always approaches a finite limit when one or more eigenvalues tend to zero, its second time derivative does not necessarily do so, see Appendix 10.2.

This fact is important also because, in the setup illustrated in Fig. 5.1, system B is initially pure by design, i.e., ρ_B initially possesses some vanishing eigenvalues. Consequently, the leading order change in the coherent information diverges irrespective of the state of System A, due to the presence of $\ddot{S}(B)$ in the expression. Indeed, there are a number of further subtleties associated with the perturbative expansion, which we discuss in Appendix 10.5.

In the next section, we therefore introduce a generalisation of the coherent information which is stable as it does not require the taking of the limit $\epsilon \to 0$.

5.5 Generalisation: n-Coherent Information, n-Durability and n-Exposure

In the previous section we demonstrated that the leading order change in the coherent information suffers a divergence (see Fig. 5.1) tracing back to the fact that the coherent information is conventionally defined as the difference of von Neumann entropies with the von Neumann entropy being the potentially divergent limit as $n \to 1$ of the class of n-Rényi entropies. In this section, we therefore generalise the notion of coherent information to the entire class of n-Rényi entropies. In the literature, studies of the wider class of n-Rényi entropies are greatly increasing in significance due to the usefulness of these entropies in extracting information about the entanglement spectrum of a quantum system, providing richer information than the von Neumann entropy alone [86, 116]. We note also that work is ongoing in developing novel entanglement measures from the Rényi entropies [158, 150, 168].

5.5.1 The n-Coherent Information

We now define the class of n-coherent informations, I_n, based on the n-Rényi entropy, through

$$I_n^d = H_n(A') - H_n((A\tilde{A})') = H_n(A') - H_n(B'), \tag{5.28}$$

$$I_n^c = H_n(B') - H_n((B\tilde{A})') = H_n(B') - H_n(A'), \tag{5.29}$$

where the superscripts d and c refer to the direct and complementary channels, respectively. In particular, we have:

$$I_n^d = -I_n^c \tag{5.30}$$

To see this, recall that the two reduced density matrices of two subsystems making up a pure system possess the same nonzero eigenvalues including their multiplicities. The 1-coherent information is the traditional coherent information based on the von Neumann entropy.

As we now show, for integer $n > 1$ the leading order change of the n-coherent information remains well-defined across the whole state space of System A, in contrast to the 1-coherent information. Furthermore, as we will discuss, the n-Rényi entropies may themselves serve as measures of quantum correlations.

5.5.2 The n-Durability

To evaluate the leading order time evolution of the n-coherent information, let us recast Eq. (5.18) in the form

$$\ddot{H}_n(A)|_{t=0} = \frac{2n(\Delta B)^2 D_{n,A}}{(n-1)}, \tag{5.31}$$

where we defined $D_{n,A}$ as:

$$D_{n,A} := -\frac{\mathrm{Tr}_A\left[\rho_A^{n-1}\left[\hat{A},\rho_A\right]\hat{A}\right]}{\gamma_{n,A}}. \tag{5.32}$$

We will refer to the quantity $D_{n,A}$ as the 'n-durability', for reasons which will become clear as we progress. First, we restrict our attention to integer $n \geq 1$ and we notice that the n-durability is a strictly positive quantity. To see this, consider the trace term as expressed in terms of the eigenvalues of the ρ_A:

$$\mathrm{Tr}_A\left[\rho_A^{n-1}\left[\hat{A},\rho_A\right]\hat{A}\right] = \sum_{i,j}\lambda_j^{n-1}(\lambda_i - \lambda_j)|a_{ij}|^2. \tag{5.33}$$

Noting that $0 \leq \lambda_i \leq 1$, let us consider two eigenvalues, λ_x and λ_y with $\lambda_x < \lambda_y$. We will therefore have a positive contribution to the sum of the form $\lambda_x^{n-1}(\lambda_y - \lambda_x)|a_{xy}|^2$. However, we then also have a negative contribution to the sum of the form $-\lambda_y^{n-1}(\lambda_y - \lambda_x)|a_{xy}|^2$. This negative contribution always outweighs the positive contribution as $\lambda_y^{n-1} > \lambda_x^{n-1}$. Hence, the n-durability defined with the negative sign as in Eq. (5.32) obeys $D_{n,A} \geq 0$.

Not only is the n-durability a positive quantity, it also has the useful property that it reduces to the variance in the case of pure states. To see this, we note that if ρ_A is pure then $\rho_A^2 = \rho_A$, and

$$\begin{aligned} D_{n,A} = -\frac{\mathrm{Tr}_A\left[\rho_A^{n-1}\left[\hat{A},\rho_A\right]\hat{A}\right]}{\mathrm{Tr}_A[\rho_A^n]} &= -\frac{\mathrm{Tr}_A\left[\rho_A\left[\hat{A},\rho_A\right]\hat{A}\right]}{\mathrm{Tr}_A[\rho_A]} \\ &= -\mathrm{Tr}_A\left[\rho_A\hat{A}\rho_A\hat{A}\right] + \mathrm{Tr}_A\left[\rho_A\hat{A}^2\right] \\ &= -\sum_i \Big(\langle i|\,|\psi\rangle\,\langle\psi|\,\hat{A}\,|\psi\rangle\,\langle\psi|\,\hat{A}\,|i\rangle - \langle i|\,|\psi\rangle\,\langle\psi|\,\hat{A}^2\,|i\rangle \Big) \\ &= \langle\psi|\,\hat{A}^2\,|\psi\rangle - \langle\psi|\,\hat{A}\,|\psi\rangle^2 \\ &= (\Delta A)^2, \end{aligned} \tag{5.34}$$

where we defined $\rho_A = |\psi\rangle\langle\psi|$ and $\{|i\rangle\}$ is a set of orthonormal basis vectors, one of which can be chosen equal to $|\psi\rangle$. Hence:

$$D_{n,A} \xrightarrow{\text{purity}} (\Delta A)^2. \tag{5.35}$$

We note here already that the variance does not constitute a bound on the n-durability, as we will explicitly see later.

Let us now consider the role that the n-durability plays in the early time evolution of the n-coherent information. The leading order change in the n-coherent information of the direct channel (δI_n^d) is given by

$$\begin{aligned} \delta I_n^d &= \frac{t^2}{2}\left(\ddot{H}_n(A)\big|_{t=0} - \ddot{H}_n(B)\big|_{t=0}\right) \\ &= \frac{nt^2}{n-1}\Big((\Delta B)^2 D_{n,A} - (\Delta A)^2 D_{n,B}\Big) \\ &= -\frac{nt^2(\Delta B)^2}{n-1}\Big((\Delta A)^2 - D_{n,A}\Big), \end{aligned} \tag{5.36}$$

Here, we used the fact that System B is pure at $t = 0$ such that, through Eq. (5.35), $D_{n,B} = (\Delta B)^2$. By the same reasoning, we see that if system A is pure, then $D_{n,A} = (\Delta A)^2$ and $\delta I_n^d = 0$, as expected.[2]

5.5.3 The n-Exposure

Eq. (5.36) demonstrates that it is not merely the overall amount of quantum correlations that system A initially possesses with the ancilla $\tilde{A}$ which determines the rate at which the n-coherent information changes at the onset of interaction. Rather, the n-coherent information is sensitive to the amount of system A's entanglement which is 'exposed' to the action of interaction Hamiltonian, as determined by the difference between the variance and the n-durability. We will therefore refer to this difference as the 'n-exposure', $E_{n,A}$:

$$E_{n,A} := \Big((\Delta A)^2 - D_{n,A}\Big) \tag{5.37}$$

We see from Eq. (5.35) that in the case that system A is pure, $E_{n,A}$ is zero. This is of course to be expected because if system A does not possess quantum correlations with $\tilde{A}$ to begin with, then no quantum correlations can be transferred during the interaction and the n-coherent information should not change. Conversely, if system A possesses quantum correlations with $\tilde{A}$, the exposure is, in general, non-zero.

However, as we anticipated, the value of the n-exposure depends not only on the absolute extent to which System A is entangled or quantum correlated with $\tilde{A}$, but also on the extent to which these quantum correlations are 'accessible' or 'exposed' to the operator $\hat{A}$ in the interaction Hamiltonian. For illustration, consider the following scenario:

Let system A be comprised of two subsystems, A_1 and A_2, with a bipartite density matrix of the form $\rho_{A_1} \otimes \rho_{A_2}$. Assume that operator $\hat{A}$ acts only on system A_1, such that we may represent the operator on the Hilbert space of A_1 and A_2 as $\hat{A}_1 \otimes \hat{\mathbb{I}}_2$. Let us now evaluate the numerator and denominator of $D_{n,A}$. The numerator is given by:

$$\begin{aligned}
&\mathrm{Tr}_{A_1}\,\mathrm{Tr}_{A_2}\left[\rho_{A_1}^{n-1} \otimes \rho_{A_2}^{n-1}\big[\hat{A}_1 \otimes \hat{\mathbb{I}}_2, \rho_{A_1} \otimes \rho_{A_2}\big]\hat{A}_1 \otimes \hat{\mathbb{I}}_2\right] \\
&= \mathrm{Tr}_{A_1}\,\mathrm{Tr}_{A_2}\left[\rho_{A_1}^{n-1}\big[\hat{A}_1, \rho_{A_1}\big]\hat{A}_1 \otimes \rho_{A_2}^{n}\right] \\
&= \mathrm{Tr}_{A_1}\left[\rho_{A_1}^{n-1}\big[\hat{A}_1, \rho_{A_1}\big]\hat{A}_1\right]\mathrm{Tr}_{A_2}\left[\rho_{A_2}^{n}\right],
\end{aligned} \tag{5.38}$$

[2] See Appendix 10.5 for a discussion of the non-trivial limit of Eq. (5.36) as $n \to 1$.

while the denominator (n-purity) is given by:

$$\begin{aligned}\gamma_{n,A} &= \mathrm{Tr}_{A_1}\,\mathrm{Tr}_{A_2}\left[\rho_{A_1}^n \otimes \rho_{A_2}^n\right] \\ &= \mathrm{Tr}_{A_1}\left[\rho_{A_1}^n\right]\mathrm{Tr}_{A_2}\left[\rho_{A_2}^n\right].\end{aligned} \tag{5.39}$$

Hence, the $\mathrm{Tr}_{A_2}\left[\rho_{A_2}^n\right]$ terms cancel in the numerator and denominator, and we find that

$$E_{n,A} = (\Delta A)^2 - D_{n,A_1}, \tag{5.40}$$

where, as it should be, the only contribution to the variance comes from system A_1. Hence, there even exist extreme cases in which system A overall is highly entangled with system $\tilde{A}$ (from Fig. 5.1), but where this entanglement can be entirely accounted for by subsystem A_2 while subsystem A_1 may not be entangled with $\tilde{A}$ at all. In this case, while system A as a whole is highly entangled with the ancilla $\tilde{A}$, the degree to which that entanglement is 'exposed' to the action of the operator $\hat{A}$ is vanishing, since operator $\hat{A}$ has non-trivial action only on subsystem A_1. Notice that, due to our results in Section 5.2, remarkably, this conclusion holds true, to second order in time, even in the presence of free Hamiltonians on system A, which generically includes an interaction between A_1 and A_2.

5.5.4 Properties of the n-Exposure

The n-exposure determines the leading order change of the n-coherent information of the direct and complementary channels that arise at the onset of the interaction of systems A and B. Intuitively, the n-exposure is the extent to which pre-existing entanglement between A and $\tilde{A}$ is 'exposed' to the interaction Hamiltonian of A and B. The higher the exposure, the faster the coherent informations of the direct and complementary channels change at the onset of the interaction. We found that, in the case of interaction Hamiltonians of the form $\hat{A} \otimes \hat{B}$, the n-exposure is the difference between two terms: $E_{n,A} = (\Delta A)^2 - D_{n,A}$, where $(\Delta A)^2$ is the variance in the observable $\hat{A}$ and where $D_{n,A}$ is the n-durability of system A. Both are properties of system A only: to calculate the n-exposure of system A merely requires knowledge of the operator $\hat{A}$ of the interaction Hamiltonian and the initial reduced density matrix, ρ_A.

For initially pure states of A, the n-durability equals the variance, i.e., the n-exposure vanishes for pure states. For initial states of A that are mixed, the n-durability can be smaller than the variance. In this case, the n-exposure is positive, implying that the n-coherent information of the complementary channel rises while, due to Eq. (5.30), that of

the direct quantum channel drops at the onset of the interaction. Conversely, there also exist initial mixed states of A for which the n-durability exceeds the variance. In such cases, the n-exposure is negative, and the n-coherent information of the complementary channel drops while that of the direct channel rises at the onset of the interaction.

To further illustrate the significance of negative and positive changes in the n-coherent information, let us consider the example of $n = 2$. For $n = 2$, the n-Rényi entropy is a simple function of the purity, $\mathrm{Tr}[\rho^2]$,

$$H_2(A) = -\log(\gamma_{2,A}), \tag{5.41}$$

where γ_2 is the purity. The purity is useful in that even for mixed bipartite states it is possible to prove that entanglement exists between the subsystems if the purity of one subsystem is lower than the purity of the bipartite system as a whole [79, 86]. In our case, if

$$\gamma_2(A) < \gamma_2(\tilde{A}A), \tag{5.42}$$

or equivalently,

$$H_2(A) > H_2(\tilde{A}A), \tag{5.43}$$

then entanglement must exist between subsystems A and $\tilde{A}$. In fact, the same inequality applies for any n-Rényi entropy [78]. This inequality is known to be a valuable tool to infer the presence of entanglement under non-ideal experimental conditions [127]. Furthermore, we note that the 2-Rényi entropy provides a direct lower bound on the von Neumann entropy, while stricter bounds can be obtained using higher order Rényi entropies [45]:

$$H_1(A) \geq H_2(A), \tag{5.44}$$

$$H_1(A) \geq 2H_2(A) - H_3(A). \tag{5.45}$$

Hence, the n-coherent information behaves similarly to the traditional 1-coherent information in the sense that positivity indicates the presence of quantum correlations. In order, for example, to prevent loss of quantum correlations to an environment system B, it is advisable to avoid input states for which the n-coherent information decreases to leading order. This is to prevent the n-coherent information from becoming negative, at which point we would no longer fulfill inequality Eq. (5.43) that guarantees bipartite entanglement between A and $\tilde{A}$. Meanwhile, input states which lead to an increase in the n-coherent information are desirable, as they provide a 'safe zone' in which the inequality is increasingly fulfilled.

Therefore, while the n-coherent information does not constitute a direct measure of bipartite entanglement, its behavior does provide an indication of which input states of A

are more or less vulnerable to losing quantum correlations with $\tilde{A}$ to an environment, B. Indeed, in order to obtain the quantum channel capacity from the coherent information, one maximises over all possible input states of the $\tilde{A}A$ system and over multiple parallel uses of the channel. In this optimisation, some states will induce a positive change in the coherent information, while others will lead to a negative change. The preferred input state depends on whether the desired outcome is the transmission or retention of pre-existing quantum correlations between A and $\tilde{A}$.

In the next section, we will apply the notion of n-coherent information to the light-matter interaction. We will explore how the leading order behaviour of the n-coherent information, as determined by the n-exposure, varies with the input state. We will focus on the $n = 2$ case for simplicity, but note that a similar analysis can be performed straightforwardly for other n.

5.6 Application to the Light-Matter Interaction

In practice, much of quantum communication relies upon the interaction between light and matter. In this section, we apply our results to a simplified model of the light-matter interaction, namely the Unruh-De Witt model. At its core, this model describes a quantum system coupled to a massless scalar field. Many variations of this model exist, and are applied across a broad range of applications [125, 165, 77]. In the present context, we consider a particularly simple variation of this model in which a stationary qubit interacts with a single mode of a quantum field. The qubit and the field are chosen initially unentangled and in a product state $\rho_f \otimes \rho_q$. We assume the initial state of the field, ρ_f, to be the vacuum state $\rho_f = |0\rangle\langle 0|$. We allow the initial state, ρ_q, of the qubit to be arbitrary. Expressed in terms of the eigenstates of the σ_z Pauli operator it reads

$$\rho_q = \delta |z^+\rangle\langle z^+| + \alpha |z^+\rangle\langle z^-| + \alpha^* |z^-\rangle\langle z^+| + (1-\delta) |z^-\rangle\langle z^-|, \tag{5.46}$$

where $\sigma_z |z^+\rangle = |z^+\rangle$ and $\sigma_z |z^-\rangle = -|z^-\rangle$. We then consider the interaction of a single field mode with the qubit, governed by an interaction Hamiltonian H_{int} of the form

$$H_{\text{int}} = \nu \sigma_z \otimes (a + a^\dagger) \tag{5.47}$$

where a and $a^\dagger$ are the annihilation and creation operators of the mode considered and where ν is the effective coupling constant. Since we will neglect the free Hamiltonians, we can set $\nu = 1$ and instead absorb the ν-dependence in the t-dependence. We will now solve the problem non-perturbatively in order to then obtain an exact expression for the time

evolution of the n-Rényi entropy, and compare its second time derivative to our Eq. (5.18). Note that while the particularly simple form of the interaction Hamiltonian invoked here allows for a non-perturbative calculation to be performed, this is not always the case. See Appendix 10.1 for details.

We first express the time-evolved system as:

$$\rho(t) = e^{it\sigma_z \otimes (a+a^\dagger)}(\rho_q \otimes \rho_f)e^{-it\sigma_z \otimes (a+a^\dagger)}. \tag{5.48}$$

For the density matrix of the qubit this gives, see [107] for details:

$$\rho_q(t) = \delta \left|z^+\right\rangle \left\langle z^+\right| + \alpha e^{-2t^2} \left|z^+\right\rangle \left\langle z^-\right| + \alpha^* e^{-2t^2} \left|z^-\right\rangle \left\langle z^+\right| + (1-\delta) \left|z^-\right\rangle \left\langle z^-\right|. \tag{5.49}$$

Working in the eigenbasis of the qubit, we have:

$$H_n(\rho_q(t)) = \frac{1}{1-n} \log \left(\sum_i \lambda_i^n \right), \tag{5.50}$$

$$\dot{H}_n(\rho_q(t)) = \frac{\sum_i n\lambda_i^{n-1}\dot{\lambda}_i}{\sum_i \lambda_i^n}, \tag{5.51}$$

$$\ddot{H}_n(\rho_q(t)) = \frac{1}{1-n} \left(\frac{\sum_i \left(n(n-1)\lambda_i^{n-2}\dot{\lambda}_i^2 + n\lambda_i^{n-1}\ddot{\lambda}_i \right)}{\sum_i \lambda_i^n} - \frac{\left(\sum_i n\lambda_i^{n-1}\dot{\lambda}_i \right)^2}{\left(\sum_i \lambda_i^n \right)^2} \right). \tag{5.52}$$

Let us therefore consider the eigenvalues of $\rho_q(t)$. Diagonalising Eq. (5.49), we obtain:

$$\lambda^\pm(t) = \frac{1 \pm \sqrt{1 - 4(\delta - \delta^2 - |\alpha|^2 e^{-4t^2})}}{2}, \tag{5.53}$$

such that

$$\dot{\lambda}^\pm(t) = \mp \frac{8|\alpha|^2 t e^{-4t^2}}{\sqrt{1 - 4(\delta - \delta^2 - |\alpha|^2 e^{-4t^2})}}, \tag{5.54}$$

and

$$\ddot{\lambda}^\pm(t) = \mp \left(\frac{8|\alpha|^2 e^{-4t^2}(1 - 8t^2)}{\sqrt{1 - 4(\delta - \delta^2 - |\alpha|^2 e^{-4t^2})}} + \frac{128|\alpha|^4 t^2 e^{-8t^2}}{\left(1 - 4(\delta - \delta^2 - |\alpha|^2 e^{-4t^2})\right)^{3/2}} \right). \tag{5.55}$$

From here, we readily see that $\dot{\lambda}^{\pm}|_{t=0} = 0$, such that

$$\ddot{H}_n(\rho_q(t=0)) = \frac{n\sum_i \lambda_i^{n-1}\ddot{\lambda}_i}{(1-n)\sum_i \lambda_i^n}\bigg|_{t=0}, \tag{5.56}$$

where

$$\ddot{\lambda}^{\pm}\big|_{t=0} = \mp\frac{8|\alpha|^2}{\sqrt{1-4(\delta-\delta^2-|\alpha|^2)}} \tag{5.57}$$

Denoting the $t=0$ eigenvalues as $\lambda^{\pm}$, we finally obtain:

$$\ddot{H}_n(\rho_q(t=0)) = \frac{-8n|\alpha|^2\big(\lambda^{-n-1}-\lambda^{+n-1}\big)}{\big(n-1\big)\big(\lambda^+-\lambda^-\big)\big(\lambda^{-n}+\lambda^{+n}\big)} \tag{5.58}$$

Let us now compare this result to Eq. (5.18). In Eq. (5.18), all quantities are evaluated at $t=0$. Therefore, we simply work with the initial qubit state ρ_q. In order to then evaluate Eq. (5.18), we re-express the system in the eigenbasis of ρ_q. We have:

$$\lambda^{\pm} = \frac{1\pm\sqrt{1-4(\delta-\delta^2-|\alpha|^2)}}{2}, \tag{5.59}$$

$$|\lambda^+\rangle = \frac{1}{\sqrt{1+|x|^2}}\Big(|z^+\rangle + x\,|z^-\rangle\Big), \qquad |\lambda^-\rangle = \frac{1}{\sqrt{1+|y|^2}}\Big(|z^+\rangle + y\,|z^-\rangle\Big), \tag{5.60}$$

where

$$x := \frac{-(\delta-\lambda^+)}{\alpha}, \qquad y := \frac{1-(\delta+\lambda^+)}{\alpha}. \tag{5.61}$$

We may now re-express $\sigma_z = |z^+\rangle\langle z^+| - |z^-\rangle\langle z^-|$ in terms of the eigenbasis of ρ_q. We have:

$$\begin{aligned}\sigma_z = \frac{1}{|x-y|^2}\Big(&(1+|x|^2)(|y|^2-1)\,|\lambda^+\rangle\langle\lambda^+| \\ &+\sqrt{(1+|x|^2)(1+|y|^2)}(1-yx^*)\,|\lambda^+\rangle\langle\lambda^-| \\ &+\sqrt{(1+|x|^2)(1+|y|^2)}(1-xy^*)\,|\lambda^-\rangle\langle\lambda^+| \\ &+(1+|y|^2)(|x|^2-1))\,|\lambda^-\rangle\langle\lambda^-|\Big).\end{aligned} \tag{5.62}$$

Working in this eigenbasis, we have:

$$\mathrm{Tr}_q\Big[\rho_q^{n-1}[\sigma_z,\rho_q]\sigma_z\Big] = \sum_{i,j}\lambda_j^{n-1}(\lambda_i-\lambda_j)|\sigma_{zij}|^2$$

$$= \left(\lambda^{-n-1} - \lambda^{+n-1}\right)\left(\lambda^{+} - \lambda^{-}\right)|\sigma_{z+-}|^2$$
$$= \frac{4|\alpha|^2\left(\lambda^{-n-1} - \lambda^{+n-1}\right)}{\left(\lambda^{+} - \lambda^{-}\right)}, \tag{5.63}$$

where the characteristic equation, $\lambda^{+2} - \lambda^{+} + \delta - \delta^2 - |\alpha|^2 = 0$, is used to convert the σ_z components into expressions in terms of $\lambda^{\pm}$. Taking into account that the field variance in this case is 1, and substituting the above result into Eq. (5.18), we again arrive at Eq. (5.58) for $\ddot{H}_n(\rho_q(t=0))$, which indeed confirms the validity of the perturbative approach we have employed in the previous sections.

Using these non-perturbatively verified results, we can assess how the n-exposure depends upon the precise configuration of the qubit. We have:

$$E_{n,q} = (\Delta\sigma_z)^2 - D_{n,q} = 4(\delta - \delta^2) + \frac{4|\alpha|^2\left(\lambda^{-n-1} - \lambda^{+n-1}\right)}{\left(\lambda^{+} - \lambda^{-}\right)\left(\lambda^{-n} + \lambda^{+n}\right)}. \tag{5.64}$$

From this expression, we see that the n-exposure does not depend on the phase of α. Indeed, the n-exposure can be expressed in terms of δ and $|\alpha|^2$ alone.

As discussed in Section 5.4, the leading order behaviour of the $n \to 1$ coherent information is non-trivial. This is due to the divergence in the second time derivative of the von Neumann entropy of the environment system.[3] Hence, we will restrict our attention to $n > 1$ and choose the simplest case ($n = 2$) to illustrate the features of the n-exposure. In Fig. 5.2, we present a contour plot of the 2-exposure as a function of these two variables.[4] We also include isocurves of the 2-Rényi entropy. Crucially, we see that the isocurves of the exposure follow different trajectories to the isocurves of the entropy through the $(\delta, |\alpha|^2)$ plane. This illustrates that the leading order change in the 2-coherent information is not simply a function of the total amount of entanglement present, but depends upon the precise configuration of the qubit. The right hand side of Fig. 5.2 highlights this phenomenon by plotting the variation in the 2-exposure along isocurves of constant 2-Rényi entropy.

One may also consider the n-exposure of the qubit in the Bloch sphere representation. We first set:

$$\rho_q = \frac{1}{2}(\mathbb{I} + a_x\sigma_x + a_y\sigma_y + a_z\sigma_z), \tag{5.65}$$

[3]Note that the divergent second derivative does not imply a divergence in the von Neumann entropy itself - see Appendix 10.2.

[4]Note that the positivity of the eigenvalues requires $|\alpha|^2 \leq \delta - \delta^2$.

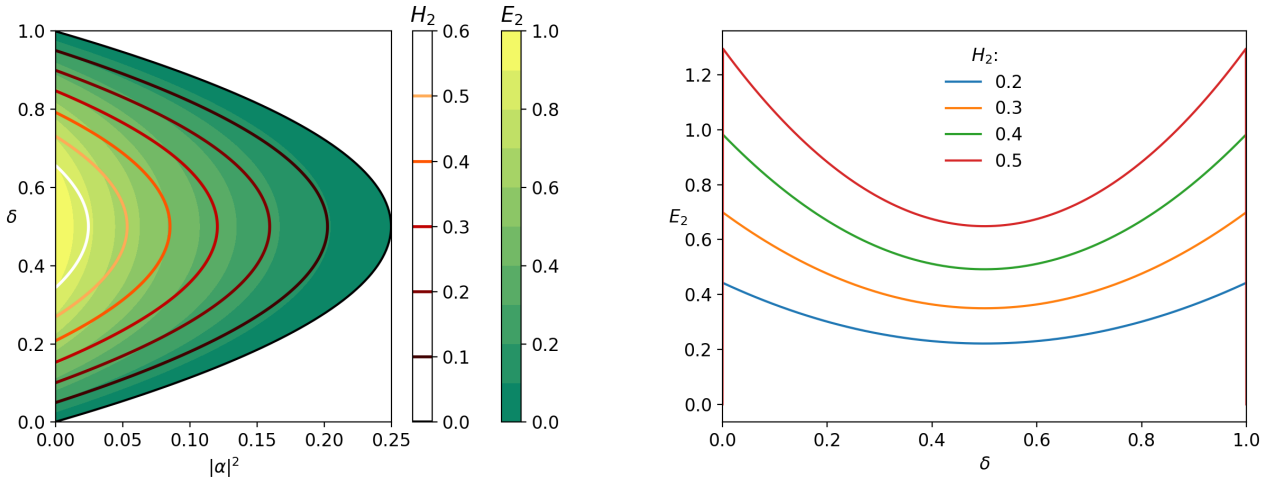

Figure 5.2: Left: contour plot of the 2-exposure of the qubit across the $(\delta, |\alpha|^2)$ plane (green). Also included are contours of the 2-Rényi entropy, which do not align with the 2-exposure contours. Right: variation in the 2-exposure as a function of δ for constant values of 2-Rényi entropy.

where the Bloch vector is $\vec{a} = (a_x, a_y, a_z)$. This then leads to the following transformation:

$$\delta = \frac{1 + a_z}{2}, \qquad |\alpha|^2 = \frac{|a_x|^2 + |a_y|^2}{4}. \tag{5.66}$$

We may use these expressions to convert Fig. 5.2 into the Bloch sphere representation. We note that in this representation, the exposure is independent of the phase in the (a_x, a_y) plane, so that it is sufficient to plot only a cross section in the (a_x, a_z) plane. We illustrate the 2-exposure in the Bloch sphere representation in Fig. 5.3. Again, we also plot isocurves of the 2-Rényi entropy to illustrate that the exposure is a non-trivial function of the distribution of the entanglement in the state space of the qubit.

In particular, we note that in order to minimise exposure at the onset of an interaction, we should tune the distribution of the entanglement in the initial system. In this example we see from Fig. 5.3 that for the same initial 2-Rényi entropy, the 2-exposure is minimised along the a_x axis, while it is maximised along the a_z axis. This indicates the optimal state of the qubit in the Bloch sphere representation in order to minimise the leading order change in the second Rényi entropy. The same analysis can be applied to more complex systems in order to identify the ideal initial configuration for the minimisation or maximisation of the exposure.

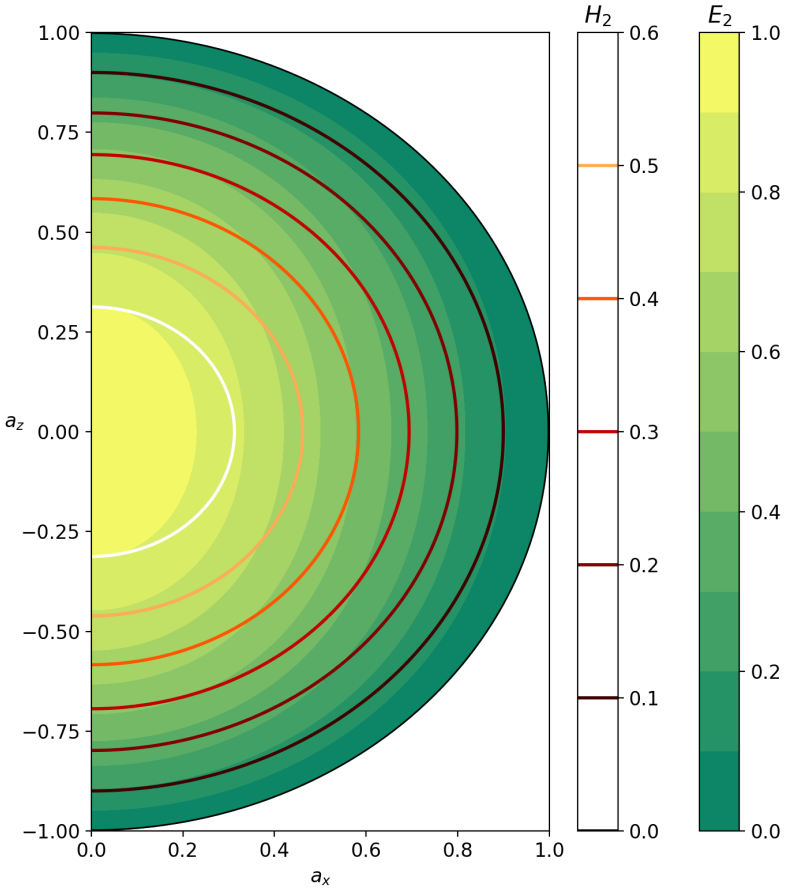

Figure 5.3: 2-exposure of the qubit in the Bloch sphere representation. Again we see that the isocurves of the 2-Rényi entropy are disaligned with those of the exposure, indicating that it is not simply the amount of entanglement, but the way in which it is distributed that determines the exposure. In this case, if avoidance of transmission is desired then the equatorial direction is 'safer' than the polar direction.

Fig. 5.2 and Fig. 5.3 illustrate that in the qubit case, the 2-exposure is always positive. This is due to the simplicity of the qubit state space. In the next section, however, we will consider a qutrit system, for which the higher dimensionality leads to more complex results.

5.7 Application to Qutrit Systems

In this section, we provide a visualisation of the 2-exposure for a simple qutrit system. As we augment the qutrit density matrix, we will see how the exposure can vary in non-trivial ways, and in particular, that it can change sign. To this end, let us first consider the general form of the qutrit density matrix:

$$\rho = \begin{pmatrix} \omega_x & \frac{-ia_z - q_z}{2} & \frac{-ia_y - q_y}{2} \\ \frac{ia_z - q_z}{2} & \omega_y & \frac{-ia_x - q_x}{2} \\ \frac{ia_y - q_y}{2} & \frac{ia_x - q_x}{2} & \omega_z \end{pmatrix}. \tag{5.67}$$

While this generic qutrit state possesses eight degrees of freedom, we may restrict our attention to the case where all off-diagonal matrices are purely imaginary ($q_j = 0$). We then have:

$$\rho = \begin{pmatrix} \omega_x & \frac{-ia_z}{2} & \frac{-ia_y}{2} \\ \frac{ia_z}{2} & \omega_y & \frac{-ia_x}{2} \\ \frac{ia_y}{2} & \frac{ia_x}{2} & \omega_z \end{pmatrix}, \tag{5.68}$$

where $0 \leq a_j \leq 1$, $0 \leq \omega_j \leq 1$, and $\sum_j \omega_j = 1$. The non-negativity of this simplified density matrix is ensured through the following conditions [111]:

$$4\omega_j\omega_k \geq a_l^2, \tag{5.69}$$

$$4\omega_j\omega_k\omega_l \geq \omega_j a_j^2 + \omega_k a_k^2 + \omega_l a_l^2. \tag{5.70}$$

From here, we can simplify further by enforcing $\omega_j = \omega_k = \omega_l = 1/3$. In this case, conditions Eq. (5.69) and Eq. (5.70) can be re-written as a single condition, namely

$$\frac{4}{9} \geq a_x^2 + a_y^2 + a_z^2, \tag{5.71}$$

which describes a space of a_x, a_y, and a_z values enclosed by an octant of a sphere of radius $2/3$. Given a choice of an operator acting on the qutrit system, we may then examine the variation of the exposure as we move through this space of states.

The unitary dynamics of a qutrit can be described through a set of three different types of transformations [111]. Namely, rotations, single-axis twisting, and dual-axes counter-twisting. We can build the full space of Hamiltonians from the following three matrices:

$$S_x = \begin{pmatrix} 0 & 0 & 0 \\ 0 & 0 & -i \\ 0 & i & 0 \end{pmatrix}, \qquad S_y = \begin{pmatrix} 0 & 0 & i \\ 0 & 0 & 0 \\ -i & 0 & 0 \end{pmatrix}, \qquad S_z = \begin{pmatrix} 0 & -i & 0 \\ i & 0 & 0 \\ 0 & 0 & 0 \end{pmatrix}. \tag{5.72}$$

We may now calculate the 2-exposure for different qutrit configurations and different Hamiltonians according to Eq. (5.37). Since our space of possible states is a three-dimensional octant of a sphere, we represent the results as cross-sections in the (a_x, a_y) plane. In Section 5.7 we illustrate the exposure at the $a_z = 0.5$ plane for two arbitrary Hamiltonians. We also include isocurves of constant 2-Rényi entropy, demonstrating that the n-exposure is not simply dependent upon the total amount of entanglement present, but rather on the precise distribution of this entanglement. For each example Hamiltonian we also see that, depending upon the precise configuration of the input state, the 2-exposure can be either positive or negative, indicating, e.g., in the case where B is an environment, 'safe' and 'unsafe' configurations, respectively.

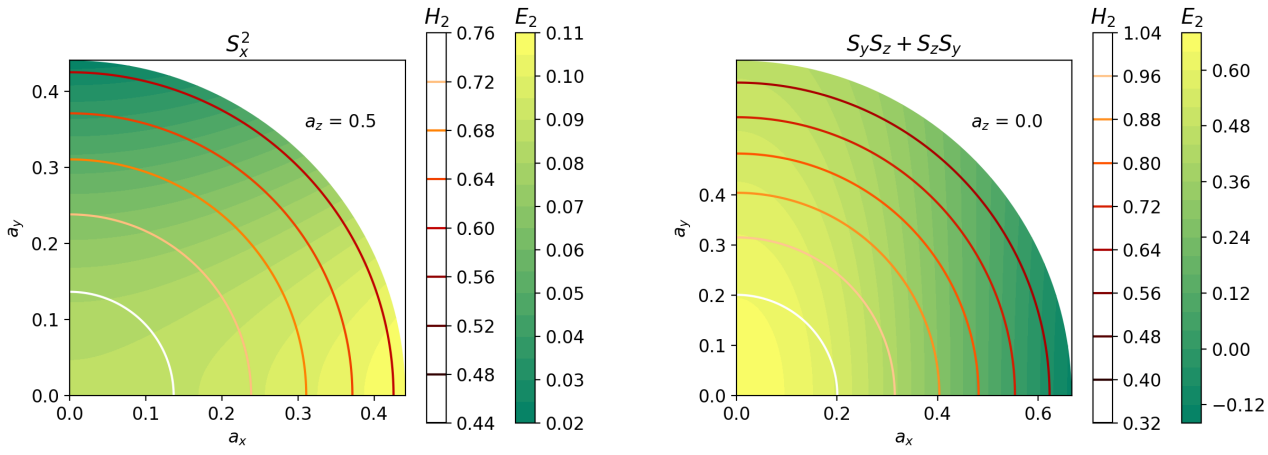

Figure 5.4: Left: 2-exposure across the a_x, a_y plane at $a_z = 0.5$ for the Hamiltonian S_x^2. Right: 2-exposure for the Hamiltonian $S_yS_z + S_zS_y$ across the a_x, a_y plane at $a_z = 0.0$. In this case we see regions of negative exposure. Also plotted are the 2-Rényi entropy isocurves.

5.8 Summary and Outlook

In this work, we have considered a setup where a system A is initially entangled with and purified by an ancilla $\tilde{A}$. System A then starts to interact with a system B and may, therefore, become entangled with B. Through the interaction, A may lose some of its quantum correlations with $\tilde{A}$ and B may acquire quantum correlations with $\tilde{A}$. We identified the maps of reduced density matrices, from A to A' and from A to B' (primes denoting a later time) the direct and the complementary channel respectively.

Because the quantum capacity of a quantum channel is defined by optimization of the coherent information over input states and parallel channel uses, we have calculated the leading order change in coherent information of each channel. This, in turn, poses a lower bound on the quantum channel capacity.

In quantum technologies, depending on the application, it can be desirable to maximize the direct channel, in order to protect existing quantum correlations from leakage to an environment B. Conversely, it may be desirable to maximize the complementary channel for purposes of quantum communication from A to B. It is therefore of interest to determine the factors which govern the leading order change in coherent information at the onset of a quantum channel, so that quantum systems may be initialised in a configuration most favourable to the application.

To calculate the leading order behaviour of the coherent information, we first showed that the free Hamiltonians do not contribute to leading (second) order. This dramatically simplifies the calculations, as the interaction Hamiltonian may be considered alone. Moreover, this has the important implication that resonance phenomena, which require free Hamiltonians, do not contribute to leading order. This is of particular significance in systems which make use of the light-matter interaction, in which resonance phenomena are commonly encountered. The significance of this finding will be investigated further in future work.

We then found that the leading order term in the perturbative expansion of the coherent information diverges when system B is initially pure. We therefore generalized the notion of coherent information to the family of n-coherent information, via the n-Rényi entropies. The n-coherent information is always regular for $n > 1$. Calculation of the dynamics of the n-coherent information, and therefore of the n-Rényi entropies, is desirable because it implicitly also determines the dynamics of the entire spectrum of the underlying density matrix. This is because the family of n-Rényi entropies (unlike the von Neumann entropy alone) is sufficient to reconstruct the spectrum of the density matrix.

A further, useful property of the n-coherent information arises from the fact that the

n-Rényi entropies of two subsystems that together constitute a pure supersystem are identical, as is the case also for the von Neumann entropy. Therefore, and because $H_n(\tilde{A})'' = 0$, calculating the leading order n-Rényi entropies and n-coherent informations of the direct and complementary channels implies also knowledge of the leading order of all other coherent informations that can be formed among the three subsystems $A, \tilde{A}, B$. For example, when $(H_n(A) - H_n(AB))$ becomes positive, this indicates that quantum correlations between A and B are becoming established, and we have $(H_n(A) - H_n(AB))'' = H_n(A)''$ since $H_n(AB)'' = H_n(\tilde{A})'' = 0$.

We then explicitly calculated the leading order time evolution of the $n-$coherent information of the direct and complementary channels, for the case of interaction Hamiltonians of the form $\hat{A} \otimes \hat{B}$ and showed that the leading order is determined by a quantity that we call the n-exposure. Intuitively, the n-exposure quantifies how much of the pre-existing quantum correlations in system $A\tilde{A}$ are exposed to the interaction Hamiltonian between systems A and B. The larger the exposure, the faster does the coherent information of the direct and complementary channel change. Importantly, we have shown that the $n-$exposure is not proportional to the amount of pre-existing entanglement (as measured by the von Neumann entropy), nor is it proportional to the $n-$Rényi entropy. Instead, it depends non-trivially on the initial state of A, such that two initial configurations with the same initial entanglement may exhibit entirely different behaviours at the onset of the quantum channel. We illustrated how the n-exposure dependends on the initial state of A, and on the interaction Hamiltonian, in a simple model of the light-matter interaction and in qutrit systems.

In future work, it will be very interesting to calculate the analog of the n-exposure for interaction Hamiltonians of the more general form $\sum_r \hat{A}_r \otimes \hat{B}_r$. Interestingly, in this case the contributions to the leading order change in the n-coherent information of the direct and complementary channels do not simply factorize into separate contributions from systems A and B. It will then also be interesting to revisit the limit $n \to 1$ (see also Appendix 10.5).

In practice, for example in the running of quantum processors, it may be possible to use the notion of exposure to optimize their performance, for example, by extremizing the exposure to maximize a desired transfer of quantum correlations, or conversely, to minimize exposure in order to reduce leakage of quantum correlations to an environment. We also anticipate that the notion of $n-$exposure may prove useful in the implementation of quantum algorithms when certain qubits are idle. In particular, one may rotate a qubit in its Bloch sphere along an isocurve of n-Rényi entropy, thus preserving its n-coherent information with the rest of the qubits, but to a location in the Bloch sphere that decreases its exposure to decohering. This principle should also be extendable to multiple qubits at

a time, possibly utilizing supervised machine learning with a cost function that contains the exposure. Work in this direction is in progress.

In this work we have focused on the dynamics of the coherent information, which we note is not itself an entanglement monotone. Indeed, given that our study involves a tripartite system, traditional measures of entanglement such as the von Neumann entropy are insufficient to describe true tripartite entanglement. Hence, work is ongoing to extend our results using the logarithmic negativity as an entanglement monotone of tripartite systems. Nevertheless, coherent information remains a critical tool in the assessment of quantum channel capacity since any finite coherent information value provides a lower bound on the quantum channel capacity. This is because quantum channel capacity is obtained as the supremum over multiple parallel uses of the channel and arbitrary encoding on inputs.

Chapter 6

Superoscillations and Super-Phenomena

In this chapter we first describe a new method to generate superoscillatory functions in Sections 6.1 - 6.5. We then briefly review the generalization of superoscillations to super-phenomena in Section 6.6, and finally in Section 6.7 describe a position observable super-phenomenon, which we called the "quantum prison break".

6.1 Introduction

Superoscillatory functions are functions that locally oscillate faster than the fastest Fourier component that they contain. Superoscillations were first named and made the subject of investigation in work that includes, in particular [30, 6, 7, 9, 21, 22, 144, 94]. In hindsight, examples of superoscillatory behavior had previously been seen experimentally, e.g., in optics, and also in theory, where, for example, certain so-called prolate spheroidal functions are superoscillatory.

In the meantime, both the theory, see, e.g., [60, 102, 62, 61, 33, 163, 39, 142, 106, 115, 73, 25, 4, 24, 3], and applications, see, e.g., [50, 8, 82, 148, 121, 23, 92, 53, 84, 83, 157, 17, 56, 173, 5], of superoscillations have been actively explored.

Functions with superoscillatory behavior are the subject of intense investigation for multiple reasons. One reason is that they offer an opportunity for superresolution, i.e., for resolution beyond the diffraction limit. Superresolution is of particular interest in the presence of natural bandwidth limitations, such as the ultraviolet cutoff expected to arise

at the Planck scale, see, e.g., [95, 96, 72, 97, 98, 143, 1], in the presence of practical bandwidth limitations, for example, arising from absorption bands in media, e.g., in the case of radar [101, 26, 99], or in the presence of imposed bandwidth limitations, e.g., to avoid deleterious ionization in biological tissue, e.g., in optogenetics [137, 49, 131, 90, 37], see [26, 99].

In certain media, the use of superoscillatory waves for superresolution is obstructed because of the existence of dissipative processes that are faster than the superoscillations. Even in these circumstances, the use of superoscillatory waves can be useful, for example, to explore these fast dissipative processes, [26, 99].

Also in information theory, see, e.g., [42], the rôle of superoscillatory behavior in communication signals is of interest. There, the study of superoscillatory signals has the potential, for example, for a noise-model independent generalization of the Shannon Hartley theorem [26, 99].

In quantum theory, superoscillatory behavior has been described early on in the context of weak measurement theory. The further exploration of the quantum mechanics as well as the quantum thermodynamics of superoscillatory behavior is of high interest, see, e.g., [33, 163, 39, 142, 106, 3, 99].

Superoscillatory behavior is known to come with a cost, however, which is that the superoscillatory part of a function necessarily possesses relatively small amplitudes compared to the amplitudes in the rest of the function. In particular, it was proven in [60, 102, 62] that the superoscillatory behavior obeys two scaling laws: for fixed L^2-norm, the amplitudes in the superoscillating region necessarily diminish polynomially with the frequency of the imposed superoscillations and they necessarily diminish exponentially with the number of imposed superoscillations.

6.2 Motivation

The focus of the first part of this chapter is the question of how superoscillatory functions can be constructed. At first, it had appeared that superoscillatory functions with numerous fast superoscillations are hard to construct, in the sense that the calculation is numerically unstable. For example, in [94], a method was presented that allows one, for any fixed $\Omega > 0$, to construct Ω-bandlimited and square integrable functions that pass through any finite number of prescribed points. These points can be chosen arbitrarily. If they are chosen such as to force the constructed function to possess superoscillations then the calculation involves the need to invert a matrix that is ill-conditioned. The matrix becomes the more

ill-conditioned and, therefore, the harder to invert numerically, the more superoscillations are being prescribed and the smaller their wavelength.

Fortunately, however, numerical instabilities in the construction of superoscillatory functions can be avoided, as was first shown in [39]. In prior approaches, such as [94], the superoscillatory function was constructed by adding a number of non-superoscillatory Ω-bandlimited functions with coefficients that had to be extremely fine-tuned in order to achieve superoscillatory behavior for the resulting sum of these functions, hence the numerical instability. Instead, the method in [39] constructs a superoscillatory function as the product of non-superoscillatory functions whose bandwidth adds up to Ω (recall that as functions are multiplied, their bandwidths add). The multiplicative method of [39] allows one to construct superoscillatory functions with any number of arbitrarily close-by zero crossings because the function function inherits the zeros of each of its factors - and these factors can be chosen arbitrarily close to another. The method is numerically stable because no fine tuning is needed to obtain the product function. This method was then used in the later paper [122] to approximate sinusoidal superoscillations.

Here, we also build on [39]. We obtain a numerically stable method for constructing superoscillatory functions whose superoscillatory stretch exhibits any desired behavior to any desired accuracy, in any number of dimensions.

6.3 New method to Efficiently and Numerically Stably Generate Superoscillatory Functions with Arbitrary Target Behavior in any Number of Dimensions

Let us consider the problem of finding a square integrable function $g : \mathbb{R}^d \to \mathbb{R}$ of a given bandlimit Ω which, in some given region $B \subset \mathbb{R}^d$, is approximating some arbitrary given smooth target function $f : \mathbb{R}^d \to \mathbb{R}$ while meeting an arbitrarily given accuracy goal $\epsilon > 0$:

$$|g(x) - f(x)| < \epsilon \quad \forall x \in B \tag{6.1}$$

Since there is no assumption of bandlimitation for f, the behavior of f in B can be chosen arbitrarily highly oscillatory, i.e., the to-be-constructed $\Omega-$bandlimited function g may have to be arbitrarily highly superoscillatory.

We now show how such a function g, that approximates the behavior of f in B to arbitrary given accuracy, can be generated efficiently and numerically stably.

The idea is to construct g as the product of two functions, one of bandlimit zero that ensures accuracy, namely a Taylor polynomial of the target function f, and one function of bandlimit Ω that ensures square integrability without spoiling the accuracy of the approximation.

Concretely, the method consists of first Taylor expanding the target function f around some point $p \in B$ to a finite order n. By Taylor's theorem, we can always choose n large enough so that the Taylor polynomial f_n approximates f in B to meet any given accuracy goal $\epsilon_1 > 0$:

$$|f_n(x) - f(x)| < \epsilon_1 \qquad \forall\ x \in B \tag{6.2}$$

We note that f_n possesses vanishing bandwidth because the Fourier transform of a polynomial is a linear combination of Dirac deltas and their derivatives. We also note that f_n diverges polynomially and that it is therefore not square integrable.

Second, we therefore also construct an Ω-bandlimited function $c : \mathbb{R}^d \to \mathbb{R}$ which obeys two conditions:

1. In the region B, we require the function c to stay close to 1 up to some accuracy goal $\epsilon_2 > 0$:
$$|c(x) - 1| < \epsilon_2\ \forall x \in B \tag{6.3}$$
2. We require the function c to decay to zero for $|x| \to \infty$ sufficiently fast so that $g(x) := f_n(x)c(x)$ is square integrable in $\mathbb{R}^d$.

For any ϵ_2, such a function c can be obtained as the product $c(x) = \prod_{i=1}^{m} c_i(x)$ of a sufficiently large number, m, of Ω/m-bandlimited functions, c_i, that each take a local maximum of value 1 at the Taylor expansion point, p. Condition (1) is obeyed by choosing m sufficiently large because $c(x)$ becomes increasingly flat around p. To see this, we notice that since c takes a local maximum value of 1 at p, its first derivative vanishes, and its second derivative decays with increasing m. For example, in one dimension, $(r(x/m)^m)''|_p = r''(x/m)|_p/m$ since $r'(x/m) = 0|_p$. In addition, condition 2 is obeyed by choosing $m > n$.

Clearly, $g := cf_n$ is Ω-bandlimited and square integrable. We now show that also any accuracy goal ϵ can be met. To this end, we can choose $\epsilon_1 := \epsilon/2$. This determines n such that f_n differs from f at most by ϵ_1 in B. In B, $|f_n|$ takes on a maximum, say M at $x_M \in B$. We then meet the overall accuracy goal by choosing any $\epsilon_2 > 0$ obeying $M - M(1 - \epsilon_2) < \epsilon_1$, i.e., by choosing any ϵ_2 obeying $0 < \epsilon_2 < \epsilon_1/M = \epsilon/2M$. Finally, the choice of ϵ_2 determines m.

The complexification of the method is straightforward. Also, instead of the Taylor expansion, other polynomial expansions may be used. The function c may be called a canvas function because it is designed to provide the blank backdrop on which the pattern of the target function is to be drawn.

6.4 Example: a One-Dimensional Implementation

Here, we will demonstrate the new method for Ω-bandlimited functions $\mathbb{R} \to \mathbb{R}$. We require the to-be-constructed superoscillatory function, g, to approximate the behavior of a target function, f, in the interval $B := [-1, 1]$. To this end, we take the MacLaurin series approximation of f

$$f_n(x) := \sum_{k=0}^{n-1} \frac{f^{(k)}(0)}{k!} x^k \approx f(x). \tag{6.4}$$

to order n. By Taylor's theorem, we can always find an n large enough to meet any accuracy goal ϵ_1 in $[-1, 1]$. We then obtain the desired superoscillatory function

$$g(x) := f_n(x)c(x) \tag{6.5}$$

if we can also construct a suitable Ω-bandlimted canvas function c that stays close to 1 in $[-1, 1]$ and that counteracts the x^{n-1} divergence of f_n for $x \to \pm\infty$. To construct such a function that decays at least as fast as $\frac{1}{x^n}$, we can make, for example, the ansatz:

$$c(x) = \text{sinc}\left(\frac{\Omega x}{m}\right)^m \tag{6.6}$$

Using the method of integration by differentiation [103, 104, 89], we quickly find the Fourier transform of this function:

$$\begin{aligned} \tilde{c}(k) &= \frac{1}{\sqrt{2\pi}} \int_{-\infty}^{\infty} \text{sinc}\left(\frac{\Omega x}{m}\right)^m e^{ikx} dx \\ &= \frac{\sqrt{2\pi}}{\Omega} \frac{\left(\frac{m}{2}\right)^m}{(m-1)!} \sum_{j=0}^{m} \binom{m}{j} (-)^j T_{\frac{1}{m}}^{m-2j} \theta\left(\frac{k}{\Omega}\right) \left(\frac{k}{\Omega}\right)^{m-1} \end{aligned} \tag{6.7}$$

Here, T_a is the translation operator $T_a = e^{a\Omega\partial/\partial_k}$.

The work [122] which followed up on [39] also studied the properties of powers of sinc functions. For our purposes here, we will find it useful to further investigate the peculiar

property that, near 0, the sequence of powers of sinc functions approaches a Gaussian in the limit of large m. To show this, we could consider the behavior of the binomial coefficients in the Fourier transform in Eq. (6.7) to investigate how the Fourier transform approaches a Gaussian. Instead, let us work directly in the x domain. We use a defining property of Gaussians, $\mathcal{G}(x) := e^{-x^2/(2\sigma^2)}$, namely that they obey:

$$\frac{\mathcal{G}'(x)}{\mathcal{G}(x)} = -\frac{x}{\sigma^2}, \tag{6.8}$$

In comparison, the canvas function, $c(x) = \mathrm{sinc}(\frac{\Omega x}{m})^m$ obeys for large m:

$$\frac{c'(x)}{c(x)} = -\frac{\Omega^2}{3}\frac{x}{m} - \frac{\Omega^4}{45}\left(\frac{x}{m}\right)^3 + O\left(\left(\frac{\Omega x}{m}\right)^5\right). \tag{6.9}$$

Therefore, as long as $x \ll m$, the function $c(x)$ is a good approximation to a Gaussian with variance $\frac{\sqrt{3m}}{\Omega}$. As desired, for increasing m, the function $c(x)$ approximates a wider and wider Gaussian so that its amplitude stays closer and closer to 1 up to $|x|$ of order m. Only from about $x = \frac{1}{\Omega}\pi n$, where $c(x)$ first drops to zero, $c(x)$ no longer approximates a Gaussian.

Finally, we also need c to meet the accuracy goal ϵ_2. To this end, we notice that while $c(0) = 1$, at the ends of the interval $[-1, 1]$, the function c falls to approximately $\mathrm{sinc}(\frac{\pm\Omega}{n})^n = 1 - \frac{\Omega^2}{6n}$, where we can again bound the error, and therefore meet any accuray goal ϵ_2 by using Taylor's theorem.

6.5 Summary and Outlook

The new method presented here allows one to construct, efficiently and numerically stably, a superoscillatory function that possesses any desired smooth behavior in the superoscillating region. The new method should, therefore, be useful for applications ranging from superresolution and the study of fast dissipative processes in media to applications of superoscillations in communication channels or measurement devices, in particular, in scenarios where the channel capacity is limited chiefly by the bandwidth and not by the availability of a large dynamic range.

In practice, the new method for constructing custom superoscillatory wave forms is straightforward to apply in any circumstances where the desired superoscillatory waveform can be

calculated and then produced by a wave form generator, e.g., in acoustics. However, wave form generators can only generate frequencies up to a certain range and at higher frequencies, such as in the optical range, methods other than wave form generators need to be employed to create superoscillatory waves, see e.g., [82, 148]. In this case, the presented method may, however, be applicable directly, namely if the experimental setup allows the physical multiplication of wave forms. In electronics, the multiplication of signals for the purpose of obtaining a superoscillating signal is relatively straightforward through the use of transistors for multiplication. It would be very interesting to explore, for example, the use of photo transistors for the purpose of creating custom superoscillatory electromagnetic waves in optics.

Finally, in the next sections, we will describe the generalization of the notion of superoscillations, and new related ideas.

6.6 Super-Phenomena: A Generalized Notion of Superoscillations

In this section we will review super-phenomena. In [91] superoscillations are described as an aspect of weak measurements. Namely, the key property of superoscillations, local oscillations faster than the fastest Fourier component of the field, is described as follows. The *local wavenumber* $k(x)$ of a function $\psi(x)$ is defined by the natural choice:

$$k(x) = \mathrm{Im}\left[\frac{d}{dx}\ln\psi(x)\right], \tag{6.10}$$

i.e., it is the imaginary part of the derivative of the logarithm. If, e.g., the function $\psi(x)$ is a plane wave e^{ikx}, then $k(x) = k$ is a constant function, corresponding to the wavenumber of the plane wave. On the other hand, if we construct a superoscillatory wavefunction, using, e.g., the method described in the previous chapter, we may find that, though the function is bandlimited to a range of wavenumbers $[k_{min}, k_{max}]$, the local wavenumber can be outside that range.

If $\psi(x)$ is a wavefunction, then $k(x)$ may also be understood as a weak value of the momentum operator $\hat{p} = -i\frac{d}{dx}$. Namely, we can rewrite the Eq. (6.10):

$$k(x) = \mathrm{Im}\left[\frac{d}{dx}\ln\psi(x)\right] = \mathrm{Im}\left[\frac{1}{\psi(x)}\frac{d}{dx}\psi(x)\right], \tag{6.11}$$

to yield the desired expression of a weak value:

$$\hbar k(x) = \mathrm{Re}\frac{\langle x|\,\hat{p}\,|\psi\rangle}{\langle x|\psi\rangle}. \tag{6.12}$$

It is easy to see what the candidate regions of superoscillatory behaviour are, i.e., the regions where $k(x)$ is outside of the bandlimitation: whenever $\langle x|\psi\rangle = \psi(x)$ approaches a number close to zero, local wavenumber $k(x)$ becomes a large value, and can be larger than the largest k in the momentum spectrum. This is in accordance with a known property of superoscillatory functions: the amplitudes in the superoscillatory part of the function are suppressed compared to the rest of the function: exponentially in the local wavenumber, and polynomially in the number of superoscillations.

The notion of superoscillations, understood via weak values of the momentum operator, can be generalized to any observable. *A super-phenomenon* is defined [91] via the weak value of some quantum observable $\hat{O}$. The analogue of a superoscillatory function's local wavenumber is the local super-observable $s(x)$:

$$s(x) = \frac{\langle x|\,\hat{O}\,|\psi\rangle}{\langle x|\psi\rangle}. \tag{6.13}$$

6.7 Super-Phenomenon of the Position Observable: Quantum Prison Break

We will now present a new idea, an interesting application of super-phenomena of the position observable $\hat{X}$. We will take a superoscillatory function $\psi(k)$ to be a function in the momentum space, rather than the position space. The support in the position space will be in some finite interval $\mathcal{I} = [0, L] \in \mathbb{R}$. Because the function $\psi(k)$ is superoscillatory in the variable k the position observable can yield results outside of the interval $\mathcal{I}$:

$$x(k) = \frac{\langle k|\,\hat{X}\,|\psi\rangle}{\langle k|\psi\rangle}, \tag{6.14}$$

where $x(k) \notin \mathcal{I}$ for some finite interval of momentum values k. Thus we may say that the quantum state described by the wavefunction $\psi(k)$ can *locally in momentum space* yield position measurements outside the support of the wavefunction $\psi(x)$ in the position

representation. We will call this *quantum prison break*[1] since it can be viewed as a way for a quantum state to escape the interval $x \in \mathcal{I}$ on which it has support.

As a model of the aforementioned concept, suppose we are considering a quantum system of finite size, for example a particle trapped in a well in one dimension, whose Schrödinger equation is:

$$i\hbar \frac{\partial \psi(x)}{\partial t} = \left(\frac{-\hbar^2}{2m} \frac{\partial^2}{\partial x^2} + V(x) \right) \psi(x), \tag{6.15}$$

with the potential: $V(x) = V_0 = \text{const.}$ for $x \in \mathcal{O} = [0, L]$, and $V(x) = +\infty$ for finite intervals $x \in [-\epsilon, o] \cup [L, L + \epsilon]$. Otherwise the potential is equal to zero, therefore the infinite walls are of finite size. In this case tunnelling is not possible.

Let us take some superoscillatory function $\psi(k)$, which we may generate, e.g., by the method described in Chapter 6. We will generate this function with the property of its Fourier transform $\psi(x)$ having a compact support in $\mathcal{I}$. Now, we define the *position (local in momentum space)* $x(k)$:

$$x(k) = -\text{Im} \left[\frac{d}{dk} \ln \psi(k) \right]. \tag{6.16}$$

Due to the superoscillatory property of $\psi(k)$ in some range of momenta $k \in [k_1, k_2]$, $x(k)$ will be outside the interval $\mathcal{I}$. Moreover, it can be exactly prescribed, since we can choose to generate such a superoscillatory function $\psi(k)$, so that $x(k) = x_0$, for any $x_0 \in \mathbb{R}$.

Operationally, we may first project the wavefunction onto the superoscillatory interval $k \in [k_1, k_2]$, perhaps using the combination of a low-pass and high-pass frequency filter. If the projection is successful, i.e., the quantum object passes the filter, then its position will be outside of the original "prison"[2].

In summary, in order to escape, the quantum prisoner first needs to be in a superoscillatory quantum state $\psi(k)$. Then, in order to escape, it needs to pass through a momentum filter, which leaves behind only the superoscillatory interval $[k_1, k_2]$. If successful, the prisoner has escaped. It is typically, though, more likely that it will be unsuccessful, since generically the wavefunction's amplitude in the superoscillatory interval is much smaller than the amplitudes outside.

[1] Name suggestion thanks to Achim Kempf.

[2] This is analogous to a superoscillatory wavefunction in position space passing through a slit in the wall. If the slit is positioned so that it matches the superoscillatory interval, and the quantum object goes through, its momentum will be larger than the wavefunction's bandwidth.

Note, if the description of a quantum object includes the wavefunction $\psi(k)$ and an, e.g., spin state $|\varphi\rangle = \alpha\,|\uparrow_z\rangle + \beta\,|\downarrow_z\rangle$, $|\alpha|^2 + |\beta|^2 = 1$, the complete quantum state $|\chi\rangle$ is:

$$|\chi\rangle = |\psi\rangle \otimes |\varphi\rangle\,, \tag{6.17}$$

i.e., it is a tensor product of $\psi(x)$ and its spin degree of freedom. In this case, the quantum prison break might seem to be an alternative method for teleportation.

However, it has a significant downside. The need for postselection necessarily implies that some attempts will not be successful, i.e., a potentially significant number of outcomes need to be discarded. It is interesting to see if there is an inherent trade-off between the probability of loss and the distance of "teleportation". We leave the details to future work, though we note that we can roughly estimate such a tradeoff: the bigger the x_0, the smaller is the amplitude of the superoscillatory interval in momentum space $k \in [k_1, k_2]$. It is known from previous studies [102, 62] in superoscillations, that the amplitude becomes polynomially smaller in the interval $[k_1, k_2]$, compared to the rest of the wavefunction, as x_0 increases (this is because x_0 measures the local frequency of the superoscillatory function). Therefore, the probability of a successful "teleportation" falls polynomially with the distance of teleportation. It is an interesting effect, since the standard teleportation has in principle constant success probability as a function of distance, while the probability of quantum tunnelling, roughly speaking, falls exponentially with the distance, therefore the quantum prison break is in between these two phenomena.

In summary, as an alternative method for teleportation, it has the disadvantage of sometimes failing, due to postselection, and the failure rate increases with the distance of teleportation. However, it has the advantage that it does not use entangled pairs as a resource for teleportation.

Chapter 7

Conclusion

In this thesis we studied several aspects of quantum interactions. We began by describing the Unruh-DeWitt detector model of light-matter interactions. It is a simple, useful model of a 2-level quantum system interacting with a quantum field, and the most convenient framework for deriving the famous Unruh effect. Using this model we found two new acceleration-induced effects in light-matter interactions. First, we showed that the presence of photons stimulates the Unruh effect. The stimulation of resonant transitions, arising from the rotating wave interaction terms, was known. We showed that the non-resonant transitions, responsible for the Unruh effect, can be stimulated as well. The stimulation increases the probability for the Unruh effect type of transitions by many orders of magnitude, bringing it closer to experimental observability. Given that we only wanted to measure the Unruh effect, we needed to suppress the resonant transitions. This lead to the idea of *acceleration-induced transparency*, the phenomenon where a suitably chosen trajectory of the Unruh-DeWitt detector leads to the suppression of the resonant excitations of the detector. The suppression can be either partial, or as was also proven in the thesis and [85], the resonant transitions can be fully suppressed. Combined, the two effects lead to a new way to measure the Unruh effect in the laboratory, with an anticipated experimental enhancement of about 15 orders of magnitude which may finally bring the effect into the range of experimental detection.

Both of these effects are methods to modulate the probability of transitions in light-matter interactions: stimulating the Unruh effect can greatly increase the probability of the non-resonant transitions, while the acceleration-induced transparency is a method to decrease, even down to zero, the probability of measuring resonant transitions.

Additionally, since gravity and acceleration are related via the equivalence principle, the

new acceleration-induced effects suggest studying their gravity-induced analogs. The work on gravity-induced transparency and the stimulated Hawking effect is in progress.

We then conjectured that the trajectories which produce the acceleration induced transparency are not rare. We first argued that it is likely that the trajectories are ubiquitous enough to extend the acceleration-induced transparency beyond the first order in perturbation theory. Therefore the transparency phenomenon may occur for interactions with a strong coupling constants. We also conjectured that it is possible to find transparency inducing trajectories for more than one mode of the quantum field. Therefore an Unruh-DeWitt detector would become transparent for multiple energy level transitions, if the detector is an $N > 2$-level quantum system. Proving these conjectures, will require finding the trajectories which give rise to acceleration-induced transparency for multiple wavelengths of light, or, the transparency for a transition at higher orders of perturbation theory. Proving them would be interesting since it would allow greater control over the strength of interactions in light-matter interactions, with possible applications to, e.g., photon-based quantum computing.

We then generalized the notion of acceleration-induced transparency. Its analog was described in a general scenario of interactions, where we have control over some parameters in the interaction Hamiltonian. Therefore the idea of acceleration-induced transparency is no longer limited to light-matter interactions. We showed that it is possible to suppress some transitions at will by varying the coupling constants or the interaction Hamiltonian in time. Because we are varying the parameters of the interaction to switch off transitions, we named it *parametrically induced decoupling*. While the mathematical framework and the ideas were introduced, more work is in progress. It would be interesting to find applications of the framework to, e.g., problems in quantum control. Perhaps the most straightforward application would be to adiabatic quantum computing, since parametrically induced decoupling is a method to switch off transitions. In adiabatic quantum computing the interaction terms responsible for excitations from the ground state are directly responsible for the slow-down of computation, and it would be desirable to apply the previously mentioned method to switch off those transitions, and consequently speed up computations. This possibility may be related to the QAOA algorithm which mimics adiabatic quantum computing in finite, and not necessarily adiabatic, steps.

Moreover, the outcome of the conjecture on the ubiquity of acceleration-induced transparency will significantly influence the applicability of parametrically induced decoupling. This is because we used the proof of its existence to show the existence of the decoupling. Therefore, more results on acceleration-induced transparency will lead to more ways to parametrically induce decoupling, in general interaction scenarios.

We also introduced a new mathematical tool to describe quantum interactions called Newton's cradle spectra. It is a result in linear algebra, and therefore widely applicable. We presented exact expressions that relate the eigensystems of a self-adjoint operator before and after adding to it a rank-one projector. Most notably, the expressions are valid for any coupling constant multiplying the rank-one projector. Since, via the spectral theorem, any self-adjoint operator can be decomposed into a sum over such projectors, this gives a new method to understand non-perturbative physics. We can use the Newton's cradle spectra results iteratively, by adding the projectors one by one, the total sum equaling the interaction Hamiltonian. As a consequence of the Newton's cradle spectra results, we refined the understanding of Cauchy's interlacing theorem. We derived the expression for finding the eigenvalues of the matrix obtained by deleting a row and a column of a matrix (represented in some Hilbert space basis), with known eigenvalues and eigenvectors. We also found that level repulsion can be explained by the new results. Since the eigenvalue related to an eigenvector orthogonal to the projector does not change as we vary the coupling constant, and it does otherwise, level repulsion is generic. This is because the probability of an inner product of two random vectors to be zero occurs with zero probability (it happens only for a set of lower dimension). The Newton's cradle spectra results are widely applicable to essentially any field which uses linear algebra as mathematical framework, including engineering. We especially discussed the application to adiabatic quantum computing, where this work provides insight on how algorithmic complexity translates to the narrowing of the gap and therefore also the slowdown of computation. Using Newton's cradle spectra we also succeeded in formulating the finite Shannon sampling theory. And, as an example, a calculation of a dressed vacuum in light-matter interactions was presented.

The results we derived for the addition of a rank-one projector suggest investigations into the behaviour of eigenvalues and eigenvectors under the full addition of self-adjoint operators. We observed that the eigenvalues in Newton's cradle spectra for self adjoint operators behave like Newtonian particles, with "momentum conservation", and well defined "forces" between the eigenvalues. It would be interesting to understand what can be understood about the full addition of Hamiltonians, given this observation, since we may use analytical results from classical mechanics to derive some properties of spectral dynamics, i.e., the behaviour of eigenvalues under the full addition of Hamiltonians.

Further, in order to better understand and control the ability of interactions to transmit quantum information, we investigated parameters which influence the rate at which a quantum channel arises at the onset of interactions between two systems. We found it useful in the calculations to extend the conventional coherent information to n-coherent information defined via the n-Rényi entropy. We found that the rate of change of n-coherent information at the onset of the interaction is determined by n-exposure. The quantity n-

exposure measures how much of the initial coherent information between a system A and its ancilla $\tilde{A}$ is available to another system B, given the interaction Hamiltonian between A and B. Examples in qubits and light-matter interactions are presented.

Finally, we studied superoscillations, as aspects of weak measurements. They occur when a function locally oscillates faster than its fastest Fourier component. We first presented a new method to generate superoscillatory function. This method was based on the observation that polynomials have zero bandwidth, which we used in order to prescribe the shape of the superoscillatory part of the function. The shape is given by some function on an interval, it is then approximated by its Taylor polynomial to the desired accuracy. The non-zero finite badnwidth, and the convergence of the function at infinity is achieved by multiplying the Taylor polynomial by a power of the sinc function. The multiplication results in a finite-bandwidth superoscillatory function of arbitrary shape.

Building on this work, we then briefly reviewed the generalization of superoscillations, the super-phenomena. Super-phenomena allow more to be locally extracted from an observable than its highest eigenvalue, given that the system is in a specially prepared quantum states. Analogously, they also allow that locally a smaller value of an observable is found than its lowest eigenvalue. This is a valuable aspect of quantum interactions, precisely because it allows us to extract more (or less) from a quantum state than we would naively expect. Finally, inspired by this, we described a new application of the position observable super-phenomenon: *quantum prison break*. It arises when the wavefunction is superoscillatory in the momentum space, and it allows a quantum object, initally contained in some finite space, the "prison", to escape to a predetermined position outside the "prison", conditioned on the postselection of the momentum measurement. It is likely that there are more phenomena, like the quantum prison break, ready to be discovered.

References

[1] David Aasen, Tejal Bhamre, and Achim Kempf. Shape from sound: toward new tools for quantum gravity. *Physical Review Letters*, 110(12):121301, 2013.

[2] Dorit Aharonov, Wim Van Dam, Julia Kempe, Zeph Landau, Seth Lloyd, and Oded Regev. Adiabatic quantum computation is equivalent to standard quantum computation. *SIAM Review*, 50(4):755–787, 2008.

[3] Y. Aharonov, F. Colombo, I. Sabadini, D. Struppa, and J. Tollaksen. *The mathematics of superoscillations*, volume 247. Memoirs of the American Mathematican Society, 2017.

[4] Y. Aharonov, F. Colombo, I. Sabadini, D. C. Struppa, and J. Tollaksen. Some mathematical properties of superoscillations. *Journal of Physics A: Mathematical and Theoretical*, 44(36):365304, aug 2011.

[5] Y. Aharonov, F. Colombo, I. Sabadini, D. C. Struppa, and J. Tollaksen. Evolution of superoscillatory data. *Journal of Physics A: Mathematical and Theoretical*, 47(20):205301, May 2014.

[6] Y. Aharonov, S. Popescu, and D. Rohrlich. How can an infra-red photon behave as a gamma ray. *Tel-Aviv University Preprint*, page 1847–1890, 1990.

[7] Yakir Aharonov, Jeeva Anandan, Sandu Popescu, and Lev Vaidman. Superpositions of time evolutions of a quantum system and a quantum time-translation machine. *Phys. Rev. Lett.*, 64:2965–2968, Jun 1990.

[8] Yakir Aharonov, Noam Erez, and Benni Reznik. Superoscillations and tunneling times. *Phys. Rev. A*, 65:052124, May 2002.

[9] Yakir Aharonov, Sandu Popescu, Daniel Rohrlich, and Lev Vaidman. Measurements, errors, and negative kinetic energy. *Phys. Rev. A*, 48:4084–4090, Dec 1993.

[10] Aida Ahmadzadegan and Achim Kempf. On the unruh effect, trajectories and information. *Classical and Quantum Gravity*, 35:184002, 2017.

[11] Naum Ilyich Akhiezer and Izrail Markovich Glazman. *Theory of Linear Operators in Hilbert Space*. Dover Books on Mathematics. Dover Publications, 2013.

[12] L. Allen and J. H. Eberly. *Optical Resonance and Two-level Atoms*. Dover, 1987.

[13] J. M. Arias, J. Dukelsky, and J. E. García-Ramos. Quantum phase transitions in the interacting boson model: integrability, level repulsion, and level crossing. *Physical Review Letters*, 91(16):162502, 2003.

[14] J. M. Arrazola, V. Bergholm, K. Brádler, T. R. Bromley, M. J. Collins, I. Dhand, A. Fumagalli, T. Gerrits, A. Goussev, L. G. Helt, J. Hundal, T. Isacsson, R. B. Israel, J. Izaac, S. Jahangiri, R. Janik, N. Killoran, S. P. Kumar, J. Lavoie, A. E. Lita, D. H. Mahler, M. Menotti, B. Morrison, S. W. Nam, L. Neuhaus, H. Y. Qi, N. Quesada, A. Repingon, K. K. Sabapathy, M. Schuld, D. Su, J. Swinarton, A. Száva, K. Tan, P. Tan, V. D. Vaidya, Z. Vernon, Z. Zabaneh, and Y. Zhang. Quantum circuits with many photons on a programmable nanophotonic chip. *Nature*, 591(7848):54–60, Mar 2021.

[15] M. Aspelmeyer, C. Brukner, and A. Zeilinger. Course 9 - entangled photons and quantum communication. In Daniel Estève, Jean-Michel Raimond, and Jean Dalibard, editors, *Quantum Entanglement and Information Processing*, volume 79 of *Les Houches*, pages 337–355. Elsevier, 2004.

[16] Jinho Baik, Gérard Ben Arous, and Sandrine Péché. Phase transition of the largest eigenvalue for nonnull complex sample covariance matrices. *The Annals of Probability*, 33(5):1643–1697, 2005.

[17] D. G. Baranov, A. P. Vinogradov, and A. A. Lisyansky. Abrupt rabi oscillations in a superoscillating electric field. *Opt. Lett.*, 39(21):6316–6319, Nov 2014.

[18] J. S. Bell and J. M. Leinaas. The Unruh effect and quantum fluctuations of electrons in storage rings. *Nuclear Physics B*, 284:488–508, January 1987.

[19] J. S. Ben-Benjamin, M. O. Scully, S. A. Fulling, D. M. Lee, D. N. Page, A. A. Svidzinsky, M. S. Zubairy, M. J. Duff, R. Glauber, W. P. Schleich, and W. G. Unruh. Unruh acceleration radiation revisited. *International Journal of Modern Physics A*, 34(28):1941005, 2019.

[20] John J. Benedetto and Paulo J.S.G. Ferreira. *Modern sampling theory: Mathematics and Applications*. Springer Science & Business Media, 2001.

[21] Michael Berry. Evanescent and real waves in quantum billiards and gaussian beams. *Journal of Physics A: Mathematical and General*, 27(11):L391, jun 1994.

[22] Michael Berry. Faster than fourier. In J.A. Anandan and J. Safko, editors, *Fundamental Problems in Quantum Theory*, pages 55–65. World Scientific, Singapore, 1994.

[23] Michael Berry. A note on superoscillations associated with bessel beams. *Journal of Optics*, 15(4):044006, apr 2013.

[24] Michael Berry. Suppression of superoscillations by noise. *Journal of Physics A: Mathematical and Theoretical*, 50(2):025003, dec 2016.

[25] Michael Berry and Sandu Popescu. Evolution of quantum superoscillations and optical superresolution without evanescent waves. *Journal of Physics A: Mathematical and General*, 39(22):6965, may 2006.

[26] Michael Berry, Nikolay Zheludev, Yakir Aharonov, Fabrizio Colombo, Irene Sabadini, Daniele C Struppa, Jeff Tollaksen, Edward T. F. Rogers, Fei Qin, Minghui Hong, Xiangang Luo, Roei Remez, Ady Arie, Jörg B Götte, Mark R Dennis, Alex M H Wong, George V Eleftheriades, Yaniv Eliezer, Alon Bahabad, Gang Chen, Zhongquan Wen, Gaofeng Liang, Chenglong Hao, C-W Qiu, Achim Kempf, Eytan Katzav, and Moshe Schwartz. Roadmap on superoscillations. *Journal of Optics*, 21(5):053002, apr 2019.

[27] N. D. Birrell and P. C. W. Davies. *Quantum Fields in Curved Space*. Cambridge Monographs on Mathematical Physics. Cambridge University Press, 1982.

[28] Nicholas David Birrell, Nicholas David Birrell, and PCW Davies. *Quantum fields in curved space*. Cambridge University Press, 1984.

[29] Andrea Bonfiglioli and Roberta Fulci. *Topics in noncommutative algebra: the theorem of Campbell, Baker, Hausdorff and Dynkin*, volume 2034. Springer Science & Business Media, 2011.

[30] James A. Bucklew and Bahaa E. A. Saleh. Theorem for high-resolution high-contrast image synthesis. *J. Opt. Soc. Am. A*, 2(8):1233–1236, Aug 1985.

[31] James R Bunch, Christopher P Nielsen, and Danny C Sorensen. Rank-one modification of the symmetric eigenproblem. *Numerische Mathematik*, 31(1):31–48, 1978.

[32] Pasquale Calabrese and Alexandre Lefevre. Entanglement spectrum in one-dimensional systems. *Phys. Rev. A*, 78:032329, Sep 2008.

[33] Matt S. Calder and Achim Kempf. Analysis of superoscillatory wave functions. *Journal of Mathematical Physics*, 46(1):012101, 2005.

[34] H. B. G. Casimir. On the Attraction Between Two Perfectly Conducting Plates. *Indag. Math.*, 10:261–263, 1948.

[35] Augustin-Louis Cauchy. On the equation which helps one determine the secular inequalities in the movements of the planets. *Complete Works (Serie 2)*, 9, 1829.

[36] Aidan Chatwin-Davies, Achim Kempf, and Robert TW Martin. Natural covariant planck scale cutoffs and the cosmic microwave background spectrum. *Physical Review Letters*, 119(3):031301, 2017.

[37] Shuo Chen, Adam Z. Weitemier, Xiao Zeng, Linmeng He, Xiyu Wang, Yanqiu Tao, Arthur J. Y. Huang, Yuki Hashimotodani, Masanobu Kano, Hirohide Iwasaki, Laxmi Kumar Parajuli, Shigeo Okabe, Daniel B. Loong Teh, Angelo H. All, Iku Tsutsui-Kimura, Kenji F. Tanaka, Xiaogang Liu, and Thomas J. McHugh. Near-infrared deep brain stimulation via upconversion nanoparticle–mediated optogenetics. *Science*, 359(6376):679–684, 2018.

[38] Yu-Ao Chen, Qiang Zhang, Teng-Yun Chen, Wen-Qi Cai, Sheng-Kai Liao, Jun Zhang, Kai Chen, Juan Yin, Ji-Gang Ren, Zhu Chen, Sheng-Long Han, Qing Yu, Ken Liang, Fei Zhou, Xiao Yuan, Mei-Sheng Zhao, Tian-Yin Wang, Xiao Jiang, Liang Zhang, Wei-Yue Liu, Yang Li, Qi Shen, Yuan Cao, Chao-Yang Lu, Rong Shu, Jian-Yu Wang, Li Li, Nai-Le Liu, Feihu Xu, Xiang-Bin Wang, Cheng-Zhi Peng, and Jian-Wei Pan. An integrated space-to-ground quantum communication network over 4,600 kilometres. *Nature*, 589(7841):214–219, Jan 2021.

[39] Leilee Chojnacki and Achim Kempf. New methods for creating superoscillations. *Journal of Physics A: Mathematical and Theoretical*, 49(50):505203, nov 2016.

[40] Yang-Zhi Chou and Matthew S Foster. Chalker scaling, level repulsion, and conformal invariance in critically delocalized quantum matter: Disordered topological superconductors and artificial graphene. *Physical Review B*, 89(16):165136, 2014.

[41] C. Cohen-Tannoudji, J. Dupont-Roc, and G. Grynberg. *Atom-Photon Interactions: Basic Processes and Applications*. Wiley, 2004.

[42] T.M Cover and J.A. Thomas. *Elements of Information Theory*. John Wiley & Sons, Ltd, 2nd edition, 2005.

[43] L. C. B. Crispino, A. Higuchi, and G. E. A. Matsas. The unruh effect and its applications. *Rev. Mod. Phys.*, 80:787, 2008.

[44] Álvaro Cuevas, Massimiliano Proietti, Mario Arnolfo Ciampini, Stefano Duranti, Paolo Mataloni, Massimiliano F. Sacchi, and Chiara Macchiavello. Experimental detection of quantum channel capacities. *Phys. Rev. Lett.*, 119:100502, Sep 2017.

[45] A. J. Daley, H. Pichler, J. Schachenmayer, and P. Zoller. Measuring entanglement growth in quench dynamics of bosons in an optical lattice. *Phys. Rev. Lett.*, 109:020505, Jul 2012.

[46] Kiril Datchev and Hamid Hezari. Inverse problems in spectral geometry. *Inverse problems and applications: Inside Out II*, 60:455–486, 2011.

[47] H. Ted Davis and Kendall T. Thomson. *Linear Algebra and Linear Operators in Engineering: With Applications in Mathematica*. ISSN. Elsevier Science, 2000.

[48] Manuel De la Sen. On cauchy's interlacing theorem and the stability of a class of linear discrete aggregation models under eventual linear output feedback controls. *Symmetry*, 11(5):712, 2019.

[49] Karl Deisseroth. Optogenetics. *Nature Methods*, 8(1):26–29, 2011.

[50] Mark R. Dennis, Alasdair C. Hamilton, and Johannes Courtial. Superoscillation in speckle patterns. *Optics Letters*, 33(24):2976, December 2008. arXiv: 0810.1948.

[51] Peter B. Denton, Stephen J. Parke, Terence Tao, and Xining Zhang. Eigenvectors from eigenvalues: A survey of a basic identity in linear algebra. *Bulletin of the American Mathematical Society*, 59(1):31–58, feb 2021.

[52] P. A. M. Dirac. The Quantum Theory of the Emission and Absorption of Radiation. *Proceedings of the Royal Society A*, 114(767):243–265, 1927.

[53] M. Dubois, E. Bossy, S. Enoch, S. Guenneau, G. Lerosey, and P. Sebbah. Time-driven superoscillations with negative refraction. *Phys. Rev. Lett.*, 114(1):013902, 2015.

[54] Albert Einstein. Strahlungs-Emission und Absorption nach der Quantentheorie. *Deutsche Physikalische Gesellschaft*, 18:318–323, January 1916.

[55] Albert Einstein. Zur Quantentheorie der Strahlung. *Physikalische Zeitschrift*, 18:121–128, January 1917.

[56] Y. Eliezer and A. Bahabad. Super-transmission: the delivery of superoscillations through the absorbing resonance of a dielectric medium. *Optics Express*, 22(25):31212–31226, 2014.

[57] Edward Farhi, Jeffrey Goldstone, and Sam Gutmann. A quantum approximate optimization algorithm. *arXiv preprint arXiv:1411.4028*, 2014.

[58] Edward Farhi, Jeffrey Goldstone, Sam Gutmann, Joshua Lapan, Andrew Lundgren, and Daniel Preda. A quantum adiabatic evolution algorithm applied to random instances of an np-complete problem. *Science*, 292(5516):472–475, 2001.

[59] Edward Farhi, Jeffrey Goldstone, Sam Gutmann, and Michael Sipser. Quantum computation by adiabatic evolution, 2000.

[60] Paulo J. S. G. Ferreira and Achim Kempf. The energy expense of superoscillations. In *2002 11th European Signal Processing Conference*, pages 1–4, 2002.

[61] Paulo J. S. G. Ferreira, Achim Kempf, and M. J. C. S. Reis. Construction of aharonov–berry's superoscillations. *Journal of Physics A: Mathematical and Theoretical*, 40(19):5141, apr 2007.

[62] Paulo J.S.G. Ferreira and Achim Kempf. Superoscillations: Faster than the nyquist rate. *IEEE Transactions on Signal Processing*, 54(10):3732–3740, 2006.

[63] Steven T. Flammia, Alioscia Hamma, Taylor L. Hughes, and Xiao-Gang Wen. Topological Entanglement Rényi Entropy and Reduced Density Matrix Structure. *Phys. Rev. Lett.*, 103(26):261601, 2009.

[64] Michael Fleischhauer, Atac Imamoglu, and JP Marangos. Electromagnetically induced transparency: Optics in coherent media. *Reviews of Modern Physics*, 77:633–673, 2005.

[65] P. Forn-Díaz, L. Lamata, E. Rico, J. Kono, and E. Solano. Ultrastrong coupling regimes of light-matter interaction. *Reviews of Modern Physics*, 91(2):025005, June 2019.

[66] Stephen A. Fulling. *Aspects of quantum field theory in curved spacetime*. Number 17. Cambridge University Press, 1989.

[67] Sevag Gharibian, Yichen Huang, Zeph Landau, and Seung Woo Shin. Quantum hamiltonian complexity. *Foundations and Trends in Theoretical Computer Science*, 10(3):159–282, 2015.

[68] Roy Glauber. Coherent and Incoherent States of the Radiation Field. *Physical Review*, 131(6):2766–2788, 1963.

[69] M. Göppert-Mayer. Elementary processes with two quantum transitions. *Annalen der Physik*, 18(7-8):466–479, 2009.

[70] Thomas Guhr, Axel Müller-Groeling, and Hans A Weidenmüller. Random-matrix theories in quantum physics: common concepts. *Physics Reports*, 299(4-6):189–425, 1998.

[71] Laszlo Gyongyosi, Sandor Imre, and Hung Viet Nguyen. A Survey on Quantum Channel Capacities. *arXiv e-prints*, page arXiv:1801.02019, January 2018.

[72] Yufang Hao and Achim Kempf. On a non-fourier generalization of shannon sampling theory. In *2007 10th Canadian Workshop on Information Theory (CWIT)*, pages 193–196, 2007.

[73] Yufang Hao and Achim Kempf. On the stability of a generalized shannon sampling theorem. In *2008 International Symposium on Information Theory and Its Applications*, pages 1–6, 2008.

[74] Yufang Hao and Achim Kempf. Filtering, sampling, and reconstruction with time-varying bandwidths. *IEEE Signal Processing Letters*, 17(3):241–244, 2009.

[75] S. W. Hawking. Black hole explosions. *Nature*, 248:30–31, 1974.

[76] S. W. Hawking. Particle creation by black holes. *Communications in Mathematical Physics*, 43(3):199–220, 1975.

[77] Lee Hodgkinson and Jorma Louko. Static, stationary and inertial Unruh-DeWitt detectors on the BTZ black hole. *Phys. Rev. D*, 86:064031, 2012.

[78] R. Horodecki, P. Horodecki, and M. Horodecki. Quantum α-entropy inequalities: independent condition for local realism? *Physics Letters A*, 210(6):377–381, 1996.

[79] Ryszard Horodecki and Michal Horodecki. Information-theoretic aspects of inseparability of mixed states. *Phys. Rev. A*, 54:1838–1843, Sep 1996.

[80] Jen-Tsung Hsiang and Bei-Lok Hu. Ground State Excitation of an Atom Strongly Coupled to a Free Quantum Field. *Phys. Rev. D*, 100(12):125019, 2019.

[81] Theodore C Hsu and JC Angles d'Auriac. Level repulsion in integrable and almost-integrable quantum spin models. *Physical Review B*, 47(21):14291, 1993.

[82] Fu Min Huang, Yifang Chen, F Javier Garcia de Abajo, and Nikolay I Zheludev. Optical super-resolution through super-oscillations. *Journal of Optics A: Pure and Applied Optics*, 9(9):S285, aug 2007.

[83] Kun Huang, Huapeng Ye, Jinghua Teng, Swee Ping Yeo, Boris Luk'yanchuk, and Cheng-Wei Qiu. Optimization-free superoscillatory lens using phase and amplitude masks. *Laser & Photonics Reviews*, 8(1):152–157, 2014.

[84] Heikki J. Hyvärinen, Shakil Rehman, Jani Tervo, Jari Turunen, and Colin J. R. Sheppard. Limitations of superoscillation filters in microscopy applications. *Opt. Lett.*, 37(5):903–905, Mar 2012.

[85] Barbara Šoda, Vivishek Sudhir, and Achim Kempf. Acceleration-induced effects in stimulated light-matter interactions. *Phys. Rev. Lett.*, 128:163603, Apr 2022.

[86] Rajibul Islam, Ruichao Ma, Philipp M. Preiss, M. Eric Tai, Alexander Lukin, Matthew Rispoli, and Markus Greiner. Measuring entanglement entropy in a quantum many-body system. *Nature*, 528(7580):77–83, Dec 2015.

[87] E. T. Jaynes and F. W. Cummings. Comparison of Quantum and Semiclassical Radiation Theories with Application to the Beam Maser. *Proceedings of the IEEE*, 51:89–109, 1963.

[88] Abdul J. Jerri. The shannon sampling theorem—its various extensions and applications: A tutorial review. *Proceedings of the IEEE*, 65(11):1565–1596, 1977.

[89] Ding Jia, Eugene Tang, and Achim Kempf. Integration by differentiation: new proofs, methods and examples. *Journal of Physics A: Mathematical and Theoretical*, 50(23):235201, may 2017.

[90] J.C. Jimenez, K. Su, A.R. Goldberg, V.M. Luna, J.S. Biane, G. Ordek, and P et al P. Zhou. Anxiety cells in a hippocampal-hypothalamic circuit. *Neuron*, 97(3):670–683, 2018.

[91] Andrew N. Jordan, Yakir Aharonov, Daniele C. Struppa, Fabrizio Colombo, Irene Sabadini, Tomer Shushi, Jeff Tollaksen, John C. Howell, and A. Nick Vamivakas. Super-phenomena in arbitrary quantum observables, 2022.

[92] Eytan Katzav and Moshe Schwartz. Yield-optimized superoscillations. *IEEE Transactions on Signal Processing*, 61(12):3113–3118, 2013.

[93] Achim Kempf. Uncertainty relation in quantum mechanics with quantum group symmetry. *Journal of Mathematical Physics*, 35(9):4483–4496, 1994.

[94] Achim Kempf. Black holes, bandwidths and beethoven. *J. Math. Phys.*, 41:2360–2374, 2000.

[95] Achim Kempf. Fields over unsharp coordinates. *Physical Review Letters*, 85(14):2873, 2000.

[96] Achim Kempf. Covariant information-density cutoff in curved space-time. *Physical Review Letters*, 92(22):221301, 2004.

[97] Achim Kempf. Information-theoretic natural ultraviolet cutoff for spacetime. *Physical Review Letters*, 103(23):231301, 2009.

[98] Achim Kempf. Spacetime could be simultaneously continuous and discrete, in the same way that information can be. *New Journal of Physics*, 12(11):115001, 2010.

[99] Achim Kempf. Four aspects of superoscillations. *Quantum Studies: Mathematics and Foundations*, 5(3):477–484, 2018.

[100] Achim Kempf. Replacing the notion of spacetime distance by the notion of correlation. *Frontiers in Physics*, 9:655857, 2021.

[101] Achim Kempf. Signals maximizing information return in penetrating radar, US provisional patent application #: 61/629,930 (2012).

[102] Achim Kempf and Paulo J S G Ferreira. Unusual properties of superoscillating particles. *Journal of Physics A: Mathematical and General*, 37(50):12067, dec 2004.

[103] Achim Kempf, David M Jackson, and Alejandro H Morales. New dirac delta function based methods with applications to perturbative expansions in quantum field theory. *Journal of Physics A: Mathematical and Theoretical*, 47(41):415204, sep 2014.

[104] Achim Kempf, David M Jackson, and Alejandro H Morales. How to (path-) integrate by differentiating. *Journal of Physics: Conference Series*, 626(1):012015, jun 2015.

[105] Achim Kempf and Robert Martin. Information theory, spectral geometry, and quantum gravity. *Physical Review Letters*, 100(2):021304, 2008.

[106] Achim Kempf and Angus Prain. Driving quantum systems with superoscillations. *Journal of Mathematical Physics*, 58(8):082101, 2017.

[107] Emily Kendall and Achim Kempf. The dynamics of entropies at the onset of interactions. *Journal of Physics A Mathematical General*, 53(42):425303, October 2020.

[108] Emily Kendall, Barbara Šoda, and Achim Kempf. Transmission of coherent information at the onset of interactions. *Journal of Physics A: Mathematical and Theoretical*, 55(25):255301, may 2022.

[109] Andrew D. King, Jack Raymond, Trevor Lanting, Sergei V. Isakov, Masoud Mohseni, Gabriel Poulin-Lamarre, Sara Ejtemaee, William Bernoudy, Isil Ozfidan, Anatoly Yu. Smirnov, Mauricio Reis, Fabio Altomare, Michael Babcock, Catia Baron, Andrew J. Berkley, Kelly Boothby, Paul I. Bunyk, Holly Christiani, Colin Enderud, Bram Evert, Richard Harris, Emile Hoskinson, Shuiyuan Huang, Kais Jooya, Ali Khodabandelou, Nicolas Ladizinsky, Ryan Li, P. Aaron Lott, Allison J. R. MacDonald, Danica Marsden, Gaelen Marsden, Teresa Medina, Reza Molavi, Richard Neufeld, Mana Norouzpour, Travis Oh, Igor Pavlov, Ilya Perminov, Thomas Prescott, Chris Rich, Yuki Sato, Benjamin Sheldan, George Sterling, Loren J. Swenson, Nicholas Tsai, Mark H. Volkmann, Jed D. Whittaker, Warren Wilkinson, Jason Yao, Hartmut Neven, Jeremy P. Hilton, Eric Ladizinsky, Mark W. Johnson, and Mohammad H. Amin. Scaling advantage over path-integral monte carlo in quantum simulation of geometrically frustrated magnets. *Nature Communications*, 12(1):1113, Feb 2021.

[110] Rochus Klesse. Approximate quantum error correction, random codes, and quantum channel capacity. *Phys. Rev. A*, 75:062315, Jun 2007.

[111] Paweł Kurzyński, Adrian Kołodziejski, Wiesław Laskowski, and Marcin Markiewicz. Three-dimensional visualization of a qutrit. *Phys. Rev. A*, 93(6):062126, June 2016.

[112] T. D. Ladd, F. Jelezko, R. Laflamme, Y. Nakamura, C. Monroe, and J. L. O'Brien. Quantum computers. *Nature*, 464(7285):45–53, March 2010.

[113] Felix Leditzky, Nilanjana Datta, and Graeme Smith. Useful states and entanglement distillation. *arXiv e-prints*, page arXiv:1701.03081, January 2017.

[114] Felix Leditzky, Debbie Leung, and Graeme Smith. Dephrasure Channel and Superadditivity of Coherent Information. *Phys. Rev. Lett.*, 121(16):160501, October 2018.

[115] Dae Gwan Lee and Paulo J. S. G. Ferreira. Superoscillations with optimal numerical stability. *IEEE Signal Processing Letters*, 21(12):1443–1447, 2014.

[116] Hui Li and F. D. M. Haldane. Entanglement Spectrum as a Generalization of Entanglement Entropy: Identification of Topological Order in Non-Abelian Fractional Quantum Hall Effect States. *Phys. Rev. Lett.*, 101(1):010504, July 2008.

[117] Seth Lloyd. Capacity of the noisy quantum channel. *Phys. Rev. A*, 55(3):1613–1622, March 1997.

[118] Richard Lopp and Eduardo Martín-Martínez. Quantum delocalization, gauge, and quantum optics: Light-matter interaction in relativistic quantum information. *Phys. Rev. A*, 103:013703, Jan 2021.

[119] T. H. Maiman. Stimulated optical radiation in ruby. *Nature*, 187(4736):493–494, 1960.

[120] F. Major, V. Gheorghe, and G. Werth. *Charged Particle Traps*. Springer, 2005.

[121] K.G. Makris and D. Psaltis. Superoscillatory diffraction-free beams. *Optics letters*, 36(22):4335–4337, 2011.

[122] M Mansuripur and P K Jakobsen. An approach to constructing super oscillatory functions. *Journal of Physics A: Mathematical and Theoretical*, 52(30):305202, jul 2019.

[123] Robert J. II Marks. *Introduction to Shannon sampling and interpolation theory*. Springer Science & Business Media, 2012.

[124] R.T.W. Martin and Achim Kempf. Quantum uncertainty and the spectra of symmetric operators. *Acta Applicandae Mathematicae*, 106(3):349–358, 2009.

[125] Eduardo Martín-Martínez, Miguel Montero, and Marco del Rey. Wavepacket detection with the unruh-DeWitt model. *Physical Review D*, 87(6), mar 2013.

[126] K.A. Milton. Recent developments in the casimir effect. *Journal of Physics: Conference Series*, 161(1):012001, 2009.

[127] Florian Mintert and Andreas Buchleitner. Observable entanglement measure for mixed quantum states. *Phys. Rev. Lett.*, 98:140505, Apr 2007.

[128] T. Monz, K. Kim, A. S. Villar, P. Schindler, M. Chwalla, M. Riebe, C. F. Roos, H. Häffner, W. Hänsel, M. Hennrich, and R. Blatt. Realization of universal ion-trap quantum computation with decoherence-free qubits. *Phys. Rev. Lett.*, 103:200503, Nov 2009.

[129] J. von Neumann. Allgemeine eigenwerttheorie hermitescher funktionaloperatoren. *Mathematische Annalen*, 102:49–131, 1930.

[130] John Von Neumann and Eugene Wigner. No crossing rule. *Z. Phys*, 30:467–470, 1929.

[131] S. News. Stepping away from the trees for a look at the forest. *Science*, 330(6011):1612–1613, 2010.

[132] Michael A. Nielsen and Isaac Chuang. *Quantum computation and quantum information*. American Association of Physics Teachers, 2002.

[133] Daniel Norman and Dan Wolczuk. *Introduction to Linear Algebra for Science and Engineering*. Pearson, 2011.

[134] Hasan S. Padamsee. Superconducting Radio-Frequency Cavities. *Annual Review of Nuclear and Particle Science*, 64(1):175–196, 2014.

[135] T. Padmanabhan. Why does an accelerated detector click? *Classical and Quantum Gravity*, 2(1):117–126, 1985.

[136] R. Parentani. The recoils of the accelerated detector and the decoherence of its fluxes. *Nuclear Physics B*, 454(1):227–249, November 1995.

[137] Erika Pastrana. Optogenetics: controlling cell function with light. *Nature Methods*, 8(1):24–25, 2011.

[138] Sandrine Péché. The largest eigenvalue of small rank perturbations of hermitian random matrices. *Probability Theory and Related Fields*, 134(1):127–173, 2006.

[139] KW Plumb, Kyusung Hwang, Yiming Qiu, Leland W Harriger, GE Granroth, Alexander I Kolesnikov, GJ Shu, FC Chou, Ch Rüegg, Yong Baek Kim, et al. Quasiparticle-continuum level repulsion in a quantum magnet. *Nature Physics*, 12(3):224–229, 2016.

[140] Andrea Posilicano. Self-adjoint extensions by additive perturbations. *Annali della Scuola Normale Superiore di Pisa-Classe di Scienze*, 2(1):1–20, 2003.

[141] Alejandro Pozas-Kerstjens and Eduardo Martín-Martínez. Entanglement harvesting from the electromagnetic vacuum with hydrogenlike atoms. *Physical Review D*, 94(6):064074, 2016.

[142] A. Prain. Vacuum energy in expanding spacetime and superoscillation-induced resonance. Master's thesis, University of Waterloo, 2008.

[143] Jason Pye, William Donnelly, and Achim Kempf. Locality and entanglement in bandlimited quantum field theory. *Phys. Rev. D*, 92:105022, Nov 2015.

[144] Wang Qiao. A simple model of aharonov - berry's superoscillations. *Journal of Physics A: Mathematical and General*, 29(9):2257, may 1996.

[145] I. I. Rabi, J. R. Zacharias, S. Millman, and P. Kusch. A new method of measuring nuclear magnetic moment. *Phys. Rev.*, 53:318–318, Feb 1938.

[146] Matthew Reagor, Wolfgang Pfaff, Christopher Axline, Reinier W. Heeres, Nissim Ofek, Katrina Sliwa, Eric Holland, Chen Wang, Jacob Blumoff, Kevin Chou, Michael J. Hatridge, Luigi Frunzio, Michel H. Devoret, Liang Jiang, and Robert J. Schoelkopf. Quantum memory with millisecond coherence in circuit QED. *Physical Review B*, 94(1):014506, 2016.

[147] Alfréd Rényi. On Measures of Entropy and Information. *Berkeley Symposium on Mathematical Statistics and Probability*, 4.1:547–561, 1961.

[148] Edward T. F. Rogers and Nikolay I Zheludev. Optical super-oscillations: sub-wavelength light focusing and super-resolution imaging. *Journal of Optics*, 15(9):094008, sep 2013.

[149] Andrei D Sakharov. Vacuum quantum fluctuations in curved space and the theory of gravitation. *General Relativity and Gravitation*, 32(2):365–367, 2000.

[150] Jeong San Kim and Barry C. Sanders. Monogamy of multi-qubit entanglement using Rényi entropy. *Journal of Physics A Mathematical General*, 43(44):445305, November 2010.

[151] A. L. Schawlow and C. H. Townes. Infrared and optical masers. *Phys. Rev.*, 112:1940–1949, Dec 1958.

[152] Benjamin Schumacher and M. A. Nielsen. Quantum data processing and error correction. *Phys. Rev. A*, 54(4):2629–2635, October 1996.

[153] Geoffrey L. Sewell. Quantum fields on manifolds: PCT and gravitationally induced thermal states. *Annals of Physics*, 141(2):201–224, 1982.

[154] Claude Elwood Shannon. A mathematical theory of communication. *The Bell System Technical Journal*, 27(3):379–423, 1948.

[155] Peter W. Shor. Scheme for reducing decoherence in quantum computer memory. *Phys. Rev. A*, 52:R2493–R2496, Oct 1995.

[156] Barbara Šoda and Achim Kempf. Efficient method to create superoscillations with generic target behavior. *Quantum Studies: Mathematics and Foundations*, 7(3):347–353, 2020.

[157] D. Sokolovski and Rafael Sala Mayato. "superluminal" transmission via entanglement, superoscillations, and quasi-dirac distributions. *Physical Review A*, 81:022105, 2010.

[158] Wei Song, Lin Chen, and Zhuo-Liang Cao. Lower and upper bounds for entanglement of rényi-α entropy. *Scientific Reports*, 6(1):23, Dec 2016.

[159] Gilbert Strang. *Introduction to Linear Algebra*. Wellesley-Cambridge Press, 2016.

[160] E C Sudarshan. Equivalence of semiclassical and quantum mechanical descriptions of statistical light beams. *Physical Review Letters*, 10:277–277, 1963.

[161] Vivishek Sudhir, Nadine Stritzelberger, and Achim Kempf. Unruh effect of detectors with quantized center of mass. *Physical Review D*, 103(10):105023, 2021.

[162] Shin Takagi. Vacuum Noise and Stress Induced by Uniform Acceleration Hawking-Unruh Effect in Rindler Manifold of Arbitrary Dimension. *Progress of Theoretical Physics Supplement*, 88:1–142, 1986.

[163] Eugene Tang, Lovneesh Garg, and Achim Kempf. Scaling properties of superoscillations and the extension to periodic signals. *Journal of Physics A: Mathematical and Theoretical*, 49(33):335202, jul 2016.

[164] W. G. Unruh. Notes on black-hole evaporation. *Physical Review D*, 14(4):870, 1976.

[165] W. G. Unruh and W. H. Zurek. Reduction of a wave packet in quantum brownian motion. *Phys. Rev. D*, 40:1071–1094, Aug 1989.

[166] William G. Unruh and Robert M. Wald. What happens when an accelerating observer detects a Rindler particle. *Physical Review D*, 29(6):1047–1056, 1984.

[167] Bo Wang, Xi Zhu, C Gao, Y Bai, JW Dong, and LJ Wang. Square kilometre array telescope—precision reference frequency synchronisation via 1f-2f dissemination. *Scientific reports*, 5(1):1–7, 2015.

[168] Yu-Xin Wang, Liang-Zhu Mu, Vlatko Vedral, and Heng Fan. Entanglement Rényi α entropy. *Phys. Rev. A*, 93(2):022324, February 2016.

[169] Zhaoyou Wang and Emily J. Davis. Calculating Rényi entropies with neural autoregressive quantum states. *Phys. Rev. A*, 102(6):062413, December 2020.

[170] Davis M. Welakuh, Johannes Flick, Michael Ruggenthaler, Heiko Appel, and Angel Rubio. Frequency-dependent Sternheimer linear-response formalism for strongly coupled light-matter systems. *arXiv e-prints*, page arXiv:2201.08734, January 2022.

[171] Mark M. Wilde. *Quantum Information Theory*. Cambridge University Press, 2 edition, 2017.

[172] Ahmed I. Zayed. *Advances in Shannon's sampling theory*. Routledge, 2018.

[173] Nikolay I. Zheludev. What diffraction limit? *Nature Materials*, 7(6):420–422, 2008.

[174] Leo Zhou, Sheng-Tao Wang, Soonwon Choi, Hannes Pichler, and Mikhail D Lukin. Quantum approximate optimization algorithm: Performance, mechanism, and implementation on near-term devices. *Physical Review X*, 10(2):021067, 2020.

[175] Barbara Šoda and Achim Kempf. Newton cradle spectra, 2022. arXiv:2206.09927.

APPENDICES

Chapter 8

Appendix - Acceleration Induced Effects in Stimulated Light-Matter Interaction

8.1 Exact acceleration-induced transparency for a class of trajectories

The class of trajectories for which we give the proof is the one defined in Chapter 2:

$$\dot{\alpha}(\tau) := k^0 \begin{cases} s_0 & \tau < 0 \\ s_0 + \frac{s_1 - s_0}{T_1}\tau & \tau \in [0, T_1) \\ s_1 + \frac{s_2 - s_1}{T_2 - T_1}(\tau - T_1) & \tau \in [T_1, T_2) \\ s_2 & \tau \geq T_2, \end{cases} \tag{8.1}$$

where the constants $\{s_i, T_i\}$ can be chosen arbitrarily except that we require $\dot{\alpha} > 0$ and $0 < T_1 < T_2$.

Note that these trajectories are simple, especially in the non-relativistic regime, where they correspond to the Unruh-DeWitt detector first moving inertially at some velocity $v_0 = 1 - s_0$, then uniformly decelerating for a period of T_1 to a velocity $v_1 = 1 - s_1$, then uniformly accelerating to a final velocity $v_2 = 1 - s_2$, after which it stays in that inertial motion. This can be easily seen from the definition of the phase function $\alpha(\tau) = k^\mu x_\mu$, which, for a massless scalar field simplifies to $\alpha(\tau) = k^0 (x^0(\tau) - \sum_i x^i(\tau))$.

In the relativistic case the only difference is that the acceleration is not uniform, but the pattern of inertial motion, followed by deceleration and then acceleration, finally ending in inertial motion, is preserved.

We want to show that there are some parameter values $\{s_i, T_i\}$ for which $|I_-(\Omega, k)| = 0$, where we recall that Ω is the detector gap, and k is the wavevector of the stimulated field mode. We will show that both the real and imaginary part of the integral $I_-(\Omega, k)$ go to zero by using numerical simulations in a particular way:

- First we choose a positive real number $\epsilon \ll 1$, a detector gap Ω^*, and the wavelength of the stimulating field k.
- To find the right trajectory, we sweep through a two-dimensional parameter subspace (of the full space of parameters $\{s_i, T_i\}$, subject to the aforementioned constraints), plotting the points for which the $\mathrm{Re}\left[I_-(\Omega^*, k)\right] < \epsilon$ and $\mathrm{Im}\left[I_-(\Omega^*, k)\right] < \epsilon$.
- We find regions where the (thick) lines $\mathrm{Re}\left[I_-(\Omega^*, k)\right] < \epsilon$ and $\mathrm{Im}\left[I_-(\Omega^*, k)\right] < \epsilon$ cross. The lines are thick because sampling the curves at a precision below ϵ locally gives more then one value for which they are smaller than ϵ. (See Fig. 8.1.)
- Since I_- is a continuous function of these parameters, we can then be sure that there is a point where the (exact) lines $\mathrm{Re}\left[I_-(\Omega^*, k)\right] = 0$ and $\mathrm{Im}\left[I_-(\Omega^*, k)\right] = 0$ cross, which is the point where $|I_-(\Omega^*, k)| = 0$. This concludes the proof of existence of acceleration-induced transparency.

In our proof, the two-dimensional parameter subspace we chose to vary were s_1 and T_2, and the crossing of the real and imaginary parts of the integral I_- can be seen in Fig.1.

More specifically, the parameters we vary are s_1 and δt, defined as the variation of T_2: $T_2 = T_2^{(0)} + \delta t$, where we fixed the value $T_2^{(0)}$ for numerical convenience. The other parameters s_0, s_2 and the ratio T_1/T_2 were held fixed.

8.1.1 Determining the parameters s_1 and T_2 to a desired numerical accuracy

In Chapter 2, we showed an example where the parameters we found were such that the I_- integral was suppressed with respect to the I_+ integral by a factor of about 10^{-3}. We did this by choosing a small ϵ parameter, and then sampling the real and the imaginary parts

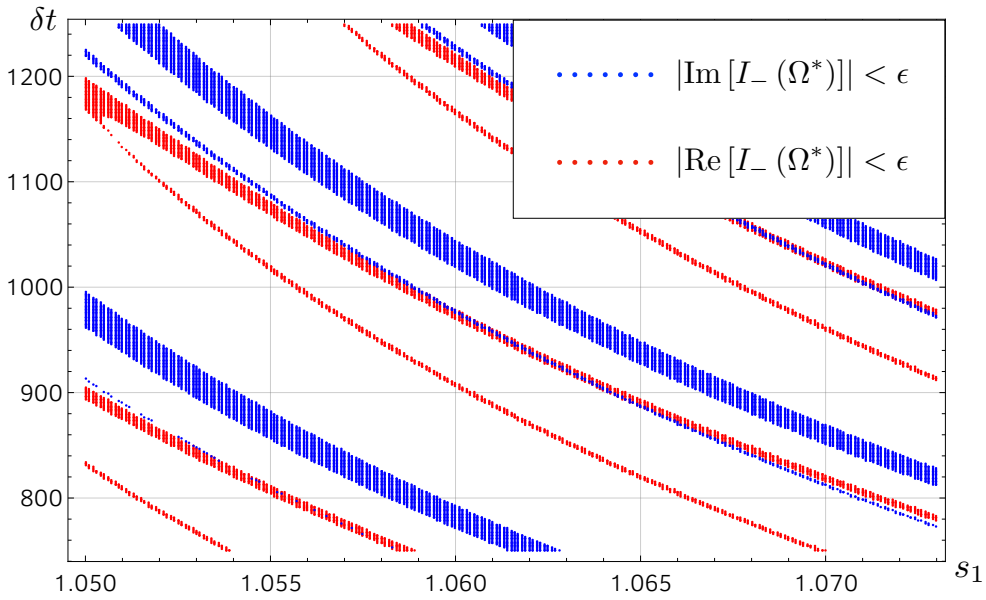

Figure 8.1: In this figure we can see a crossing of the (thick) lines $\mathrm{Re}\,[I_-(\Omega^*)] < \epsilon$ and $\mathrm{Im}\,[I_-(\Omega^*)] < \epsilon$. The existence of a crossing, together with the assumption that both $\mathrm{Re}\,[I_-(\Omega^*)]$ and $\mathrm{Im}\,[I_-(\Omega^*)]$ are continuous functions of the parameters s_1 and δt, prove that there is a point where $I_-(\Omega^*) = 0$, proving the existence of a trajectory exhibiting the phenomenon of acceleration-induced transparency.

of I_- (as functions of the parameters s_1 and T_2) densely enough around the region where the lines cross, in order to find the crossing point to a desired accuracy. In this case, we set the accuracy goal to be such that the above mentioned suppression of $\frac{I_-}{I_+}$ was about 10^{-3}. Because, in principle, this ratio could be exactly zero (as we proved above), we could set this ratio as low as desired, limited only by the available computational power.

8.2 Catalysis

At high intensity stimulation, the effect is catalysed. The ideas described above — the stimulated Unruh effect and acceleration-induced transparency — make it possible to amplify the Unruh effect by stimulating it with large photon numbers, while suppressing resonant absorption. When used in tandem, and when the stimulation is done by a field coherent state, it turns out that the resulting physical effect proceeds with little change to

the field state. To see this, note that,

$$\mathcal{A}_{|g,\alpha\rangle\to|e,\alpha\rangle}(\mathbf{k}) \propto G\left(\alpha^* I_+ + \alpha I_-\right) \neq 0. \tag{8.2}$$

That is, the field coherent state catalyses the excitation of the atom, without itself changing from the initial state $|\alpha\rangle$. The ratio of the probability for the catalysis of the stimulated Unruh process and the total probability for the stimulated Unruh process (when the field starts in a coherent state) is,

$$\frac{\left|\alpha^* I_+ + \alpha I_-\right|^2}{|\alpha|^2 |I_+ + I_-|^2 + |I_+|^2}. \tag{8.3}$$

Further, when the trajectory is chosen to be one that suppresses absorption (i.e. $|I_-| \ll |I_+|$), the fraction of the catalysed process dominates the stimulated Unruh process:

$$\frac{|\alpha|^2}{|\alpha|^2 + 1}\left[1 + \mathcal{O}\left(\left|\frac{I_-}{I_+}\right|\right)\right] \xrightarrow{|\alpha|\gg 1} 1 + \mathcal{O}\left(\left|\frac{I_-}{I_+}\right|\right). \tag{8.4}$$

Catalysis in the sense of the outgoing field state being the same as the ingoing field state also necessarily occurs in the stimulation of rotating wave terms of the Jaynes Cummings model (conventional stimulation). Here, we notice the new phenomenon that in the presence of acceleration, catalysis becomes optional. In fact, in the presence of acceleration, as Eq. (8.4) shows, we can choose α such that the numerator vanishes, implying that instead of catalysis, the process switches the ingoing field state to an orthogonal outgoing state.

8.3 Engineering of trajectories

Regarding the possible engineering of the trajectory of an Unruh-DeWitt (UDW) detector to suppress resonant transitions via the acceleration-induced transparency, let us consider the example of an UDW detector in the form of an electron whose spin provides the internal qubit with energy gap Ω when in an external magnetic field. Our aim is to demonstrate that, in principle, external electromagnetic fields can be engineered that a) enforce a prescribed trajectory $x^\mu(\tau)$ on the electron, and b) are such that the magnetic field in the electron's frame of reference is constant, meaning that it keeps the energy split Ω, induced by spin-magnetic field interaction, constant.

The trajectory, as measured by an observer in the laboratory frame, is $x^\mu = (t(\tau), 0, 0, z(\tau))$. It can be imposed by the presence of an external electromagnetic field that satisfies the Lorentz force equation:

$$m_e \frac{d^2 x^\mu}{d\tau^2} = q_e F^{\mu\nu} \frac{dx_\nu}{d\tau}. \tag{8.5}$$

The solution to this is an electric field in the z-direction, such that

$$m_e \frac{d^2 z}{d\tau^2} = q_e E_z \frac{dt}{d\tau}, \tag{8.6}$$

plus an arbitrary magnetic field in the z-direction, since it does not affect the motion. The electric field in Eq. (8.6) is given as a function of τ, but can be expressed as a function of z as well due to both $t(\tau)$ and $z(\tau)$ being invertible functions, for the trajectories we considered in Chapter 2. Hence, the electric field E can be chosen constant in time and z-dependent. It may be produced by a suitable experimental setup, for example, where the electron travels along the z-axis inside a charged, axially symmetric microwave cavity, of varying radius. Alternatively, the electron could be accelerated by a series of identical isolated rings forming a cylinder along the z-axis, with each ring's voltage chosen suitably.

We note that Lorentz transformations that are boosts along the z-axis do not alter the electric and magnetic fields parallel to the boost. As a consequence, to have a constant magnetic field in the electron's reference frame it suffices to produce a constant B field in the z direction in the lab frame. By choosing it to be in the z-direction, it does not affect the trajectory.

In summary, a suitable external electromagnetic field can be found that satisfies the two desired properties: a) it produces the desired trajectory $x^\mu(\tau)$ by means of an E field that is constant in time and suitably spatially varying, and b) it induces an energy split Ω that is constant in time through a magnetic field in the z-direction that is constant in space and time.

Chapter 9

Appendix - Newton's Cradle Spectra

We describe here the key elements of the proofs. To this end, we map self-adjoint to unitary operators, and vice versa, using the Cayley transform. An advantage of the Cayley transform is that, unlike exponentiation, the Cayley transform is bijective and hence uniquely invertible. Also, since we work here in finite-dimensional Hilbert spaces, the terms Hermitian and self-adjoint can be used interchangeably.

9.1 Relation between Hermitian and unitary Newton cradles

We claim that the left action of a representation of the unitary group $U(1)$ on a unitary operator U is mapped, via the Cayley transform, into the addition of multiples of a rank 1 projector to a Hermitian operator S. Concretely, assume U is an arbitrary fixed unitary acting on a finite-dimensional Hilbert space $\mathcal{H}$. Then its Cayley transform is defined to be the Hermitian operator S:

$$S := -i\,(U + \mathbb{1})\,(U - \mathbb{1})^{-1} \tag{9.1}$$

We multiply U from the left with an element of the $U(1)$-family $(\mathbb{1} + (e^{i\alpha} - 1)\,|w\rangle\,\langle w|)$ of unitaries where $|w\rangle$ is an arbitrary fixed normalized vector. Running through all $\alpha \in [0, 2\pi)$, we obtain a family of unitaries $U(\alpha)$:

$$U(\alpha) := U + \left(e^{i\alpha} - 1\right)|w\rangle\,\langle w|\,U \tag{9.2}$$

By Cayley transforming each of the $U(\alpha)$, we obtain a family of self-adjoint operators $S(\alpha)$

$$S(\alpha) := -i\,(U(\alpha) + \mathbb{1})\,(U(\alpha) - \mathbb{1})^{-1} \tag{9.3}$$

with $S(0) = S$. We claim that, for any fixed choice of U and $|w\rangle$, the Hermitian operators $S(\alpha)$ for varying α differ by a multiple of a rank 1 projector, i.e., that there exists a normalized vector $|v\rangle$ so that for every $\alpha \in [0, 2\pi)$ there exists a $\mu(\alpha) \in \mathbb{R}$ obeying:

$$S(\mu(\alpha)) = S + \mu|v\rangle\langle v| \tag{9.4}$$

For the proof, we start with:

$$\begin{aligned} S(\alpha) &= -i\left(\mathbb{1} + U + \left(e^{i\alpha} - 1\right)|w\rangle\langle w|U\right) && (9.5)\\ &\quad \times \left(U + \left(e^{i\alpha} - 1\right)|w\rangle\langle w|U - \mathbb{1}\right)^{-1} && (9.6)\end{aligned}$$

Acting from the right with the operator $(U + (e^{i\alpha} - 1)|w\rangle\langle w|U - \mathbb{1})$ yields:

$$\begin{aligned} &S(\alpha)\left(U + \left(e^{i\alpha} - 1\right)|w\rangle\langle w|U - \mathbb{1}\right)\\ &\quad = -i(1 + U) - i\left(e^{i\alpha} - 1\right)|w\rangle\langle w|U \end{aligned} \tag{9.7}$$

Rearranging the terms:

$$\begin{aligned} &S(\alpha)(U - \mathbb{1}) + S(\alpha)\left(e^{i\alpha} - 1\right)|w\rangle\langle w|U\\ &\quad = -i(1 + U) - i\left(e^{i\alpha} - 1\right)|w\rangle\langle w|U \end{aligned} \tag{9.8}$$

After acting with the operator $(U - \mathbb{1})^{-1}$ from the right we recognize the expression for the Cayley transform S of U and obtain:

$$S(\alpha) - S = -\left(S(\alpha) + i\right)\left(e^{i\alpha} - 1\right)|w\rangle\langle w|U(U - \mathbb{1})^{-1}. \tag{9.9}$$

Since both $S(\alpha)$ and S are self-adjoint operators, their difference, $S(\alpha) - S$, is also self-adjoint. This means that the following equation must hold for some $\mu'(\alpha) \in \mathbb{R}$:

$$-\left(S(\alpha) + i\right)\left(e^{i\alpha} - 1\right)|w\rangle = \mu'(\alpha)\left[(U - \mathbb{1})^{-1}\right]^{\dagger} U^{\dagger}|w\rangle. \tag{9.10}$$

The left $U(1)$ action on the unitary U which results in $U(\alpha)$ therefore corresponds to the addition of a multiple of a projector $\mu(\alpha)|v\rangle\langle v|$ to S, resulting in

$$S(\alpha) = S + \mu(\alpha)|v\rangle\langle v|, \tag{9.11}$$

where:

$$|v\rangle = \frac{1}{\mathcal{N}_v}\left(U^{\dagger} - \mathbb{1}\right)^{-1} U^{\dagger}|w\rangle \tag{9.12}$$

Calculating the norm of Eq. (9.12) while inserting a resolution of the identity, the normalization constant $\mathcal{N}_v$ follows:

$$\mathcal{N}_v = \sqrt{\sum_m \frac{|w_m|^2}{|u_m - 1|^2}} = \frac{\sqrt{\sum_m |w_m|^2 (s_m^2 + 1)}}{2}. \tag{9.13}$$

Recall that we use the notation $w_n := \langle s_n | w \rangle$, $v_n := \langle s_n | v \rangle$ and $U(\alpha)|u_n(\alpha)\rangle = u_n(\alpha)|u_n(\alpha)\rangle$, $S(\mu)|s_n(\mu)\rangle = s_n(\mu)|s_n(\mu)\rangle$.

9.2 Relating the eigenbases of $U(\alpha)$ and $S(\alpha)$ to those of U and S

Our aim is to construct the eigenvectors of $U(\alpha)$ (and therefore of $S(\mu)$) in terms of the eigenbasis of U (and S). We have

$$\begin{aligned} u_n(\alpha) \langle u_n(\alpha) \rangle u_m &= \langle u_n(\alpha) | U(\alpha) | u_m \rangle \\ &= \langle u_n(\alpha) | \left(U + (e^{i\alpha} - 1) |w\rangle \langle w| U \right) | u_m \rangle \\ &= \langle u_n(\alpha) \rangle u_m u_m \\ &\quad + (e^{i\alpha} - 1) \langle u_n(\alpha) \rangle w \langle w \rangle u_m u_m, \end{aligned} \tag{9.14}$$

and therefore:

$$\langle u_n(\alpha) \rangle u_m = (e^{i\alpha} - 1) \langle u_n(\alpha) \rangle w \frac{\langle w \rangle u_m u_m}{u_n(\alpha) - u_m} \tag{9.15}$$

Using

$$1 = \langle u_n(\alpha) \rangle u_n(\alpha) = \sum_m \langle u_n(\alpha) \rangle u_m \langle u_m \rangle u_n(\alpha), \tag{9.16}$$

we obtain:

$$1 = |e^{-i\alpha} - 1|^2 |\langle u_n(\alpha) \rangle w|^2 \sum_m \frac{|u_m|^2 |\langle w \rangle u_m|^2}{|u_n(\alpha) - u_m|^2} \tag{9.17}$$

This means that, in Eq. (9.15), we can express $|(e^{i\alpha} - 1) \langle u_n(\alpha) \rangle w|$ in terms of known quantities to obtain:

$$|\langle u_n(\alpha) \rangle u_m| = \left| \frac{\langle w \rangle u_m}{u_n(\alpha) - u_m} \right| \left(\sum_k \frac{|\langle w \rangle u_k|^2}{|u_n(\alpha) - u_k|^2} \right)^{-1/2}. \tag{9.18}$$

Via the Cayley transform, this yields:

$$|\langle s\rangle\, s_n| = \frac{|v_n|}{|s-s_n|}\left(\sum_k \frac{|v_k|^2}{(s-s_k)^2}\right)^{-1/2} \tag{9.19}$$

Further, the overlap function $\langle s|s_n\rangle$ can be chosen real for all s, s_n by suitably choosing the phases of the eigenvectors $|s\rangle$. To see this, we calculate:

$$\begin{aligned}\frac{s_r(\alpha)-i}{s_r(\alpha)+i}\langle s_n|s_r(\alpha)\rangle &= \langle s_n|U(\alpha)|s_r(\alpha)\rangle \\ &= \langle s_n|\left(\mathbb{1}+(e^{i\alpha}-1)|w\rangle\langle w|\right)U|s_r(\alpha)\rangle \\ = \frac{s_n-i}{s_n+i}\langle s_n|s_r(\alpha)\rangle &+ (e^{i\alpha}-1)\langle s_n|w\rangle\langle w|U|s_r(\alpha)\rangle\end{aligned} \tag{9.20}$$

This equation can be rewritten as

$$\langle s_n|s_r(\alpha)\rangle = \frac{g_n M(s_r(\alpha))}{s_r(\alpha)-s_n} \tag{9.21}$$

where we separated the n-dependent from the s-dependent terms by defining:

$$g_n := (s_n+i)\langle s_n|w\rangle \tag{9.22}$$

$$M(s_r(\alpha)) := \frac{(s_r(\alpha)+i)}{2i}(e^{i\alpha}-1)\langle w|U|s_r(\alpha)\rangle \tag{9.23}$$

We use the choice of phases of the eigenvectors $|s_n\rangle = |s_n(\alpha=0)\rangle$ so that $g_n \in \mathbb{R}$ for all n. Further, we choose the phases of the eigenvectors $|s_r(\alpha)\rangle$ for $\alpha \neq 0$ such that $M(t_r(\alpha)) \in \mathbb{R}$ for all $\alpha \neq 0$. Notice that $M(t_r(\alpha)) = 0$ for $\alpha = 0$. While these choices ensure that $\langle s_n|s_r(\alpha)\rangle \in \mathbb{R}$, the overlap function can also be made continuous through a suitable choice of signs, as described in the main text.

9.3 Velocity of the complex eigenvalues

Differentiating Eq. (9.14) at $\alpha = 0$ for $n = m$, yields:

$$\left.\frac{du_n(\alpha)}{d\alpha}\right|_{\alpha=0} = i\ |\langle u_n|w\rangle|^2 u_n \tag{9.24}$$

Since, for any α, we could choose $U(\alpha)$ to be the starting unitary U of a new Newton cradle with $|v\rangle$, the velocity of the complex eigenvalues for all α reads:

$$\frac{\mathrm{d}u_n\left(\alpha\right)}{\mathrm{d}\alpha} = i|\langle u_n\left(\alpha\right)\rangle\, w|^2 u_n\left(\alpha\right). \tag{9.25}$$

From Eq. (9.17), we have:

$$|\langle u_n\left(\alpha\right)\rangle\, w|^2 = \frac{1}{|e^{i\alpha}-1|^2}\left(\sum_m \frac{|w_m|^2}{|u_n(\alpha)-u_m|^2}\right)^{-1}. \tag{9.26}$$

Therefore, Eq. (9.25) becomes this differential equation:

$$\frac{\mathrm{d}u_n(\alpha)}{\mathrm{d}\alpha} = iu_n(\alpha)\frac{1}{|e^{i\alpha}-1|^2}\left(\sum_m \frac{|w_m|^2}{|u_n(\alpha)-u_m|^2}\right)^{-1} \tag{9.27}$$

9.4 Velocity of the real eigenvalues

The Möbius transform $u_k = (s_k - i)/(s_k + i)$ yields for the real eigenvalues of $S(\alpha)$:

$$\frac{ds_n}{d\alpha} = \frac{(s_n+i)^2}{2i}\frac{du_n}{d\alpha}. \tag{9.28}$$

The inverse Möbius transform $s_k = i(1+u_k)/(1-u_k)$, applied to Eq. (9.18), then yields for the real eigenvalues $\{s_n\}_{n\in 1,\ldots,N}$:

$$\begin{aligned}\frac{\mathrm{d}s_n}{\mathrm{d}\alpha} &= \frac{1}{2}\frac{1}{|e^{i\alpha}-1|^2}\left(\sum_m |w_m|^2\frac{s_m^2+1}{4(s_n-s_m)^2}\right)^{-1}\\ &= \frac{1}{2}\frac{1}{\sin^2(\frac{\alpha}{2})}\left(\sum_m |w_m|^2\frac{s_m^2+1}{(s_n-s_m)^2}\right)^{-1}\end{aligned} \tag{9.29}$$

9.5 Integrating the differential equation for the velocities

After separating the variables s_n and α,

$$\mathrm{d}s_n \sum_m |w_m|^2\frac{s_m^2+1}{(s_n-s_m)^2} = \frac{\mathrm{d}\alpha}{2\sin^2(\frac{\alpha}{2})}, \tag{9.30}$$

integrating with the initial conditions $s_n(\alpha = 0) = s_n$ yields:

$$\sum_m |w_m|^2 \frac{s_m^2 + 1}{s_n(\alpha) - s_m} + \sum_m |w_m|^2 s_m = \cot\left(\frac{\alpha}{2}\right) \tag{9.31}$$

As expected, since this yields a polynomial of order n in $s_n(\alpha)$, there are N solutions $\{s_n(\alpha)\}_{n=1,\ldots,N}$.

In order to express Eq. (9.31) using the components of $|v\rangle$ rather than $|w\rangle$, we express $|w\rangle$ in terms of $|v\rangle$ and the operator U:

$$|w\rangle = \mathcal{N}_v \, U \left(U^\dagger - \mathbb{1}\right) |v\rangle = \mathcal{N}_v \left(\mathbb{1} - U\right) |v\rangle \tag{9.32}$$

To obtain the components of $|w\rangle$ and $|v\rangle$, we act with $\langle u_k|$ from the left:

$$w_k = \langle u_k \rangle \, w = \mathcal{N}_v \langle u_k | \left(\mathbb{1} - U\right) |v\rangle \,, \tag{9.33}$$

$$w_k = \mathcal{N}_v \left(1 - u_k\right) v_k \tag{9.34}$$

Since only the absolute values of w_k appear in Eq. (9.31), we calculate $|w_k|^2$ and then inverse Cayley transform u_k in order to get an expression that depends on the real eigenvalues $\{s_i\}_{i=1,\ldots,N}$:

$$|w_k|^2 = |\mathcal{N}_v|^2 |1 - u_k|^2 |v_k|^2 \tag{9.35}$$

$$= |\mathcal{N}_v|^2 \frac{4}{s_k^2 + 1} |v_k|^2. \tag{9.36}$$

This yields Eq. (9.31) in terms of the v_k:

$$\begin{aligned} \cot\left(\frac{\alpha}{2}\right) &= \sum_m 4 |\mathcal{N}_v|^2 \frac{|v_m|^2}{s_n(\alpha) - s_m(0)} \\ &\quad + \sum_m |v_m|^2 4 |\mathcal{N}_v|^2 \frac{s_m}{s_m^2 + 1} s_m \end{aligned} \tag{9.37}$$

9.6 The relationship between μ and α

We claim that $\mu(\alpha)$ is given by:

$$\mu(\alpha) = \sum_m |w_m|^2 \left(s_m^2 + 1\right) \left(\cot\left(\frac{\alpha}{2}\right) - \sum_m |w_m|^2 s_m\right)^{-1} \tag{9.38}$$

We start the proof with the observation that $S(\alpha) - S = \mu|v\rangle\langle v|$ yields:

$$(s_n(\alpha) - s_m)\,\langle s_m\rangle\, s_n\,(\alpha) = \mu\,(\alpha)\,\langle s_m\rangle\, v\,\langle v\rangle\, s_n\,(\alpha) \tag{9.39}$$

We solve this equation for $(s_n(\alpha) - s_m)$ and substitute it into Eq. (9.31) to obtain:

$$\frac{1}{\mu}\sum_m |w_m|^2\left(s_m^2+1\right)\frac{\langle s_m\rangle\, s_n\,(\alpha)}{\langle s_m\rangle\, v\,\langle v\rangle\, s_n\,(\alpha)} \tag{9.40}$$

$$= \cot\left(\frac{\alpha}{2}\right) - \sum_m |w_m|^2 s_m \tag{9.41}$$

From Eq. (9.12), a Möbius transform yields

$$\langle s_m\rangle\, v = \frac{1}{\mathcal{N}_v}\frac{s_m+i}{2i}\,\langle s_m\rangle\, w, \tag{9.42}$$

i.e.,

$$(s_m+i)\,w_m = 2i\;\mathcal{N}_v\;v_m. \tag{9.43}$$

Substituting this expression into Section 9.6, we obtain:

$$\frac{1}{\mu}\sum_m 2i\;\mathcal{N}_v\,(s_m-i)\,w_m^*\frac{\langle s_m\rangle\, s_n\,(\alpha)}{\langle v\rangle\, s_n\,(\alpha)}$$

$$= \cot\left(\frac{\alpha}{2}\right) - \sum_m |w_m|^2 s_m. \tag{9.44}$$

We now insert a resolution of the identity $\mathbb{1} = \sum_m |s_m\rangle\,\langle s_m|$ into the inner product $\langle s_n(\alpha)\rangle\, v$ and use Eq. (9.12) to obtain:

$$\langle s_n\,(\alpha)\rangle\, v = \frac{1}{\mathcal{N}_v}\sum_m \langle s_n\,(\alpha)\rangle\, s_m\,\langle s_m\rangle\, w\frac{u_m^*}{u_m^*-1} \tag{9.45}$$

We then divide by $\langle s_n(\alpha)\rangle\, v$ and complex conjugate the entire expression:

$$1 = \frac{1}{\mathcal{N}_v}\sum_m w_m^*\frac{s_m-i}{-2i}\frac{\langle s_m\rangle\, s_n\,(\alpha)}{\langle v\rangle\, s_n\,(\alpha)} \tag{9.46}$$

Now we recognize the same sum as in Section 9.6, up to constants, so we can finally express μ as a function of α:

$$\mu = 4\mathcal{N}_v^2\left(\cot\left(\frac{\alpha}{2}\right) - \sum_m |w_m|^2 s_m\right)^{-1} \tag{9.47}$$

With $\mathcal{N}_v$ given in Eq. (9.13), this yields Eq. (9.38) as claimed.

9.7 Reformulation of the characteristic equation of $S(\mu)$

We now derive the equation:

$$\sum_m \frac{|v_m|^2}{s_n(\mu) - s_m} = \frac{1}{\mu}. \tag{9.48}$$

To this end, we use $|w_k|^2 = |\mathcal{N}_v|^2 \frac{4}{s_k^2+1}|v_k|^2$to express w_m in terms of v_m in Eq. (9.31):

$$4|\mathcal{N}_v|^2 \sum_m \frac{|v_m|^2}{s_n(\alpha) - s_m} = \cot\left(\frac{\alpha}{2}\right) - \sum_m |w_m|^2 s_m, \tag{9.49}$$

Using Eq. (9.47), we express the right-hand side in Eq. (9.49) in terms of $\mu(\alpha)$:

$$4|\mathcal{N}_v|^2 \sum_m \frac{|v_m|^2}{s_n(\alpha) - s_m} = 4|\mathcal{N}_v|^2 \frac{1}{\mu(\alpha)}. \tag{9.50}$$

Finally, dividing by $4|\mathcal{N}_v|^2$, and expressing the dependence on α as a dependence on μ, we obtain Eq. (9.48). We remark that an equation equivalent to Eq. (9.48), which is equivalent to the characteristic equation $\det(S(\mu) - s\mathbb{1}) = 0$ of $S(\mu)$, was used in [31] to derive a numerical algorithm for the eigenvalue problem, along with a perturbative stability analysis.

9.8 Cauchy interlacing

The Cauchy interlacing theorem arises as a special case. The theorem states that the $N-1$ eigenvalues $a_1 < a_2 < \ldots < a_{N-1}$ of any Hermitian $(N-1) \times (N-1)$ matrix A obtained by deleting the r-th row (r is arbitrary) and r-th column of a Hermitian $N \times N$ matrix S with nondegenerate spectrum are interlaced in the N eigenvalues of S, i.e.,: $s_n < a_n < s_{n+1}\ \forall n = 1 \ldots (N-1)$. It is straightforward to show that one obtains this result as the special case of the Newton cradle of S in which $|v\rangle$ is chosen to be the vector with the components $\delta_{r,i}$ in the basis in which the matrix S is given, and letting $\mu \to \infty$. Using Eq. (4.2) in Chapter 4 for $\mu \to \infty$, we can conclude more, namely that each of the interlaced eigenvalues a_n is a solution of Eq. (4.3) of the main text, which means that we can identify the interlaced eigenvalues as $a_n = s_n^*$ for $n = 1, \ldots, N-1$.

Chapter 10

Appendices - Transmission of Coherent Information at the Onset of Interactions

10.1 A non-perturbative calculation

While we have taken a perturbative approach throughout Chapter 5, we illustrate here the exact calculation of the time-evolved state of System A. We find that the exact form of ρ_A is not easily raised to the n^{th} power in general, as is required for the calculation of the n-Rényi entropies. While there are particularly simple interaction Hamiltonians such as that invoked in Section 5.6 which enable exact calculations to be performed, this is not often the case. This highlights the utility of our perturbative method. Let us first express the time-evolved state of system A as:

$$\begin{aligned}\rho_A(t) &= \mathrm{Tr}_B\left[e^{it\hat{A}\otimes\hat{B}}\rho_A\otimes\rho_B e^{-it\hat{A}\otimes\hat{B}}\right]\\ &= \sum_r \langle b_r|\, e^{it\hat{A}\otimes\hat{B}}\rho_A\otimes\rho_B e^{-it\hat{A}\otimes\hat{B}}\,|b_r\rangle\\ &= \sum_r e^{it\hat{A}b_r}\rho_A e^{-it\hat{A}b_r}\rho_{Brr},\end{aligned} \tag{10.1}$$

where, working in the eigenbasis of $\hat{B}$:

$$\rho_{Bij} = \langle b_i|\,\rho_B\,|b_j\rangle\,. \tag{10.2}$$

Representing ρ_A in the eigenbasis of $\hat{A}$:

$$\rho_A = \sum_{ij} \rho_{Aij} \left|a_i\right\rangle \left\langle a_j\right|, \tag{10.3}$$

we have:

$$\rho_A(t) = \sum_{ijk} \rho_{Aij}\rho_{Bkk} e^{itb_k(a_i-a_j)} \left|a_i\right\rangle \left\langle a_j\right|, \tag{10.4}$$

Such that

$$\gamma_{A,n}(t) = \mathrm{Tr}_A[\rho_A(t)^n], \tag{10.5}$$

where $\rho_A(t)$ is a matrix whose matrix element $\rho_A(t)_{ij}$ is given by

$$\rho_A(t)_{ij} = \rho_{Aij} \sum_k e^{itb_k(a_i-a_j)} \rho_{Bkk}. \tag{10.6}$$

10.2 Qubit von Neumann entropy in UDW example

In Fig. 10.1. we plot the exact time evolution of the von Neumann entropy of a qubit system undergoing the UDW interaction as described in Section 5.6. We illustrate that, while the second time derivative diverges for a pure input state, the von Neumann entropy itself remains finite. Nevertheless, the divergence of the second time derivative renders the second order perturbative analysis of the (1-)coherent information unsuitable as a measure of entropy transfer.

10.3 Numerical illustration of the noncommutativity of the limits $\epsilon \to 0$ and $\lambda \to 0$.

We expect that for finite eigenvalues in the small ε limit the trace term in Eq. (5.26) reduces to:

$$\lim_{\varepsilon\to 0} \sum_{i,j} (\lambda_j^{\varepsilon}\lambda_i - \lambda_j^{1+\varepsilon})|a_{ij}|^2 = \sum_{i,j} (\lambda_i - \lambda_j)|a_{ij}|^2 = 0, \tag{10.7}$$

however, numerical analysis is required to determine the range of eigenvalues for which this vanishing trace term is small enough to overcome the ε in the denominator of Eq. (5.19).

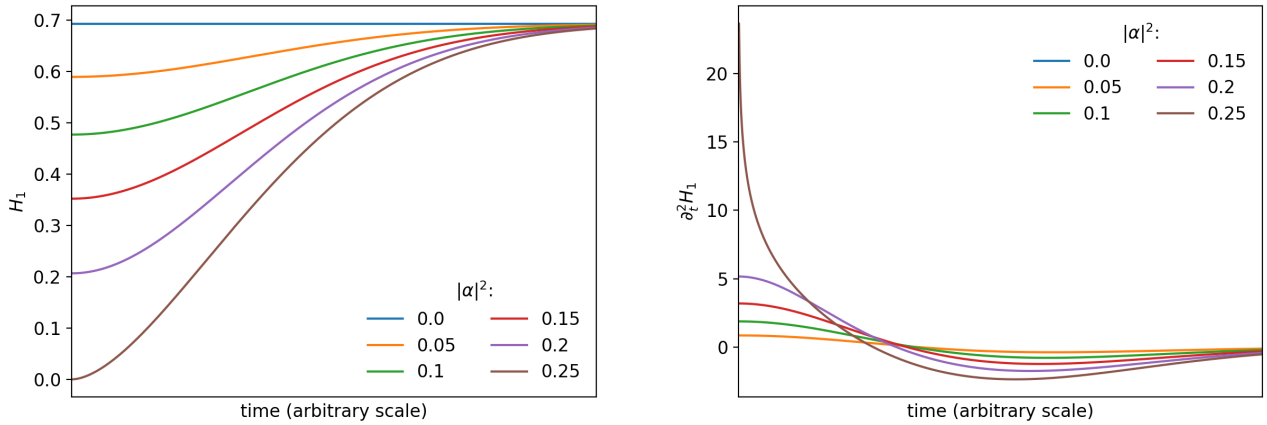

Figure 10.1: Left: the exact time evolution of the von Neumann entropy of the qubit under the UDW interaction. The $|\alpha|^2 = 0.25$ case corresponds to a pure input state. Right: the second time derivative of the von Neumann entropy of the qubit for the UDW interaction. While the second derivative is infinite at $t = 0$ for a pure state, this quickly falls off to a finite (indeed negative) value.

.

Because the values of a_{ij} are operator-dependent, let us illustrate the principle by simply setting $|a_{ij}| = 1$ for all i, j and computing the following:

$$\sum_{i,j} \lambda_j^\varepsilon (\lambda_i - \lambda_j), \tag{10.8}$$

which we refer to as the trace term. We also compute the regularised version, incorporating the ε in the denominator:

$$\frac{(1+\varepsilon)\sum_{i,j} \lambda_j^\varepsilon (\lambda_i - \lambda_j)}{\varepsilon}. \tag{10.9}$$

We illustrate the results of these computations for a qutrit system in Figure 10.2.[1] We set $\lambda_0 = 0.5$, such that $0 \leq \lambda_1 \leq 0.5$ and $\lambda_2 = 1 - \lambda_0 - \lambda_1$. We first plot the trace term, Eq. (10.8), on its own to illustrate that this tends to zero as $\varepsilon \to 0$, and then plot Eq. (10.9)

[1] We choose a qutrit rather than a qubit because in the latter case a single vanishing eigenvalue represents a pure state. Conversely, a qutrit system may have one vanishing eigenvalue without being pure. Hence, the qutrit system is the more general case.

to illustrate the range of eigenvalues for which the ε in the denominator out-competes the vanishing trace term.

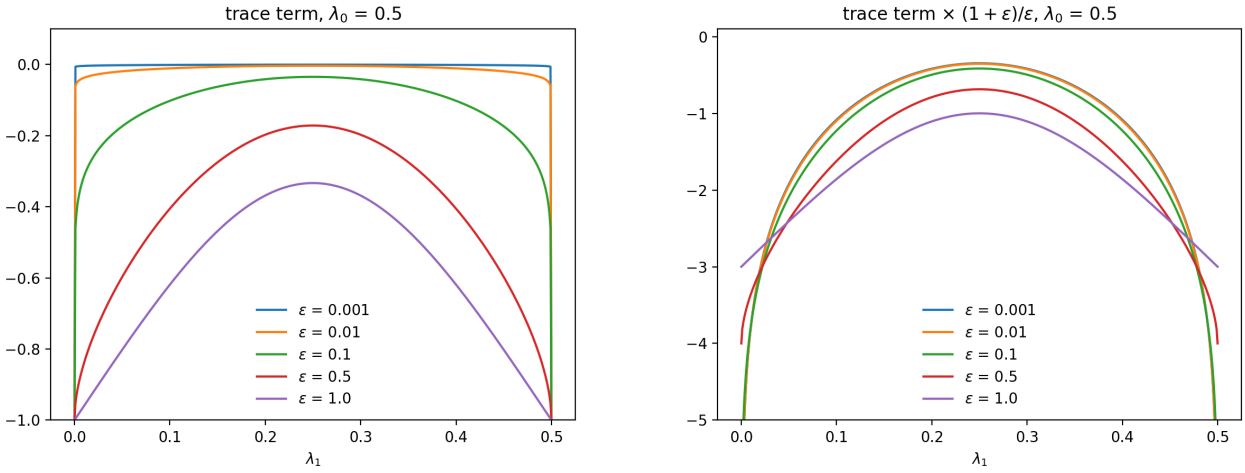

Figure 10.2: Left: plot of the sum in Eq. (10.8), where we see that this tends to zero for small ε except where an eigenvalue approaches zero, at which point an abrupt jump is observed. Right: plot of Eq. (10.9). Here we see that the jump in the left-hand plot is smoothed, but as one eigenvalue approaches zero the expression approaches a divergence.

.

On the left of Fig. 10.2, we indeed see that when ε is small, Eq. (10.8) ≈ 0 for most values of λ. However, in small λ limit this trace term demonstrates an abrupt change in value. This abrupt change, however, is not representative of a physical change in the second time derivative. Rather, the physical behaviour is represented on the right hand side, where crucially we include the ε in the denominator. The right hand side of Fig. 10.2 thus illustrates that for relatively large eigenvalues, the magnitude of the leading order change in the von Neumann entropy is small, while in the case of one or more vanishing eigenvalues, the leading order change diverges. A further example of this behaviour is given in Section 10.4, where a more general form of the interaction Hamiltonian $\hat{A}$ is used.

10.4 Supplementary example: leading order change in von Neumann entropy

While our second order calculations may not provide clarity in terms of the $(n \to 1)$ coherent information, we have demonstrated numerically that they are useful in quantifying the leading order rate of change in the von Neumann entropy of a single subsystem at the onset of an interaction. We have illustrated this numerically in Fig. 10.2, and provide in Fig. 10.3 a further numerical example. In this latter case, we choose an interaction Hamiltonian for which $|a_{ij}| \neq 1$ for all i, j. Instead, we choose an arbitrary Hermitian operator as the interaction Hamiltonian, $\hat{A}_{\text{test}}$, which acts on a qutrit system with eigenvalues $\lambda_0 = 0.5$, $0 \leq \lambda_1 \leq 0.5$, and $\lambda_2 = 1 - \lambda_0 - \lambda_1$. The interaction Hamiltonian $\hat{A}_{\text{test}}$ is:

$$\hat{A}_{\text{test}} = \begin{pmatrix} 0.2 & 0.1 & 0.5 \\ 0.1 & 0.3 & 0.5 \\ 0.5 & 0.5 & 0.5 \end{pmatrix}, \tag{10.10}$$

and the corresponding plots of

$$\text{Tr}_A \left[\rho_A^{\varepsilon} \left[\hat{A}_{\text{test}}, \rho_A \right] \hat{A}_{\text{test}} \right], \tag{10.11}$$

and

$$\frac{1+\varepsilon}{\varepsilon} \text{Tr}_A \left[\rho_A^{\varepsilon} \left[\hat{A}_{\text{test}}, \rho_A \right] \hat{A}_{\text{test}} \right], \tag{10.12}$$

are illustrated on the left and right sides of Fig. 10.3, respectively. These quantities are related to $\ddot{H}_{1+\varepsilon}(A)|_{t=0}$ according to Eq. (5.19) in Section 5.4. Importantly, we see here that non-trivial asymmetry can exist in the distribution of Eq. (10.12) across the space of possible states of System A, illustrating the way in which the leading order change in the von Neumann entropy of this system at the onset of interaction is sensitive to the precise configuration of the initial input state.

10.5 Further discussion of the $n \to 1$ $(\varepsilon \to 0)$ case

In Section 5.4, we attempted to quantify the leading (second) order change in the coherent information at the onset of a quantum channel, as illustrated in Fig. 5.1. We found, however, that the second order change in the von Neumann entropy diverges in the case of pure states. As a consequence, the leading order change in the coherent information, given by $\ddot{S}(A) - \ddot{S}(B)$, will itself always diverge, since system B is pure by definition.

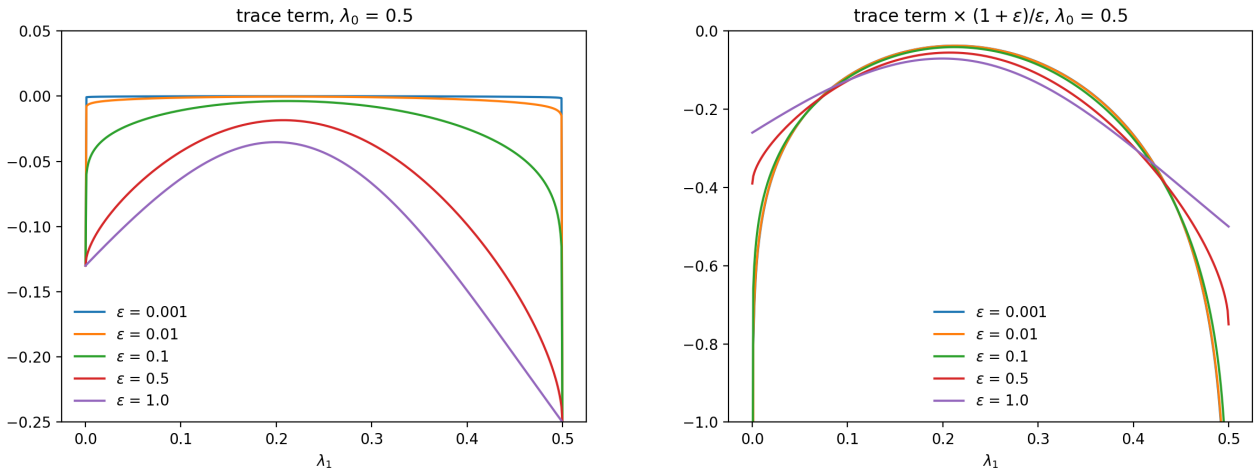

Figure 10.3: Left: Plot of Eq. (10.11) for a qutrit system with eigenvalue $\lambda_0 = 0.5$ and varying λ_1, λ_2. Right: Plot of Eq. (10.12) for the same system. The interaction Hamiltonian is $\hat{A}_{\text{test}}$, resulting in an asymmetric distribution.

.

One may naturally ask whether it is possible to quantify how the speed of the divergence depends upon the state of System A. However, we demonstrate here that a number of issues arise when we attempt to answer this question.

Let us revisit the expression for the leading order change in the n-coherent information as $n \to 1$ (or $\varepsilon \to 0$ where $n = 1+\varepsilon$). This of course corresponds to the conventional definition of the coherent information, which utilises the von Neumann entropy. Representing the n^{th} Rényi entropy as H_n, we have:

$$\delta I^d_{1+\varepsilon} = \frac{t^2}{2}\left(\ddot{H}_{1+\varepsilon}(A)\big|_{t=0} - \ddot{H}_{1+\varepsilon}(B)\big|_{t=0}\right), \tag{10.13}$$

$$= \frac{(1+\varepsilon)t^2}{-\varepsilon}\Big((\Delta B)^2 D_{1+\varepsilon,A} - (\Delta A)^2 D_{1+\varepsilon,B}\Big). \tag{10.14}$$

Because System B is pure by design, $D_{1+\varepsilon,B} = (\Delta B)^2$. Hence, we may factor out the $(\Delta B)^2$ to obtain:

$$\delta I^d_{1+\varepsilon} = \frac{(1+\varepsilon)t^2(\Delta B)^2}{\varepsilon}\Big((\Delta A)^2 - D_{1+\varepsilon,A}\Big), \tag{10.15}$$

From here, we may attempt to characterise the speed of the divergence by neglecting the prefactor of $t^2(\Delta B)^2(1+\varepsilon)/\varepsilon$, which is independent of System A, and simply consider the magnitude of the term $(\Delta A)^2 - D_{1+\varepsilon,A}$. However, we know from Section 5.4 that for $\varepsilon \to 0$, $D_{1+\varepsilon,A}$ is approximately zero across the whole state space of System A, except where one or more eigenvalues vanish. Consequently, we expect $(\Delta A)^2 - D_{1+\varepsilon,A} \approx (\Delta A)^2$ except at the positions in state space corresponding to vanishing eigenvalues. Much like the left side of Fig. 10.2, the distribution of this factor would therefore exhibit a sharp jump, approaching a discontinuity as $\varepsilon \to 0$. Such behaviour cannot be representative of a physical quantity, as this would suggest that states which were arbitrarily close to purity would exhibit vastly different behaviour to states which were exactly pure. Indeed, we showed in Section 5.4 that the $1/\varepsilon$ prefactor cannot be neglected if we want to obtain a smooth distribution across state space. However, if we are to incorporate this prefactor into the difference term $(\Delta A)^2 - D_{1+\varepsilon,A}$, we simply obtain a divergence as $\varepsilon \to 0$ because of the finite value of the $(\Delta A)^2$ term. Hence, we conclude that this approach is unsuitable for characterising the speed of the divergence in $\delta I^d_{1+\varepsilon}$.

One might also consider the possibility that System B is not completely pure. In such a case, we could not factor out $(\Delta B)^2$, and we must instead consider the difference $(\Delta B)^2 D_{1+\varepsilon,A} - (\Delta A)^2 D_{1+\varepsilon,B}$. If we were to assume that system B was not completely pure, both $D_{1+\varepsilon,A}$ and $D_{1+\varepsilon,B}$ approach zero, and there appears to be a competition between the two terms which could be regularised by the factor of $1/\varepsilon$, similar to the right hand of Fig. 10.2. However, it is important to note that in the derivation of Eq. (10.14) we required that the tripartite system $A\tilde{A}B$ be pure. Furthermore, we required that systems A and B are initially unentangled such that $\rho_{AB} = \rho_A \otimes \rho_B$. Hence, we cannot simply assume that system B is impure while ensuring the validity of Eq. (10.14).

One approach, however, may be to decompose system B into two subsystems B_1 and B_2, such that B as a whole is pure, but the individual subsystems are not. One may then restrict the interaction Hamiltonian such that it acts trivially on one subsystem, i.e. $\hat{B} = \hat{B}_1 \otimes \mathbb{I}_2$. However, this constitutes a different and more complicated physical scenario to that which we have been considering in this work. Indeed, if B_1 and B_2 are entangled, we have:

$$\rho_B = \sum_{i,j,k,l} a_{ijkl} \left|i\right\rangle \left\langle j\right|_1 \otimes \left|k\right\rangle \left\langle l\right|_2 := \sum_{i,j,k,l} a_{ijkl} \sigma_{1ij} \otimes \sigma_{2kl}. \tag{10.16}$$

Because this is not a product state, we cannot simply exchange B for B_1 in the durability expression.

Instead, we have:

$$\mathrm{Tr}_B\left[\rho_B^{n-1}\big[\hat{B},\rho_B\big]\hat{B}\right] = \mathrm{Tr}_{1,2}\left[\Big(\sum_{pqrs} a_{pqrs}\sigma_{1pq}\otimes\sigma_{2rs}\Big)^{n-1}\Big(\sum_{ijkl} a_{ijkl}\Big[\hat{B}_1,\sigma_{1ij}\Big]\hat{B}_1\otimes\sigma_{2kl}\Big)\right]. \tag{10.17}$$

This represents an interesting problem, as it may be more plausible to consider that System B is not initially completely pure. However, quantifying this slight impurity for the purpose of computing the difference term is non-trivial, and we leave further exploration of this to future work.

We anticipate that incorporating higher perturbative orders would be useful in regularising the divergences of the $n \to 1$ case. In particlar, it is likely that vanishing higher derivatives may suppress the magnitude of the entanglement transferred to the environment, even as the second derivative appears to diverge. However, we note that while the free Hamiltonians can be neglected to second perturbative order, they would need to be incorporated at higher orders. This would then significantly increase the complexity of the computations. Hence, we relegate such an approach to future work.